GAC MEDALLIST SERIES

Logan Medallist 5. Geophysics and Geology: An Essential Combination Illustrated by *LITHOPROBE* Interpretations–Part 2, Exploration Examples

Ron M. Clowes

Department of Earth, Ocean and Atmospheric Sciences
2020–2207 Main Mall
University of British Columbia
Vancouver, British Columbia, V6T 1Z4, Canada
E-mail: rclowes@eos.ubc.ca

SUMMARY

Lithoprobe (1984–2005), Canada's national, collaborative, multidisciplinary, Earth Science research project, investigated the structure and evolution of the Canadian landmass and its margins. It was a highly successful project that redefined the nature of Earth science research in Canada. One of many contributions deriving from the project was the demonstration by example that Earth scientists from geophysics and geology, including all applicable sub-disciplines within these general study areas, must work together to achieve thorough and comprehensive interpretations of all available data sets. In Part 1, this statement was exemplified through studies involving lithospheric structures. In Part 2, it is exemplified by summarizing interpretations from six exploration-related studies derived from journal publications.

In the first example, subsurface structures associated with the Guichon Creek batholith in south-central British Columbia, which hosts porphyry copper and molybdenum deposits, are better defined and related to different geological phases of the batholith. Reprocessed seismic reflection data and 2.5-D and 3-D inversions of magnetic and gravity data are combined with detailed geological mapping and drillhole information to generate the revised and improved subsurface interpretation. Research around the Bell Allard volcanogenic massive sulphide deposit in the Matagami region of northern Quebec provides the second example. A seismic reflection line over the deposit shortly after it was discovered by drilling, aided by core and geophysical logs, was acquired to test whether the deposit could be imaged. Direct detection of the ore body from the seismic section would be difficult if its location were not already known; however, structural characteristics that can be tied to lithologies from boreholes and logs were well identified. Nickel deposits and associated structures in the Thompson belt at the western limit of the Superior Province in northern Manitoba were the focus of seismic and electromagnetic (EM) studies combined with geology and physical property measurements. The combined seismic/EM image indicates that the rocks of the prospective Ospwagan Group, which have low resistivity, extend southeastward beneath the Archean gneiss and that structural culminations control the subsurface geometry of the Ospwagan Group.

The Sudbury structure in Ontario is famous for its nickel deposits, the largest in the world, which formed as the result of a catastrophic meteorite impact. To help reconcile some of the enigmas and apparent contradictions surrounding studies of the structure and to develop more effective geophysical techniques to locate new deposits, Lithoprobe partnered with industry to carry out geophysical surveys combined with the extensive geological information available. A revised structural model for the Sudbury structure was generated and a 3-D seismic reflection survey identified a nickel deposit, known from drilling results, prior to any mine development. The Athabasca Basin of northwestern Saskatchewan and northeastern Alberta is one of the world's most prolific producers of uranium from its characteristically high-grade unconformity-type deposits and is the only current uranium producer in Canada. An extensive database of geology, drillhole data and physical properties exists. Working with industry collaborators, Lithoprobe demonstrated the value of high-resolution seismic for imaging the unconformity and faults associated with the deposits. The final example involves a unique seismic reflection experiment

Geoscience Canada, v. 44, https://doi.org/10.12789/geocanj.2017.44.125 pages 135–180

to image the diamondiferous Snap Lake kimberlite dyke in the Slave Province of the Northwest Territories. The opportunity to study geological samples of the kimberlite dyke and surrounding rocks and to ground-truth the seismic results with drillhole data made available by the two industry collaborators enabled a case history study that was highly successful.

RÉSUMÉ

Lithoprobe (1984-2005), ce projet de recherche pancanadien, multidisciplinaire et concerté en sciences de la Terre, a étudié la structure et l'évolution de la croûte continentale canadienne et de ses marges. Ça a été un projet très réussi et qui a redéfini la nature de la recherche en sciences de la Terre au Canada. L'une des nombreuses retombées de ce projet a démontré par l'exemple que les spécialistes des sciences de la Terre en géophysique et en géologie, y compris toutes les sous-disciplines applicables dans ces domaines d'étude généraux, doivent travailler de concert afin de parvenir à une interprétation exhaustive de tous les ensembles de données disponibles. Dans la partie 1, cette approche s'est concrétisée par des études portant sur les structures lithosphériques. Dans la partie 2, elle a produit un résumé des interprétations tirées de six études liées à l'exploration à partir de publications dans des revues scientifiques.

Dans le premier exemple, les structures souterraines associées au batholite du ruisseau Guichon, dans le centre-sud de la Colombie-Britannique, et qui renferme des gisements porphyriques de cuivre et de molybdène, sont maintenant mieux définies et mieux reliées aux différentes phases géologiques du batholite. Un retraitement des données de sismique réflexion, et d'inversion magnétique et gravimétrique 2,5-D et 3-D combiné à une cartographie géologique détaillée et à des données de forage ont permis une interprétation révisée et améliorée du de subsurface. La recherche autour du gisement de sulfures massifs volcanogéniques de Bell Allard de la région de Matagami, dans le nord du Québec, est un deuxième exemple. Un levé de sismique réflexion réalisé au-dessus du gisement, peu après sa découverte par forage, couplé avec des diagraphies géophysiques et de carottes, a été réalisé pour vérifier si l'ensemble pouvait donner une image du gisement. La détection directe du gisement de minerai à partir de la coupe sismique serait difficile si son emplacement n'était pas déjà connu; cependant, les caractéristiques structurales qui peuvent être liées aux lithologies déduites des forages et des diagraphies ont été bien définies. Les gisements de nickel et les structures qui y sont reliées dans la bande de Thompson, à la limite ouest de la province du Supérieur, dans le nord du Manitoba, ont fait l'objet d'études sismiques et électromagnétiques (EM), combinés à des mesures de caractéristiques géologiques et physiques. L'image sismique/EM combinée indique que les roches du groupe d'intérêt d'Ospwagan, lesquelles ont une résistivité faible, s'étendent vers le sud-est sous le gneiss archéen et, les culminations structurales contrôlent la géométrie souterraine du groupe d'Ospwagan.

La structure de Sudbury, en Ontario, est réputée pour ses gisements de nickel, les plus importants au monde, lesquels se sont formés à la suite d'un impact météoritique catastrophique. Pour aider à comprendre certaines des énigmes et résoudre d'apparentes contradictions entourant les études de la structure, et pour développer des techniques géophysiques plus efficaces afin de localiser de nouveaux gisements, Lithoprobe s'est associé à l'entreprise privée pour réaliser des levés géophysiques, et les comparer aux très nombreuses informations géologiques disponibles. Une révision du modèle structural du gisement de Sudbury, ajouté à un levé sismique réflexion tridimensionnelle, ont permis de circonscrire un gisement de nickel, avant tout autre travail de développement minier. Le bassin de l'Athabasca, dans le nord-ouest de la Saskatchewan et le nord-est de l'Alberta, est l'un des producteurs d'uranium les plus prolifiques au monde provenant de gisements à haute teneur de type discordant, et est le seul producteur d'uranium au Canada. Une volumineuse base de données sur la géologie, les forages et les propriétés physiques est disponible. En collaboration avec des entreprises privées, Lithoprobe a démontré la valeur de la sismique à haute résolution pour l'imagerie de la discordance et des failles associées aux gisements. Le dernier exemple est celui d'une expérience de sismique réflexion unique visant à représenter le dyke de kimberlite diamantifère du lac Snap dans la province des Esclaves, dans les Territoires du Nord-Ouest. L'occasion d'étudier des échantillons géologiques du dyke de kimberlite, et des roches environnantes, et de valider les résultats sismiques à l'aide des données de forage mises à disposition par les deux partenaires privés, a permis une étude de cas très fructueuse.

Traduit par le Traducteur

INTRODUCTION

Lithoprobe (1984 to 2005) was Canada's national, collaborative, multidisciplinary, Earth Science research project that was established to develop a comprehensive understanding of the structure and evolution of Canada's present landmass and continental margins (Clowes 2010). Its principal scientific and operational components were built around a series of ten transects or study areas (Fig. 1), each of which was focused on carefully selected geological features that represent globally significant geotectonic processes. Among many other contributions, the project spawned a new and healthy atmosphere of scientific cooperation among Earth scientists: geophysicists and geologists (in the broadest sense of the terms) worked together, and geophysical and geological data were combined, to achieve the most thorough and comprehensive interpretation of those data, including extension of the interpretation into the third dimension, depth. In Part 1 of this two-part contribution, I exemplified this statement through a series of examples from the many Lithoprobe publications in which a combination of geophysics and geology led to high quality interpretations of lithospheric structure (Clowes 2015). In this article, I complete the series of examples, this time focusing on exploration-related results from Lithoprobe's collaboration with industry. As with the previous article, seismic reflection methods provide the primary geophysical data because such data provide the highest resolution for tying with geology and relating to subsurface interpretations, but other geophysical methods also are exemplified. Maps, drillhole information and

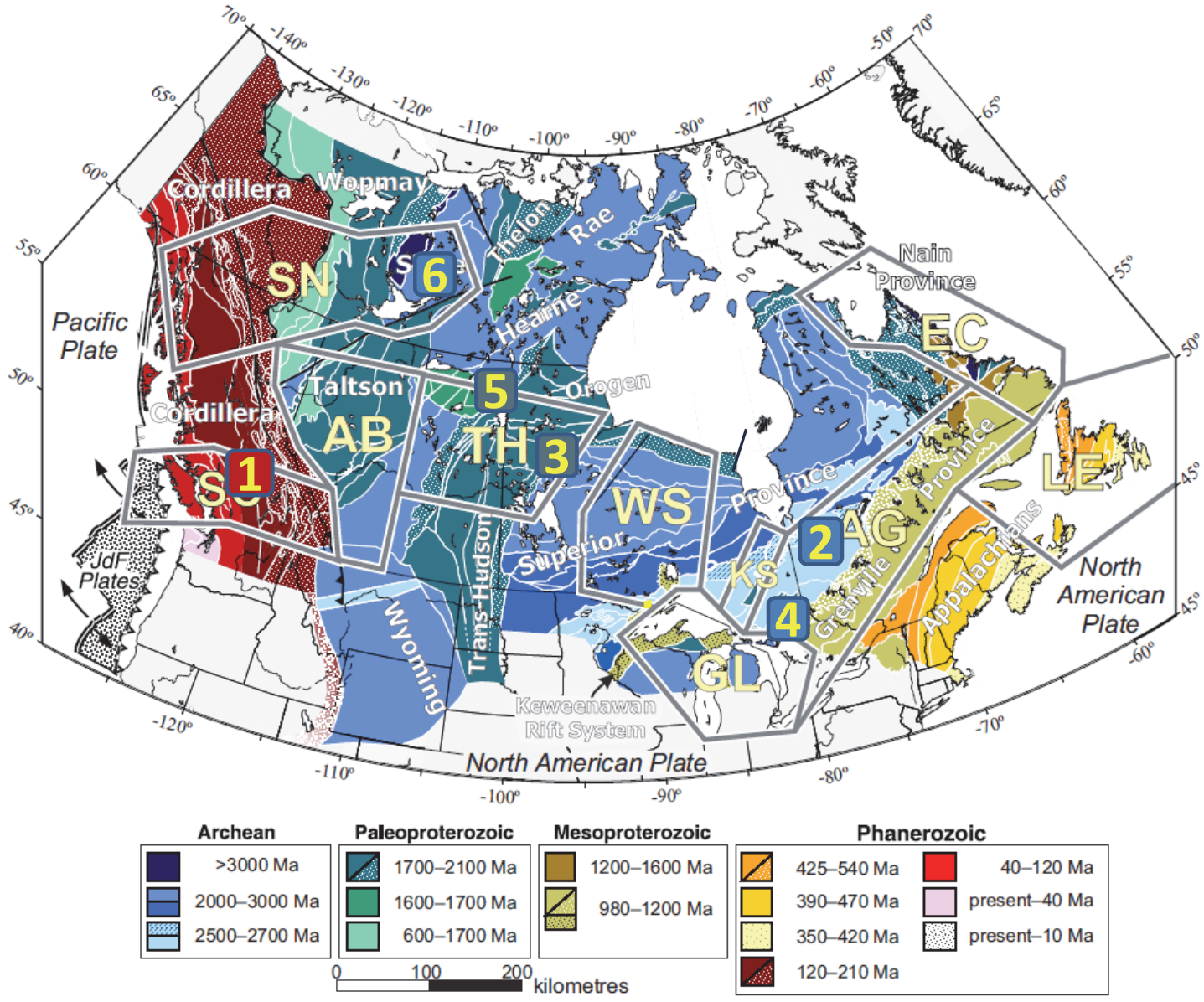

Figure 1. Simplified tectonic age map of Canada with outlines of Lithoprobe transects. White lines indicate domain divisions within the major tectonic elements. Stippling of some coloured areas indicates that the rocks may be older but they have experienced tectonic reworking during the time periods indicated by the colour. Numbers identify the general locations of the six exploration examples discussed in the text. Transect abbreviations: AB, Alberta Basement; AG, Abitibi–Grenville; EC, Eastern Canadian Shield Onshore–Offshore Transect (ECSOOT); GL, Great Lakes International Multidisciplinary Program on Crustal Evolution (GLIMPCE); KS, Kapuskasing Structural Zone; LE, Lithoprobe East; SC, Southern Cordillera; SN, Slave–Northern Cordillera Lithospheric Evolution (SNORCLE); TH, Trans-Hudson Orogen (THOT); and WS, Western Superior.

core samples, usually provided by the industry partner, are the main geological data. In general, the examples in parts 1 and 2 constitute a review of some of the important Lithoprobe results derived from a combination of geophysical and geological data.

PORPHYRY COPPER DEPOSITS, HIGHLAND VALLEY, BRITISH COLUMBIA

The Guichon Creek batholith (GCB), located in the Highland Valley of south-central British Columbia (number 1 in Fig. 1), hosts several large, low-grade copper and molybdenum deposits and is/was the principal copper reserve for British Columbia (McMillan et al. 1985). The surface geology of the batholith (about 70 km long and 30 km wide) and surrounding region is well mapped (Figs. 2 and 3a). However, only limited structural information regarding the subsurface features of the batholith, from interpretation of regional gravity data, are available. Interpretation of these data across a north-northwesterly section of the batholithic intrusion shows a funnel-shaped feature leading down to a steeply plunging conical stem more than 8 km deep (Ager et al. 1973).

The GCB, a typical calc-alkaline pluton, intruded into late Triassic arc volcanic rocks of the Nicola Group between about 213 and 196 Ma. Cutting the GCB are two major north-trend-

https://doi.org/10.12789/geocanj.2017.44.125

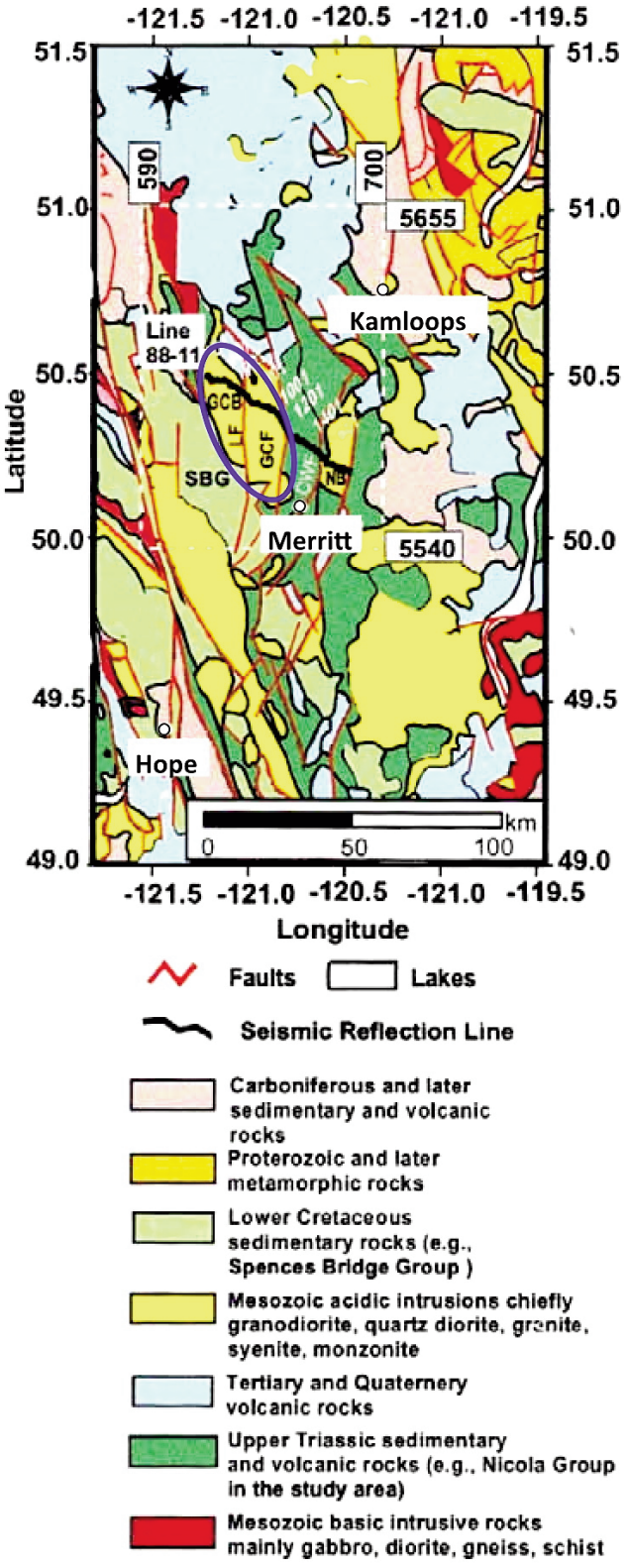

Figure 2. Simplified regional geological map showing location of Lithoprobe seismic reflection line 88-11 (location no. 1 in Fig. 1). Complex geology surrounds the Guichon Creek batholith (GCB; blue ellipse: yellow unit crossed by line 88-11). Mapped features labelled are: CWF, Coldwater fault; GCF, Guichon Creek fault; LF, Lornex fault; NB, Nicola batholith; and SBG, Spences Bridge Group. The dashed box indicates the area for which regional potential field data were used; numbers at corners are northings and eastings values. From Roy and Clowes (2000).

ing faults, the central Lornex and bounding Guichon Creek faults; the Highland Valley fault cuts the central GCB in a roughly northwesterly-southeasterly direction (Fig. 3a). Based on composition and texture, four different heterogeneous phases of the batholith are emplaced in a radially inward fashion (Northcote 1969). From outer to inner, the four phases are the Hybrid or Border (predominantly quartz diorite), Highland Valley (mainly quartz diorite and granodiorite), Bethlehem (uniform granodiorite composition) and Bethsaida (predominantly quartz monzonite) (Northcote 1969; Fig. 3a). Although mineral deposits are dispersed throughout the GCB, the principal ones, identified by name on Figure 3a, are associated with the Bethsaida phase and/or dyke swarms and faults that lie above the projection of the conical stem of the batholith (McMillan et al. 1985).

In 1988, Lithoprobe seismic reflection line 88–11, about 80 km long, was recorded along the Highland Valley across the GCB and low-grade Upper Triassic Nicola Group volcanic rocks to its east (Fig. 2). The original processing of these data to Lithoprobe specifications by commercial contractor (see Cook et al. 1992 for details) was optimized for the entire crust and thus did not generate images suitable for relating to the upper crust (depths to about 10 km). Working with support from Cominco Ltd., owners of the mine property, Roy and Clowes (2000) carried out reprocessing of the western half of line 88–11 across the batholith using commercial software available at the University of British Columbia, augmented by special processing techniques developed by Roy and Mereu (1996). They combined interpretation of the resulting seismic section with 2.5-D and 3-D interpretation of aeromagnetic and gravity data to develop a new interpretation tied to geology.

The reprocessed seismic section to two-way travel-time (TWT) of 6.0 s is shown in Figure 4. Improvements in data quality compared to the section processed by the commercial contractor enabled an interpretation of the data relative to the local geology (Fig. 4b), although near-surface structures (upper 1.5 s TWT, or 2.5 km) could not be enhanced due to limitations in the acquisition geometry. Thus, the reflection section could not be related directly to the mineral deposits. In the central part of the section at ~3 s TWT (depth of ~7 km), a fairly distinct sub-horizontal reflector is interpreted as the rim of the core of the batholith. Several other sub-horizontal seismic reflectors (dotted red lines) likely can be interpreted as layered structures formed when the pluton cooled. The east- and west-dipping reflectors (solid red lines) have been interpreted as the edges or limbs of the batholith and also may represent a layered internal structure to it, consistent with the variation in composition represented by the different phases. Drillhole information from Cominco Ltd. indicates that the Lornex and similar faults are steeply dipping. Because the reflection at ~3 s from the rim of the batholith is not visibly disrupted, Roy and Clowes (2000) presumed the faults are also high angle at 7 km depth, become listric, and/or have no physical property contrast associated with them. The stem of the batholith extends approximately from SP 541 – 781; its projection to the surface coincides approximately with the major deposits, as inferred from geology by McMillan et al. (1985).

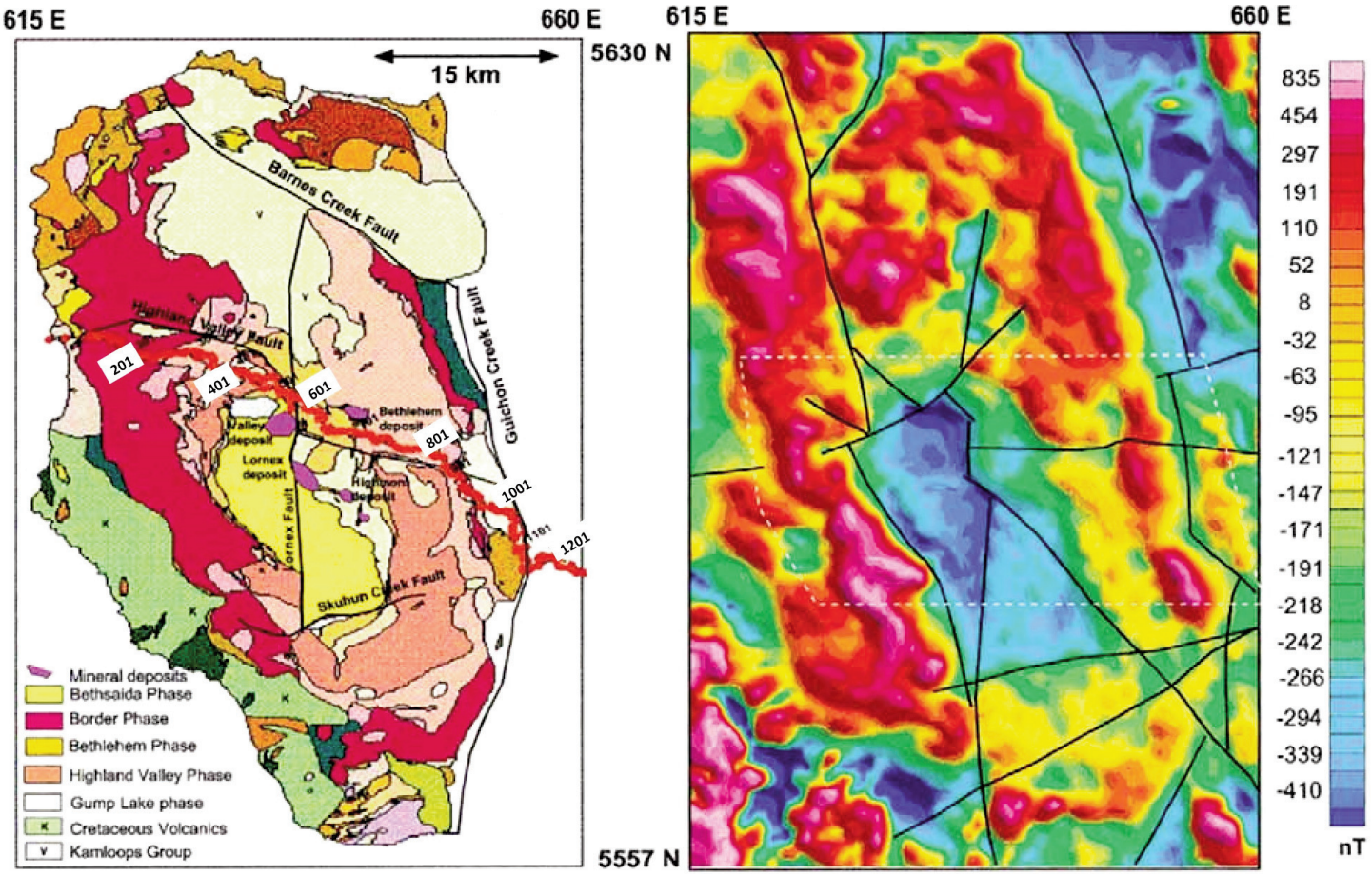

Figure 3. a) Geological map of the Guichon Creek batholith showing the different phases of intrusion (after McMillan et al. 1985; map provided by Cominco Ltd). Line 88-11 is shown by the thick red line; numbers indicate shot point locations. Individual mineral deposits are identified by name. b) Residual-field magnetic anomaly map of the same area as a); data from Cominco Ltd. Note the close similarity between the phases and the characteristics of the magnetic map. Solid black lines show surface-mapped faults. Dashed box indicates area for which high-resolution aeromagnetic data were provided by Cominco Ltd for the 3-D inversion (Fig. 5). The coordinate system is given by northings and eastings. From Roy and Clowes (2000).

Cominco Ltd acquired a high-resolution aeromagnetic survey of the GCB (Fig. 3b). A comparison of Figures 3a and 3b shows a close correspondence between variations in the magnetic anomaly field and the geology, including the different phases of the batholith. Data values for a subset of this survey (dashed white box in Fig. 3b) were provided to Roy and Clowes (2000) who carried out a 3-D inversion of these data (e.g. Li and Oldenburg 1996) to provide a 3-D volume distribution of anomalous susceptibility values. Figure 5a shows the observed high-resolution aeromagnetic map while Figure 5b shows the equivalent map predicted from the derived susceptibility values. Note the close similarity between the observed and predicted anomaly maps; all the major variations in the anomalous magnetic field variations have been recovered from the model.

Figure 5c shows depth slices of susceptibility values from the 3-D inversion results. Large lateral variation in structure and rock types resulted in highly variable susceptibility values for the 500 and 1000 m slices. Subsurface characterization of the batholith is shown by slices from 2000 to 3000 m. The low anomaly (A on 2000 m slice) lies below one of the active mining sites (A on Fig. 5b). Similar low susceptibility anomalies are noted at B and C (Fig. 5c) but these have not been investigated for mining purposes.

None of the data sets or analyses used or carried out by Roy and Clowes (2000) had sufficient resolution to provide a subsurface interpretation that reflects the complexity of the surface geology. However, based on the seismic reflection section, 2.5-D density/susceptibility structure (not discussed here), 3-D inversion results from gravity (not discussed here) and magnetics, and geology from maps and drillholes, a schematic cross-sectional model was developed (Fig. 6). Although the model is similar to the earlier interpretation of Ager et al. (1973), more details of the internal structure of the batholith and the correspondence of this structure to the observed geological phases of the GCB are shown. The Eocene Coldwater normal fault, identified farther east, truncated the stem of the batholith at about 20 km depth. The ore deposits in the GCB are fault-controlled, accounting for the low velocities and densities that were interpreted, and they occur in the granitic host rock, accounting for the low values of susceptibility. If similar geological processes that generated the ore deposit at A (Fig. 5) were active in areas represented by the low susceptibility values B and C (Fig. 5c), could other ore-bearing structures be present?

https://doi.org/10.12789/geocanj.2017.44.125

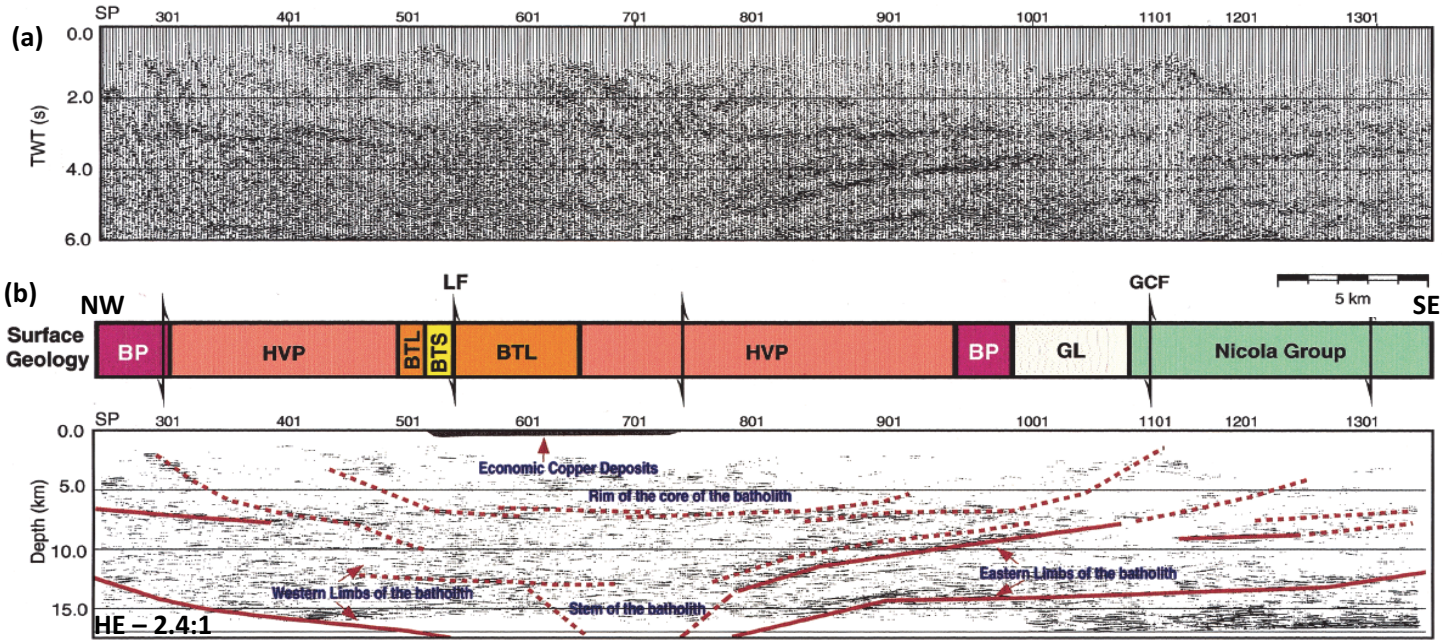

Figure 4. a) Reprocessed, stacked seismic reflection section for the western half of Lithoprobe line 88-11. Shot point (SP) numbers at the top correspond to those in Figure 3a. TWT, two-way travel-time. b) Coherency-filtered migrated section of a); an interpretation is overlain. Local geology along the line is shown by the bar strip. BP, Border phase; BTL, Bethlehem phase; BTS, Bethsaida phase; GCF, Guichon Creek fault; GL, Gump Lake phase; HVP, Highland Valley phase; LF, Lornex fault; vertical double arrows, surface faults; HE, horizontal exaggeration. From Roy and Clowes (2000).

MASSIVE SULPHIDE DEPOSITS, MATAGAMI, ABITIBI GREENSTONE BELT, QUEBEC

The Abitibi subprovince of the Archean Superior Province is the world's largest granite-greenstone belt and hosts a large proportion of Canada's mineral resources (no. 2 on Fig. 1; inset, Fig. 7). Within the greenstone belt, much of the mineral production is from volcanogenic massive sulphide (VMS) deposits formed at or near the sea floor in bimodal mafic volcanic sequences. Two examples, over which Lithoprobe ran high-resolution seismic reflection lines, are the Ansil deposit (e.g. Perron and Calvert 1998; now completely mined) within the Noranda mining camp in the southern Abitibi belt and the Bell Allard deposit (only discovered in 1992 and now being mined) within the Matagami mining district in the northern part of the belt (inset, Fig. 7). The latter is the focus of this section.

The Matagami mining district is focused on the limbs of the Galinée anticline that is cored by the Bell River complex (Fig. 7), a granophyric intrusion for which similar rocks in the area have been dated at 2724 ± 2.5 Ma using U–Pb methods (Mortensen 1993). The Bell River complex stratigraphically underlies a suite of bimodal volcanic rocks. The deeper unit, the Watson Lake Group, is largely felsic and rhyolite within it has an age similar to that of the Bell River intrusion; the upper unit, the Wabassee Group, consists of intermediate to mafic rocks (Fig. 7). The Bell River complex and its associated volcanic groups were folded into the Galinée anticline whose southwestern flank dips at about 45°. On this flank, the Watson Lake Group comprises a dacite unit overlain by rhyolite. It is separated from the overlying basaltic Wabassee Group by the Key tuffite, which is a thin (0.6–6 m) andesitic tuff with a minor hydrothermal component (Genna et al. 2014). The VMS deposits located on the southern flank of the anticline occur at the stratigraphic level of the Key tuffite horizon, and indicate that formation of the ore bodies is linked to the underlying Watson Lake Group. Five such deposits, including the Bell Allard, are identified on Figure 7.

Due to the fact that the sulphide deposits are associated with the Key tuffite horizon, it is a primary stratigraphic marker and a feature for study. Roberts (1975) carried out a detailed study of the Matagami Lake mine, located a few kilometres north of Bell Allard (Fig. 7), with emphasis on metamorphic and structural features that could be observed in underground exposures and hand specimens. Among other characteristics, he developed an orthographic projection of the contact surface between the Key tuffite and overlying basalt (Fig. 8a), which is likely representative in general of other deposits on the southern flank. Figure 8b shows a slab specimen in which the andesite–Key tuffite contact is identified. In the Matagami mining camp, a single deposit may consist of several massive sulphide lenses, the upper contact of which is sharp but the lower contact is usually gradational into a stringer zone of vein-type sulphide mineralization. Figure 8c shows an example from the Isle Dieu mine, located about 5 km north of Bell Allard (Fig. 7). The Isle Dieu deposit has two sulphide lenses, each of which overlies two or more stringer zones. The latter are considered to represent the conduits through which mineral-rich fluids circulated. The fluids were discharged onto the sea floor above and around discharge vents where they encountered cooler ocean water, which caused the precipitation of sulphides that accumulated as the sulphide lenses. The Key tuffite horizon may have been created by volcanism and

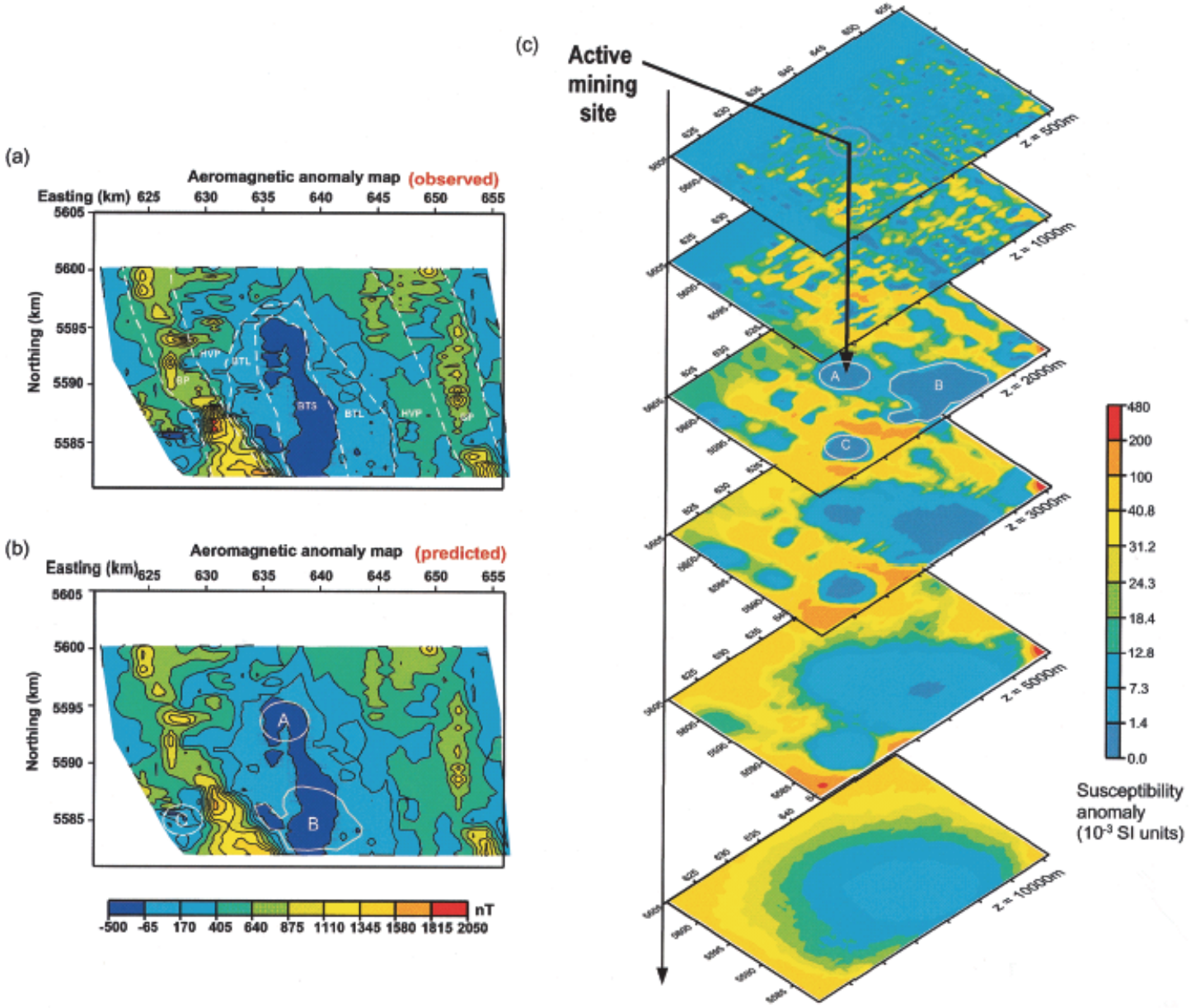

Figure 5. a) Observed high-resolution aeromagnetic anomaly map with approximate boundaries of the batholith phases (dashed lines); data provided by Cominco Ltd. A distinct low anomaly is associated with the Bethsaida phase (BTS), which hosts some of the most important mineral deposits; other abbreviations as in Figure 4. b) Predicted aeromagnetic anomaly map from the 3-D inversion. Outlines A, B and C are the surface projections of the low susceptibility anomalies identified by the same letters at z = 2000 m in (c). c) Depth slices from the 3-D inversion results. One of the active mining sites lies on top of the distinct low susceptibility anomaly shown with the arrow (event A). Events B and C identify two similar anomalies that have not been explored for mineralization. From Roy and Clowes (2000).

chemical precipitation in the waning stages of hydrothermal activity during volcanic quiescence (Calvert et al. 2003; Genna et al. 2014).

Two high-resolution Lithoprobe seismic reflection lines were acquired on the southwest flank of the Galinée anticline near known VMS deposits. The first, Line 29–3, was recorded in 1990, prior to the discovery of the Bell Allard deposit (location in Fig. 7). Its objective was to map the contact between the mafic Wabassee Group and the felsic Watson Lake Group from a known deposit (Orchan) westward to and across the Daniel fault to an area where no borehole information was available (Fig. 7; Adam et al. 1998). The second profile, Line 93A, was acquired in 1993 above the Bell Allard deposit, discovered in 1992 at depths between 900 and 1150 m, prior to any mine development (location in Fig. 7). Its objective was to test the possibility of directly detecting deep volcanogenic massive sulphide ore bodies using seismic reflection technology.

Part of the rationale for carrying out such tests results from physical property measurements of rocks and downhole logging. Boreholes in mining camps are continuously cored for assaying as well as for deployment of wireline logging tools. For the tests within the Lithoprobe umbrella, the Geological Survey of Canada carried out laboratory high pressure meas-

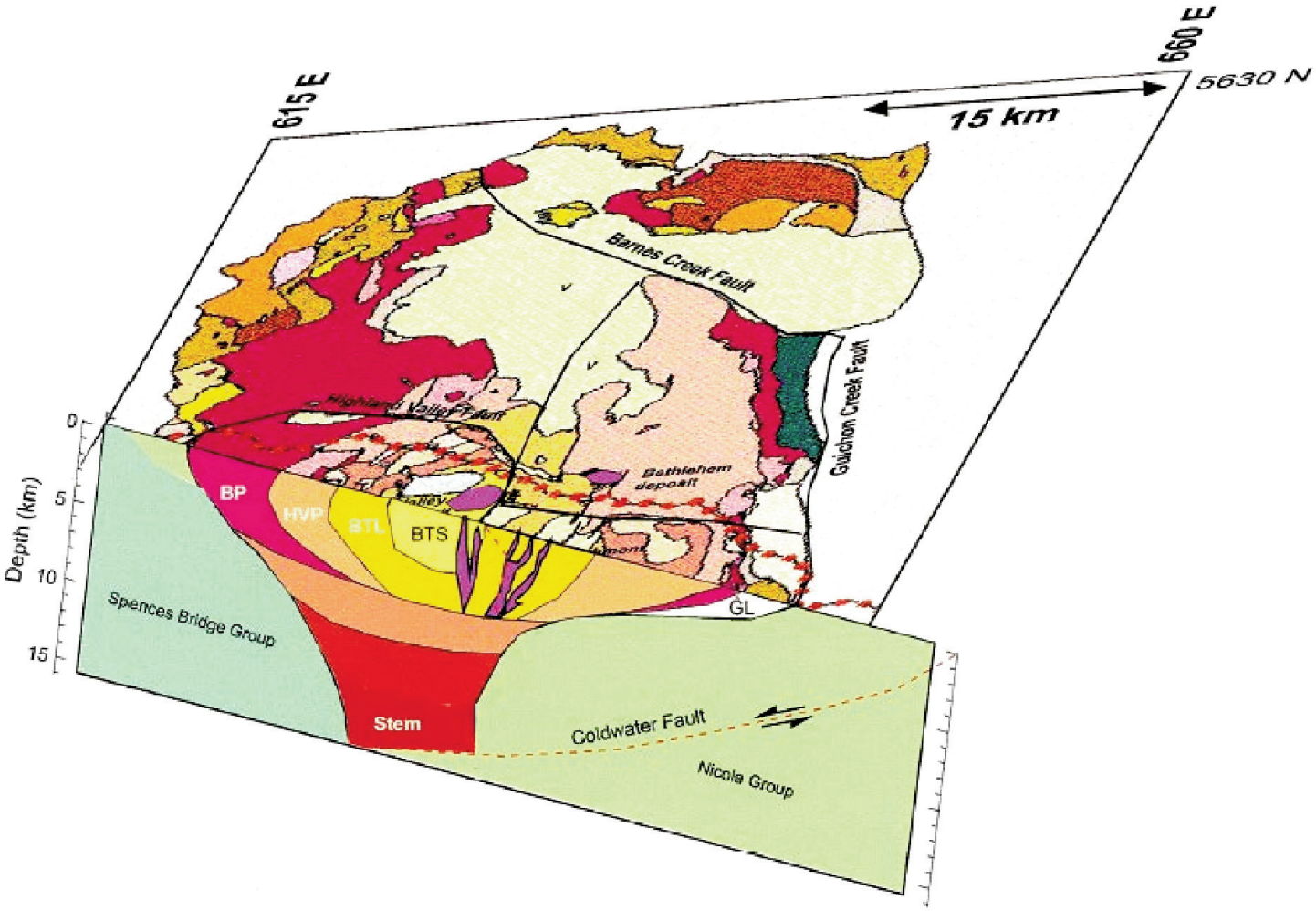

Figure 6. 2-D schematic cross-sectional model of the Guichon Creek batholith based on seismic and potential field studies tied to surface geology shown on top face. Purple 'stringers' on the cross-section and small areas on the map identify mineral deposits. Batholith phases: BP, Border; BTL, Bethlehem; BTS, Bethsaida; GL, Gump Lake; HVP, Highland Valley. From Roy and Clowes (2000).

urements of density, *P*-wave velocity and *S*-wave velocity on core samples of different lithologies, and undertook borehole logging for comparisons with the laboratory measurements (e.g. Salisbury et al. 1996, 2003). Results demonstrated that the sulphide minerals of interest exhibit anomalous density and seismic *P*-wave values relative to the host rocks and thus are suitable for generating seismic reflections. Figure 9 shows logging results for borehole BAS–95–4 located near the Bell Allard deposit and just 130 m east of Line 93A (Fig. 7). The logs show the presence of gabbro sills within a primarily basaltic volcanic stratigraphy in the upper part of the drill hole but in the lower part there is no gabbro and the stratigraphy comprises alternating layers of basalt and rhyolite. A thin layer of Key tuffite is identified at about 550 m depth. The synthetic seismogram calculated from the density and velocity values indicates that the strongest reflections probably originate from the gabbro contacts and some, but not all, of the basalt–rhyolite contacts (Calvert and Li 1999). The Key tuffite layer is too thin to generate a seismic reflection.

Figure 10a shows the seismic reflection section for Line 93A; the lithological identification, based on correlations of the borehole lithologies with the seismic section, is overlain (Calvert and Li 1999). The Key tuffite horizon (KT), which is too thin to be imaged by the frequencies prevalent in the seismic survey, is the contact between the mainly basaltic Wabassee Group and the largely rhyolitic Watson Lake Group. The associated reflectivity is likely due to the basalt–rhyolite contrast. The strongest reflections are associated with the gabbro sills and the Dumagami rhyolite (DR) within the lower Wabassee Group. The top of the Bell River intrusive complex may have been imaged (dark blue lines). Faulting is identified by discontinuities in the observed seismic reflections (red lines).

Figure 10b shows an enlargement of part of the data from Figure 10a; a geological section based on drillhole information (after Adam et al. 1997) is overlain. A strong reflection is associated with the top of the Bell Allard ore body, but this reflection is no different in amplitude than those from the gabbro sills. Thus, direct detection of the ore body from the seismic section would be difficult if its location were not already known, as is the case here. Nevertheless, structural characteristics that can be tied to lithologies from boreholes and logs are

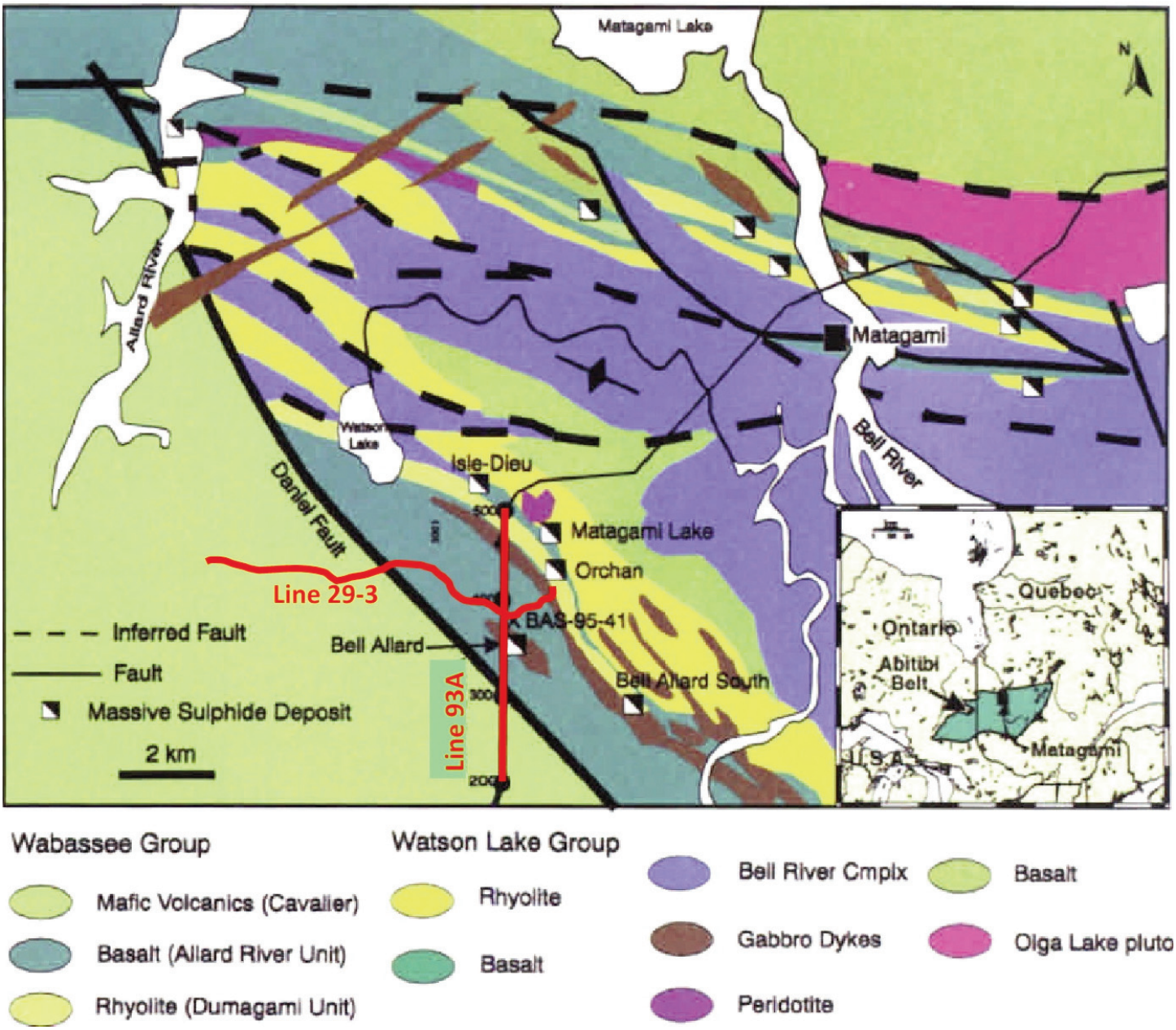

Figure 7. Geological map of the Matagami mining camp (location no. 2 in Fig. 1) showing main lithological units, seismic reflection lines 29-3 and 93A (shot point numbers are indicated), locations of main sulphide deposits, and location of borehole BAS 95-41 for which logging results are shown in Figure 9. The Bell Allard deposit lies almost directly below the highway along which the seismic line was recorded. The inset shows the general location of Matagami and the Abitibi greenstone belt in Ontario and Quebec.

well identified. Additional seismic studies, vertical seismic profiling (VSP) carried out at the Bell Allard deposit (and other mining camps as well), reveal that the strongest reflections generally do originate from the ore bodies and the basalt–rhyolite contacts are generally weaker (Adam et al. 1996).

Two-dimensional (2-D) seismic reflection surveys were shown to be limited in their applicability for ore deposit exploration so a number of mining companies and the Geological Survey of Canada, as an outgrowth of Lithoprobe studies, have tested 3-D reflection surveys at a few sites for the purpose of direct detection of massive sulphide ore bodies. One of these was at the Bell Allard deposit (Adam et al. 2003); another was at a site in the Sudbury, Ontario mining district (described in a subsequent section; Milkereit et al. 1997). Because typical ore bodies are comparable in size to the dominant wavelengths of a seismic survey, they tend to scatter, not reflect, seismic energy. Studies of the 3-D volume of seismic energy generated from these 3-D seismic surveys have demonstrated that the scattered energy from an ore body can be detected and the ore body identified. Indeed, a study in the Bathurst, New Brunswick mining camp represented the first discovery of a VMS deposit using 3-D seismic reflection methods, although the deposit was determined to be too rich in pyrite to be economically viable (Matthews et al. 2002).

https://doi.org/10.12789/geocanj.2017.44.125

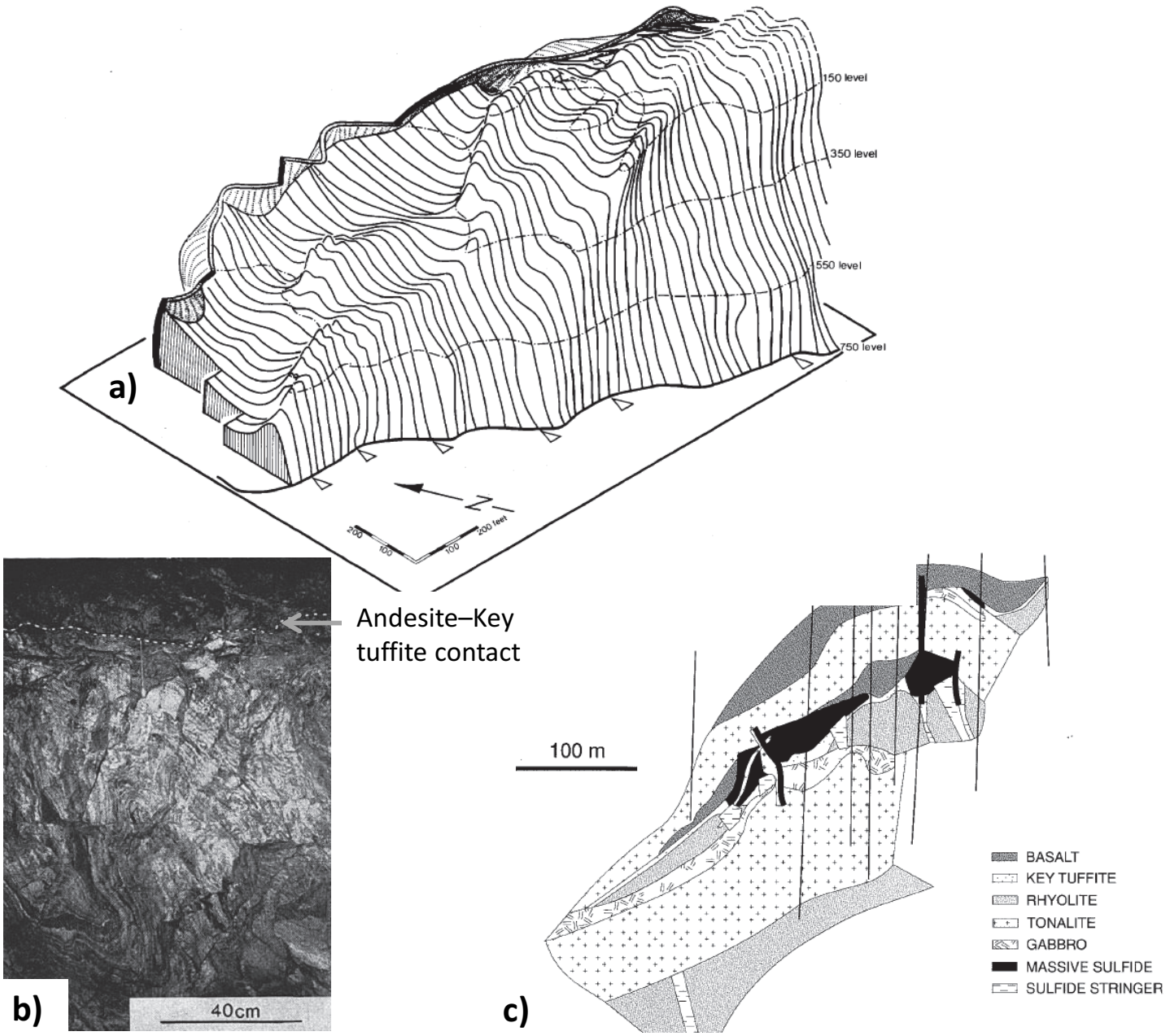

Figure 8. a) Orthographic projection of the andesite–Key tuffite surface for the Matagami Lake deposit just north of the Bell Allard deposit (location in Fig. 7) based on studies at various levels (numbers are in feet) within the mine. Fold terminates to the northwest against the south edge of a peridotite intrusive body. Gabbro dyke not shown. Surface projected above level of erosion is shown with dashed lines; from Roberts (1975). b) Slab photo of an underground exposure of the andesite–Key tuffite contact near the closure of a large fold; from Roberts (1975). c) Geological cross-section (no vertical exaggeration) of the Isle Dieu deposit located to the north of the Bell Allard deposit (location in Fig. 7). With the exception of the large tonalite intrusion, this deposit is typical of those found on the southern flank of the Bell River complex, being located at the contact of the basaltic Wabassee and deeper rhyolitic Watson Lake groups. Massive sulphide lenses are located above stringers of mineralization that likely represent conduits along which mineral-bearing fluids once flowed. From Calvert et al. (2003).

NICKEL DEPOSITS, THOMPSON BELT, MANITOBA

The Thompson belt forms the northwestern margin of the Archean Superior craton, often referred to as the Superior boundary zone, and constitutes a tectonic foreland on the eastern side of the ca. 1800 Ma Trans-Hudson Orogen (THO; no. 3 on Fig. 1; Fig. 11a). Its boundary with the Reindeer zone to the west, the internides of the THO, is the Superior Boundary fault. In contrast, its eastern limit is an irregular, poorly defined transition zone within which the main east-west structural trend of the Superior craton is progressively reworked into the northeast-southwest trend of the belt and the Archean granulite–amphibolite facies rocks of the Pikwitonei belt are retrogressed to Proterozoic amphibolite facies (e.g. Bleeker 1990). Within the Thompson belt, world-class nickel deposits have been found and produced since the early 1960s. These occur along distinct stratigraphic horizons within the thin, highly metamorphosed and deformed Paleoproterozoic Ospwagan Group sedimentary sequence. As part of Lithoprobe's 1991

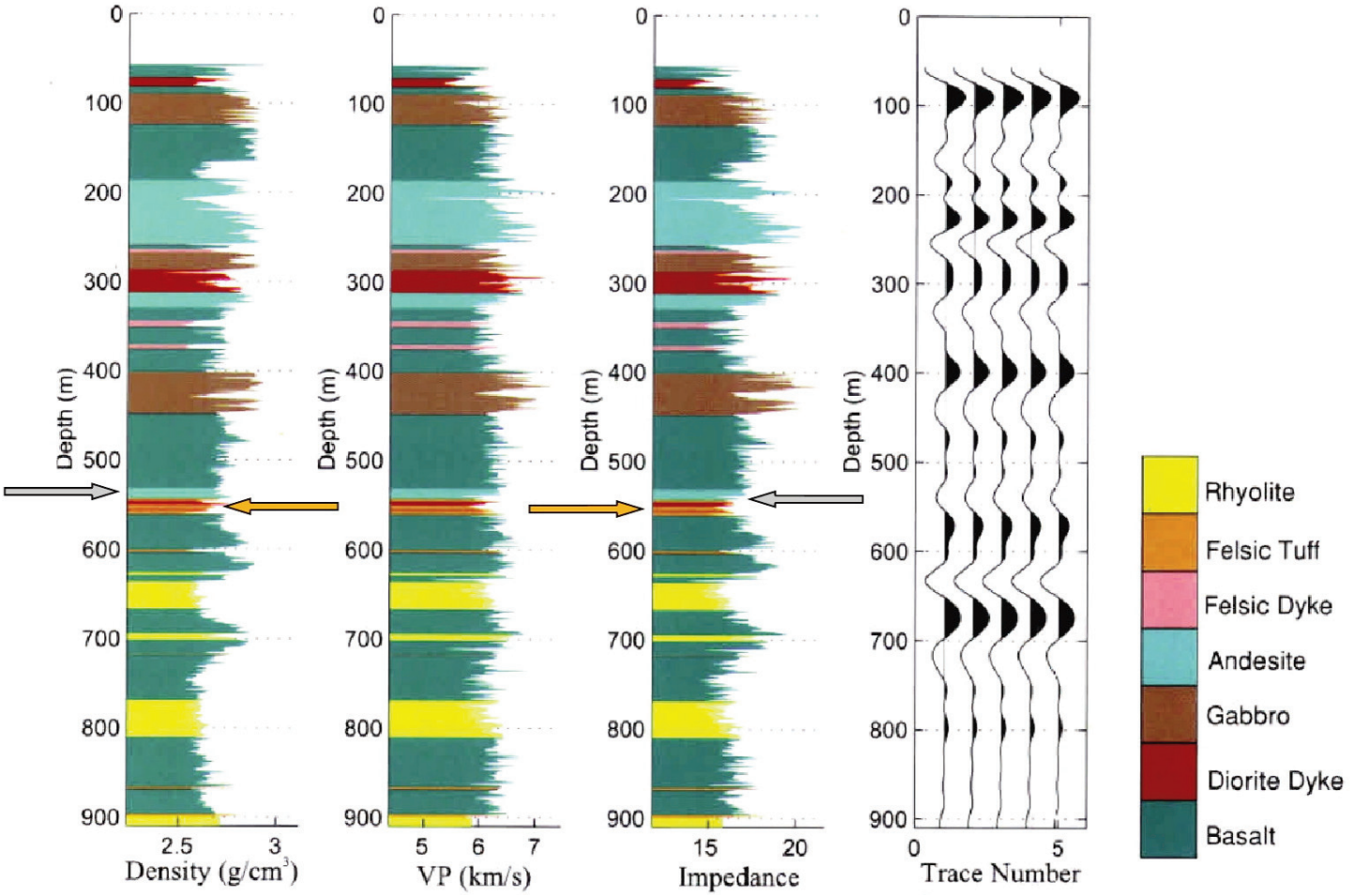

Figure 9. Density and *P*-wave sonic velocity logs from borehole BAS-95-41 coded by lithology (location in Fig. 7). The borehole extends through the gabbro sills and volcanic stratigraphy of the Wabassee Group and terminates at the upper contact of the rhyolitic Watson Lake Group. The primary reflections-only synthetic seismogram is calculated from the logs (velocity x density = impedance) using an Ormsby wavelet with corner frequencies of 25, 30, 100 and 110 Hz. Grey arrow, andesite; orange arrow, Key tuffite. From Calvert and Li (1999).

seismic reflection survey program in the THO, high resolution seismic line 1A was recorded on existing roads across the Ospwagan Group. The seismic data were complemented by a coincident electromagnetic (EM) survey that also included a profile perpendicular to the main line (Fig. 11b). The combined seismic/EM profile across the Ospwagan Group and its association with the local geology is the focus of this section.

The Ospwagan group lies unconformably on Archean basement gneiss of the Superior Province, although an early (>1880 Ma) deformation event resulted in some basement gneiss being overturned during the deformation and thus overlying the Ospwagan Group (Fig. 12). The latter includes a sequence of five metasedimentary and metavolcanic units and associated ultramafic intrusive bodies, and volcanic rocks (Bleeker 1990; Fig. 12a). Stratigraphically, the Manasan, Thompson and Pipe formations form the lower units and make up a detrital-chemical sequence representing sedimentation on a stable platform. The upper two units, the turbiditic Setting Formation and the mafic–ultramafic Bah Lake assemblage, were formed in a tectonically active setting. Mafic–ultramafic intrusive sills located at the level of the Pipe Formation host the main nickel deposit but other intrusions are present up to the middle of the Setting Formation (Machado et al. 2011). The Grass River Group (Fig. 12a) is a detrital sequence composed of a lower unit deposited in a fluvial–alluvial environment and an upper one that grades westward into the Burntwood Group of the Kisseynew domain in the Reindeer zone. Figure 12b shows a schematic cross-section representing the Archean basement gneiss and the Ospwagan Group, highlighting the mafic–ultramafic intrusive units (peridotite) associated with the major nickel deposits and mines.

The seismic reflection and EM surveys were acquired to help constrain the interpretation of subsurface geological structures since subsurface mapping of the ore-hosting Ospwagan Group is important for exploration in the Thompson belt. They represent complementary approaches. The seismic reflection method provides small-scale (10–100 m) detail of velocity–density variations and is well-suited for imaging geological features with shallow to moderate dips. The controlled source electromagnetic method typically enables imaging of resistivity anomalies that have dimensions comparable to their depth (100–1000 m) and are best suited for imaging near-vertical features.

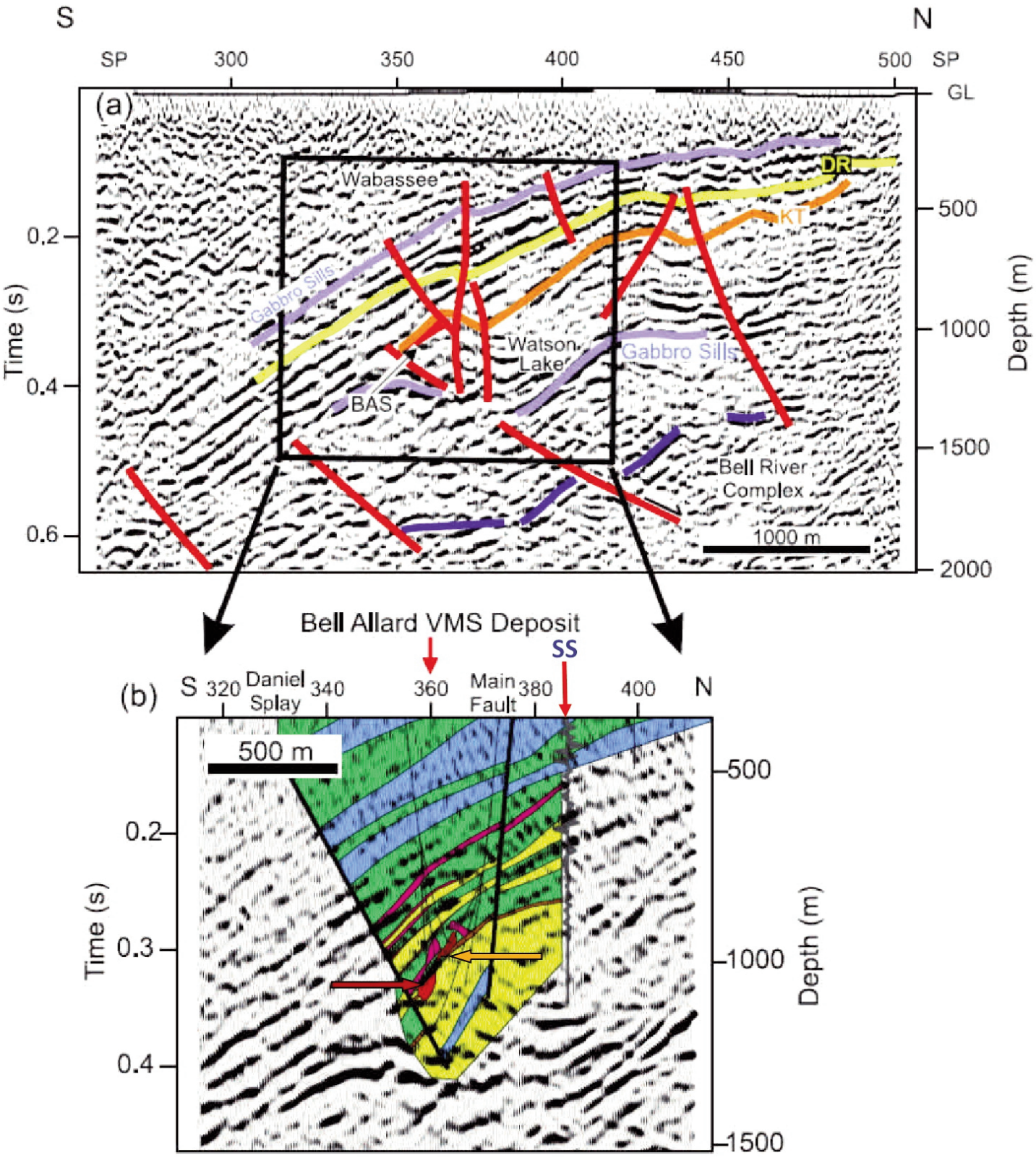

Figure 10. a) Pre-stack migrated seismic reflection section with interpretation overlain. Strong reflections are associated with gabbro sills and interlayered rhyolite and basalt within the lower Wabassee Group. BAS, Bell Allard sulphide deposit; DR, Dumagami rhyolite; KT, Key tuffite. Red lines identify faults; dark blue lines show top of Bell River complex. b) Enlargement of seismic data from a) onto which a simplified geological section through the Bell Allard deposit (after Adam et al. 1997) and the synthetic seismogram (SS) from the logs in borehole BAS-95-41 (Fig. 9) are superimposed. Thin lines show boreholes. Colours for the geological section: blue, gabbro; green, basalt; magenta, felsic tuff or dyke; red, sulphide mineralization; yellow, rhyolite; brown, mafic-intermediate dyke. Red arrow, Bell Allard deposit; orange arrow, Key tuffite. From Adam et al. (2000); modified from Calvert and Li (1999).

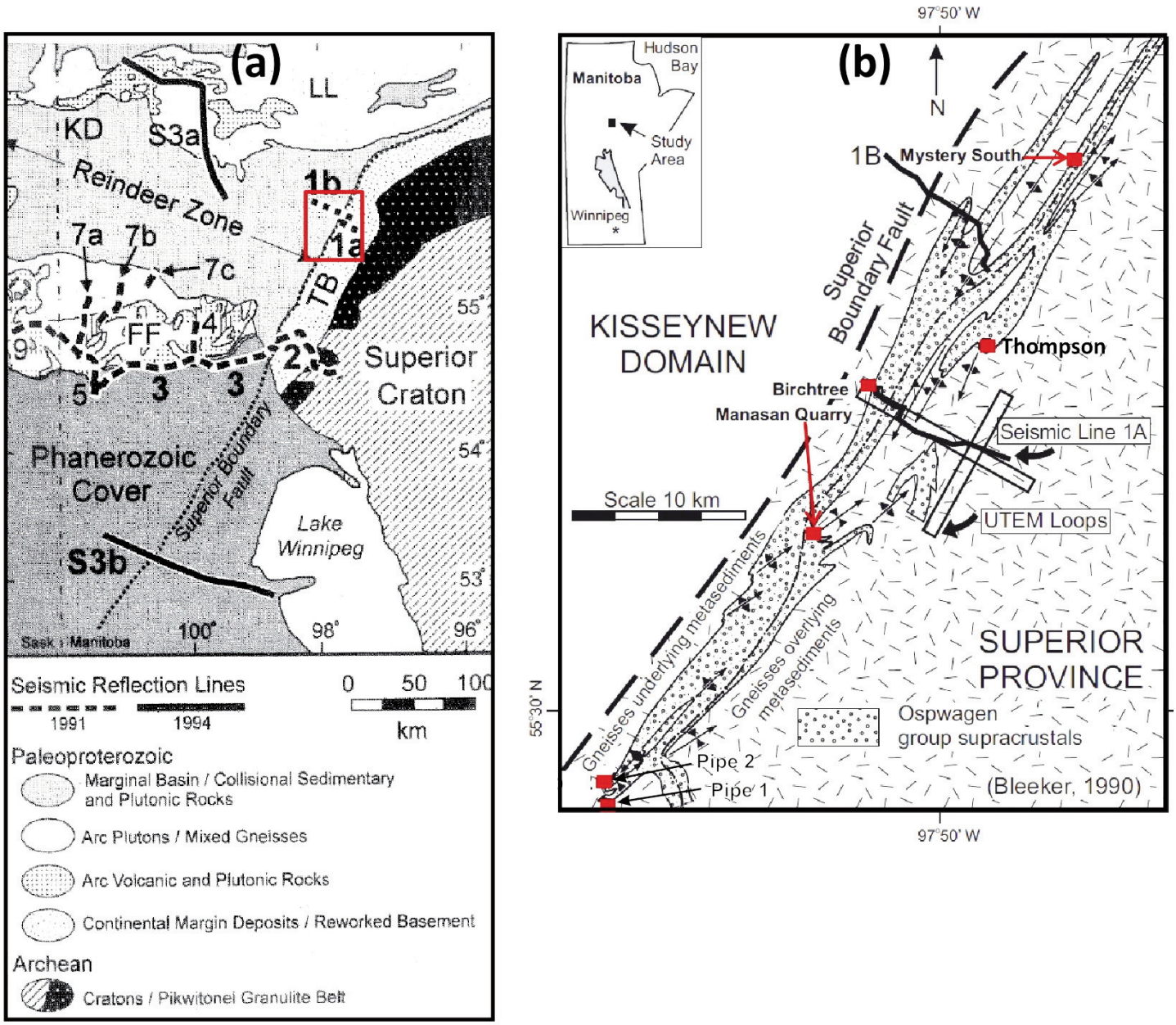

Figure 11. a) Simplified geological map of the eastern part of the Trans-Hudson Orogen (Reindeer zone) and Thompson belt (TB) showing locations of seismic reflection profiles. The red box shows the area of Figure 11b. FF, Flin Flon belt; KD, Kisseynew domain; LL, Lynn Lake belt. From Clowes (2001). b) Geological map showing location of reflection lines 1A and 1B and the electromagnetic profiles (UTEM loops), as well as the mapped occurrences of the Ospwagan Group. The gneiss is reworked Archean basement; Kisseynew domain comprises high-grade metaturbidite. Mines are named and indicated by small red squares. Base map from Bleeker (1990). Inset shows location of map in Maniboba. Modified from Eaton et al. (2010).

To be most effective, both methods can benefit from rock property measurements. Within the Thompson area, compressional wave velocities (V_p) and density measurements were made on a small suite of rock samples to assess the reflectivity of the various lithologic units (Fig. 13a; White et al. 2000). The reflectivity is controlled by variations in seismic impedance (Z, the product of velocity and density); good reflections arise from rock units or features (such as alteration zones, brittle faults or mylonite zones) with strongly contrasting impedances. From Figure 13a, we note that relatively high Z values arise from amphibolite, iron formation, pyroxenite and sulphide ore compared with other lithologies. In general, sulphide densities are uniformly high such that the seismic impedance of sulphide bodies, if present in sufficient quantity, enables them to be readily imaged (Salisbury et al. 1996, 2003). Characterization of the reflectivity of the subsurface through knowledge of the thickness, juxtaposition sequence and lateral extent of lithologies and subsequent generation of synthetic seismograms to provide guides for expected results are helpful aids for interpretation. In the Thompson area, borehole geological logs were available. By using the laboratory-measured velocities and densities in conjunction with these logs, simulat-

https://doi.org/10.12789/geocanj.2017.44.125

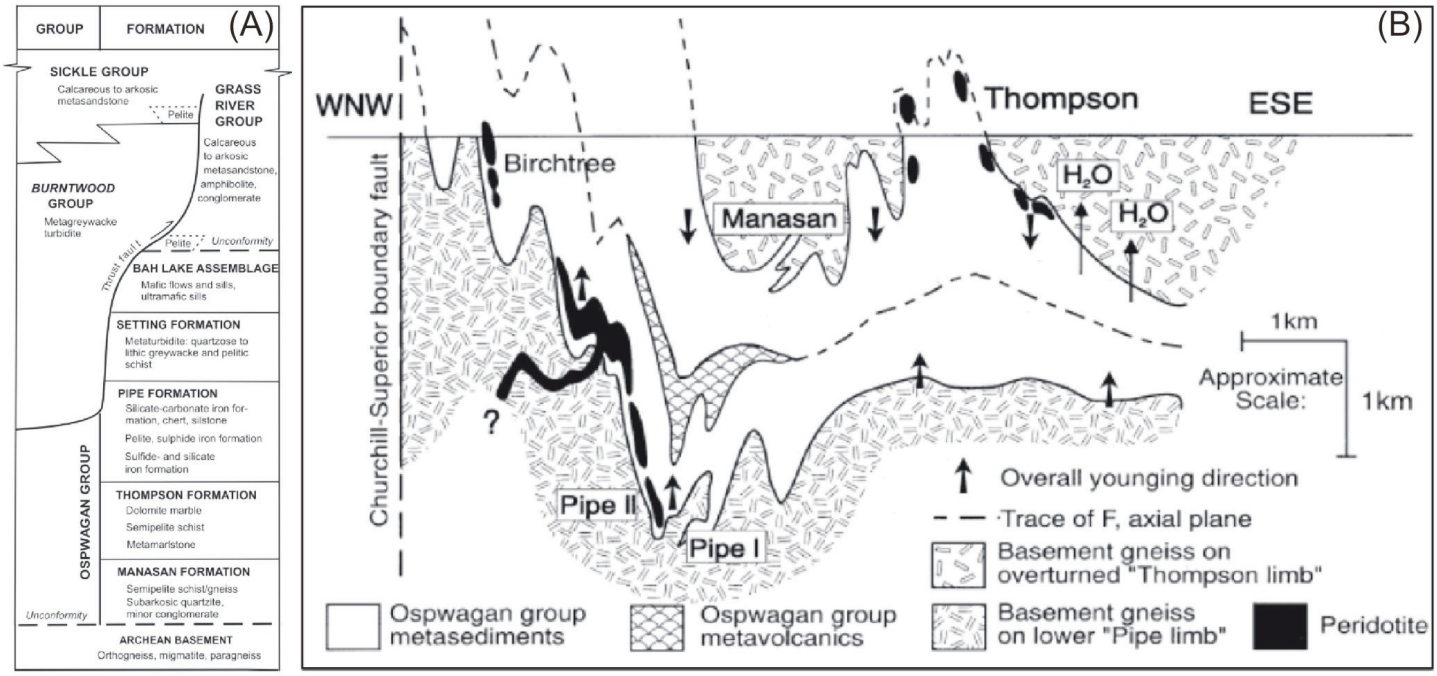

Figure 12. a) Lithostratigraphic succession of supracrustal rocks in the Thompson belt and adjacent part of the Kisseynew domain (Burntwood and Sickle groups), from Rayner et al. (2006). b) Schematic vertical depth section through the Thompson nappe structure, showing the structural positions of nickel mines, associated with the peridotite bodies, identified in Figure 11b. F1 refers to an early (>1880 Ma) deformation event that resulted in the formation of the Thompson nappe. From White et al. (2000); after Bleeker (1990).

ed seismic responses were calculated to provide guides for interpretation of the seismic data (White et al. 2000)

Similarly, rock property measurements have been shown to aid in the interpretation of EM data. Figure 13b shows resistivity and porosity measurements made on samples of various lithologies from the Thompson area (White et al. 2000). Serpentinite and peridotite are highly conductive (low resistivity) and porous, dolomite and quartzite are moderately conductive, whereas amphibolite, biotite schist, schist and orthogneiss are more resistive and show little porosity. Thus, the known conductive groups are part of the Ospwagan Group. The resistive host rocks allow for deep penetration of the EM field because they cause limited attenuation of the field. Combining this characteristic with Ospwagan Group rocks being associated with higher conductivity indicates that EM mapping methods should be capable of delineating the subsurface extent of the supracrustal rocks, a key objective of the study.

Figure 14 shows a composite of the seismic reflection and electromagnetic images with interpretation lines superimposed (White et al. 2000). Both the seismic and EM images change significantly across the Burntwood lineament, a known steep structural zone. To the west of the lineament, the poor seismic image is due to lithologic contacts with steep dips and the resistivity image is compromised at depth by the presence of strong, shallow conductors associated with an iron formation that is part of the supracrustal units, both known from borehole information. The interpretation superimposed is based on borehole information. To the east of the lineament, the combined image indicates that the rocks of the prospective Ospwagan Group (low resistivity) extend southeastward beneath the Archean gneiss and that structural culminations control the subsurface geometry of the Ospwagan Group (e.g. the Owl Lake antiform). The bottom limb of the nappe, occurring within a reflective zone below the antiform, is inferred on the basis of the thickness of Ospwagan Group rocks in the vicinity of the Birchtree mine (location on Fig. 11b). Within the highly resistive rocks at depths less than 1000 m at the eastern end, a mapped basement antiform east of the Grass River lineament appears to have been imaged within the hanging wall of the easternmost of the three major faults.

Results from the combined seismic reflection and EM study, aided by rock property measurements, borehole logs and correlation of the geophysical images with mapped surface geology, indicate that such methods can be effective in determining the subsurface configuration of the nickel ore-bearing supracrustal Ospwagan Group. The latter should generally be more seismically reflective and electrically conductive than Archean gneiss that surrounds them in fold interference structures (White et al. 2000).

MORE NICKEL DEPOSITS, SUDBURY STRUCTURE, ONTARIO

The Sudbury Structure is situated in the southernmost part of the Archean Superior Province in Ontario, near the junction of the Superior Province with the Paleoproterozoic Huronian supracrustal rocks of the Southern Province and the Mesoproterozoic rocks of the southwestern Grenville Province (no. 4, Fig. 1). Sudbury Structure is a collective term that is defined to include the elliptically shaped Sudbury Igneous Complex (SIC), the Sudbury Basin that is enclosed by the SIC and the brecciated country rocks of the Superior and Southern provinces that surround the SIC (Fig. 15; Giblin 1984). Sud-

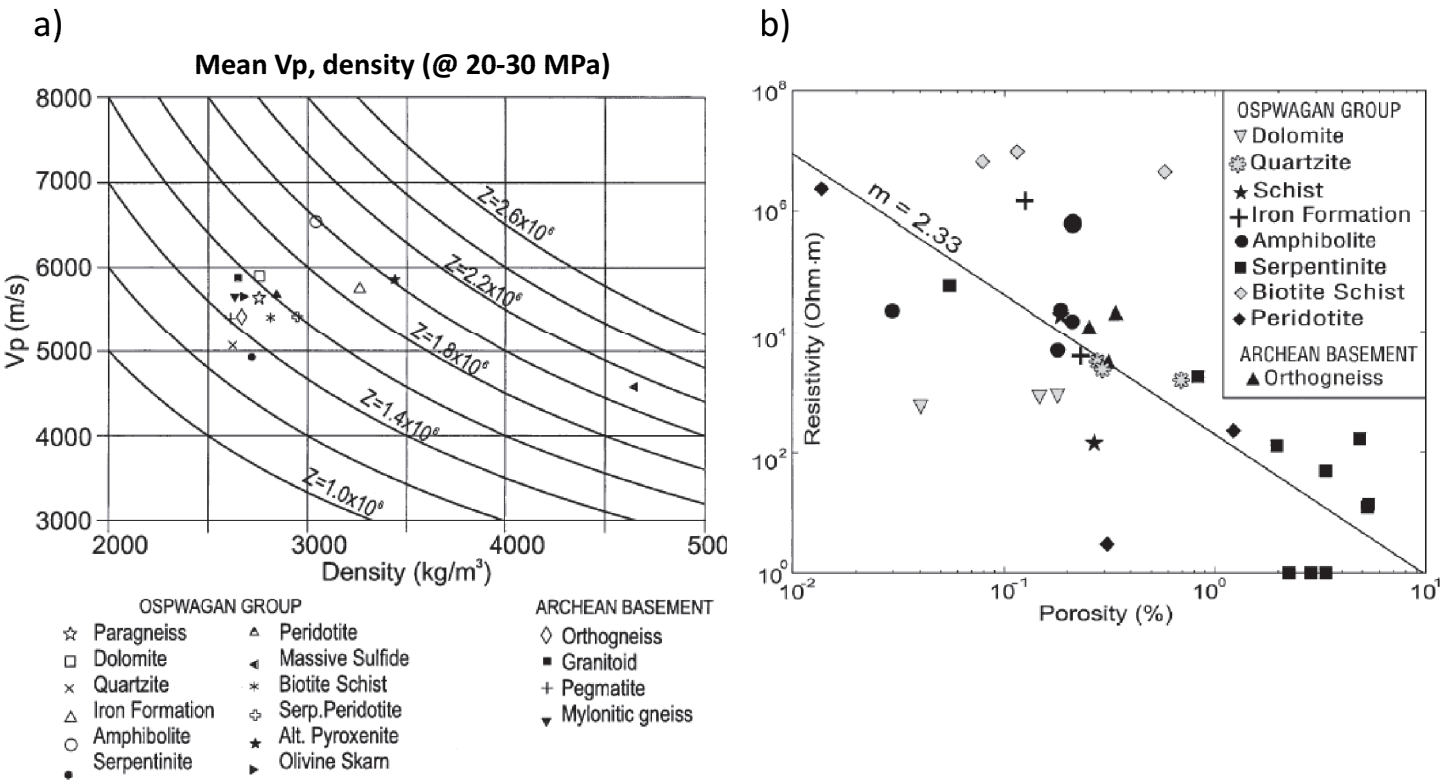

Figure 13. a) Mean *P*-wave velocities (V_p) and densities for a suite of rocks from the Thompson area. The solid curves indicate lines of constant acoustic impedance (product of V_p and density with units of kg/m^2 s). The V_p and density values for the massive sulphide are for a pyrrhotite-rich sample from Sudbury because no measurements were available for such sulphide rocks from the Thompson area. From White et al. (2000). b) The log of resistivity versus the log of porosity for a suite of samples provided by Inco Ltd., Exploration. These rock property results were used to facilitate the interpretation of conductivity in terms of ionic transport (i.e. via fluids) versus electronic conductors (i.e. metals and semiconductors). From White et al. (2000).

bury is famous for its nickel deposits that are the largest in the world (Naldrett 1999); mining has been active in the region for more than a century. Sudbury is also famous now as the site of a catastrophic meteorite impact, dated at 1850 Ma (Krogh et al. 1984), with the crater estimated at > 200 km across, probably one of the largest known impact structures in the world (Grieve et al. 1991). The meteorite generated an impact melt sheet within which the nickel deposits formed. However, this interpretation has only been extant since 1964 when Dietz (1964) recognized shock-metamorphic features characteristic of an impact origin; subsequent work has established this interpretation (e.g. Grieve et al. 1991).

Lithoprobe became involved in studies of the Sudbury Structure as part of its Abitibi–Grenville transect (see Ludden and Hynes 2000) to provide additional constraints and information to help reconcile some of the enigmas and apparent contradictions surrounding studies of the structure (Boerner et al. 2000) and to develop more effective geophysical techniques to locate new deposits to depths of at least 2500 m, a typical depth limit for modern mining methods. A comprehensive geologic knowledge base existed as a result of the lengthy mining history in the Sudbury area. Lithoprobe's interest centred on the SIC although some regional work provided constraints on the structure as a whole. As with other Lithoprobe programs, seismic reflection surveys formed the basis of the studies and set the framework within which subsequent geological interpretations were made. However, an expanded database of physical rock properties and multiple borehole logging experiments helped constrain the interpretation of seismic, electromagnetic, gravity and magnetic data, thereby contributing to the regional synthesis of geological and geophysical data. In this section, I emphasize results along the two-dimensional lines 41 and 40 (Fig. 15). These and related studies were sufficiently encouraging that the two mining companies involved, Inco Ltd. (now Vale Canada Ltd.) and Falconbridge Ltd (now Glencore plc.), and the Geological Survey of Canada funded a feasibility 3-D seismic survey (Trill), the results of which I also summarize.

Geological Background

As a result of its importance for the mining industry (Lightfoot 2016), the Sudbury area has had many years of geological mapping. Dressler (1984), collections edited by Pye et al. (1984) and Lightfoot and Naldrett (1994), including references within them, and a monograph by Lightfoot (2016) provide good introductions and extensive information relating to the area. Focusing on aspects relevant to the Lithoprobe studies, the Sudbury Structure developed as the product of four primary events: 1) establishment of structures within the Archean crust that became the foreland to subsequent orogenies; 2) construction of the Huronian margin; 3) the meteorite impact event; and 4) post-impact deformation (Boerner et al. 2000).

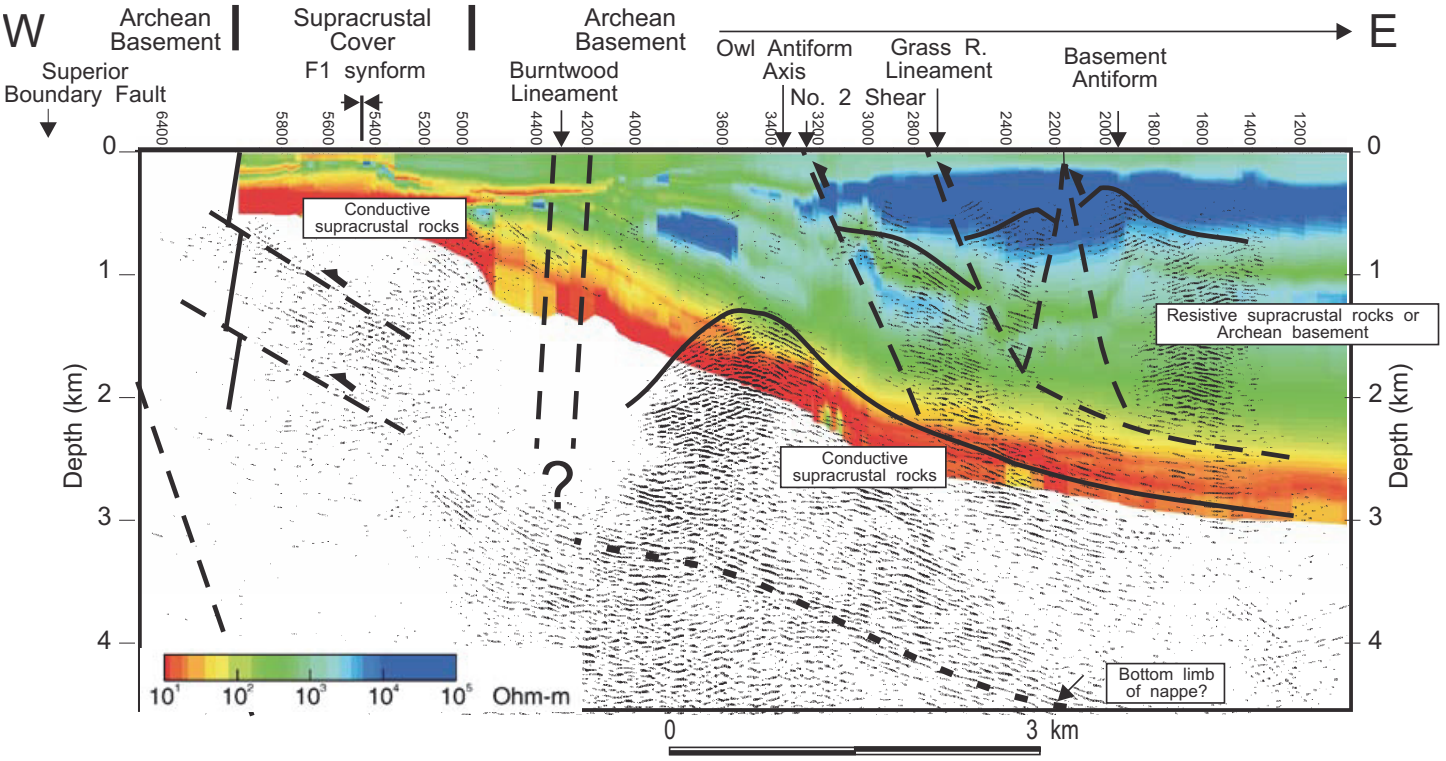

Figure 14. Migrated seismic reflection data for line 1A (Fig. 11b) overlying the colour resistivity versus depth image for the coincident electromagnetic (EM) profile with interpretation. Geological features along the profile are noted above the image. Numbers identify vibration-point stations. From White et al. (2000).

Within the Archean part of the geology, the Levack gneiss, which crystallized around 2710 Ma (James et al. 1992), forms the footwall to the north range of the Sudbury Igneous Complex (SIC) and is juxtaposed against the Cartier granite, which is about 70 m.y. younger (Meldrum et al. 1997; Fig. 15). Uplift of the Levack gneiss, a phase of the evolution of the southern margin of the Superior Province, initiated about 2660–2630 Ma (Wodicka and Card 1995) and is important as a potential source of contaminants for the SIC (e.g. Grieve et al. 1991). Following the uplift, mafic volcanism at the base of the Huronian stratigraphy marks the initial stages of continental rifting. Subsequent sedimentation into the topographical depressions, ending prior to 2200 Ma based on cross-cutting Nipissing dykes, formed the Huronian Supergroup. The region then had a 300 m.y. period of tectonic quiescence prior to experiencing distal effects of the Penokean orogeny.

The Sudbury Igneous Complex (SIC) is a product of crustal melting associated with the meteorite impact at 1850 Ma. As with other impact structures (e.g. Manicouagan in Quebec, Grieve and Head 1983; Haughton on Devon Island, Nunavut, Osinski et al. 2005), the Sudbury Structure was circular when formed but was subsequently altered in its dimensions and shape by post-impact tectonic activity; Figure 16 shows a generalized cross section of the structure prior to deformation. When the impact occurred, the target rocks included both Archean and Huronian units. The source of the metals was likely mafic rocks of the ca. 2.4 Ga East Bull Lake Intrusive Suite (Lightfoot 2016). The melt sheet was a pool of molten rock, magma, up to 2.5 km thick that flooded a large area. As the magma cooled and solidified, different minerals crystallized at different stages, forming different rock types. The mafic minerals crystallized first, forming initially the mafic rock norite (Fig. 17a), and then gabbro; felsic minerals crystallized later and formed the granitic rocks of the SIC (Fig. 17b). Because the ore minerals were heavier, they settled in depressions at the base of the norite layer, which is called the norite sublayer (Fig. 16 legend). Melt-mixing models (Grieve et al. 1991) and geochemical studies of the SIC (Ostermann and Deutsch 1997) provide strong evidence that these SIC rock types are best described by *in situ* differentiation without any need for upper mantle contributions.

The force of the meteorite impact also strongly affected rocks in the Huronian Supergroup, forming shock metamorphic features that are diagnostic of the impact, the most visible of which are shatter cones (Fig. 17c). Post-impact sedimentary rocks, the Whitewater Group, formed within the depression created by the impact and are completely encircled by the SIC (Figs. 15 and 16). The base of the Whitewater Group, the Onaping Formation, was deposited almost instantaneously following the impact (Ames et al. 1998) whereas the Onwatin and Chelmsford groups probably were deposited within a 6 m.y. period following impact (Cowan and Schwerdtner 1994).

Rock Properties and Borehole Logging

Fundamental to the successful interpretation of Sudbury Structure geophysical data, in addition to the geological studies, were results from *in situ* logging and physical rock property measurements. Composite logs from bore holes in the North

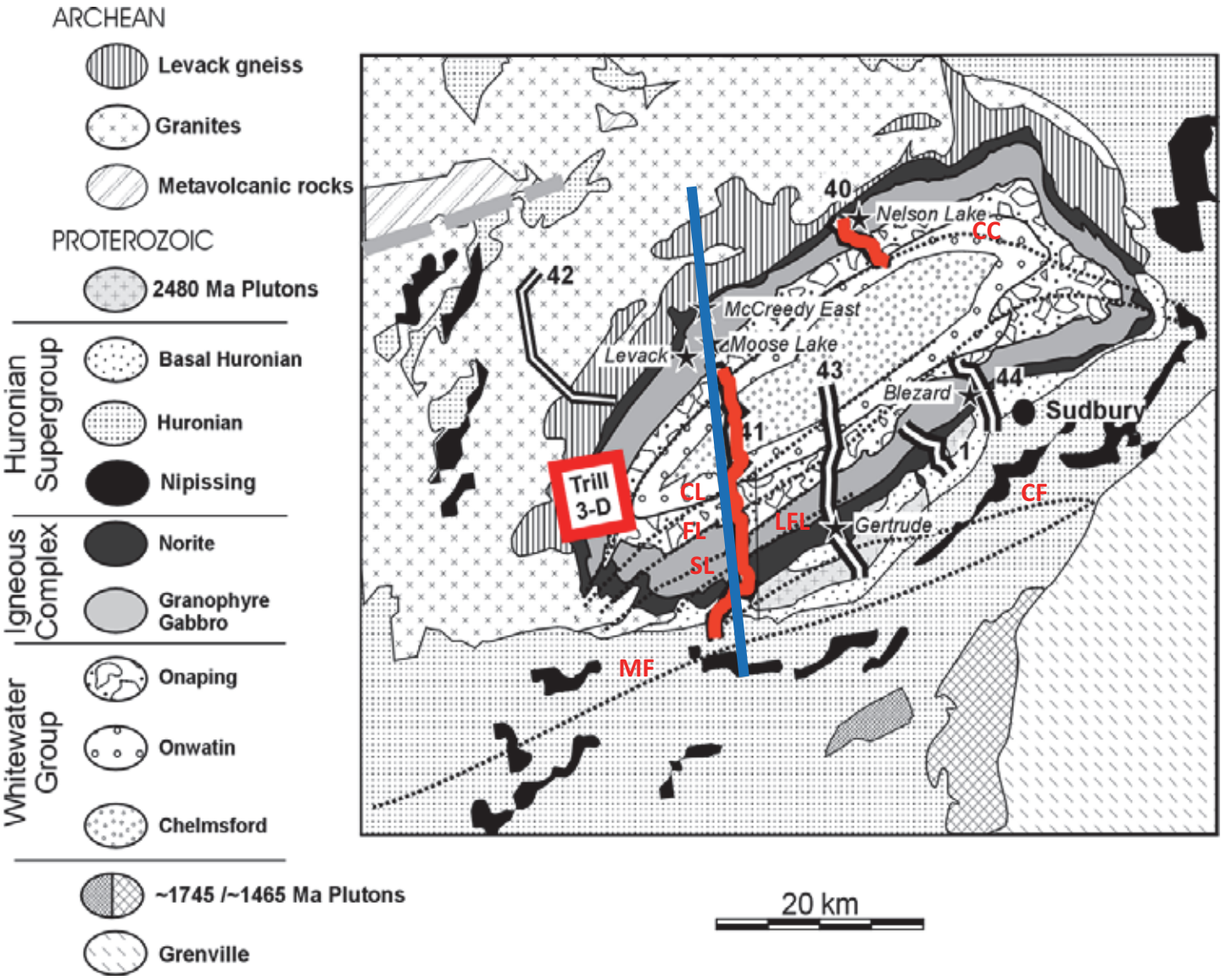

Figure 15. Geology in the region of the Sudbury Structure. Double lines with numbers are locations of reflection profiles; lines 40 and 41 highlighted in red. 'Trill 3-D' is the location of the 3-D reflection survey. Geophysical logs were recorded at borehole locations; named and indicated by stars. Blue line shows approximate location of gravity and magnetic cross sections. Dotted lines show faults: CC, Cameron Creek; CF, Creighton; CL, Cameron Lake; FL, Fairbank Lake; LFL, Little Fairbank Lake; MF, Murray; SL, Skill Lake. In legend, 'Granites' includes the Cartier granite. Modified from Adam et al. (2000).

Range were generated to provide complete logging sections through all the major rock units of the Sudbury Structure (Fig. 18). These were supplemented by full waveform sonic logs and 3-component vertical seismic profiling (VSP) measurements to identify unequivocally the sources of reflection events from the seismic reflection profiles. In general, the highest seismic velocities and densities were found in the footwall breccia due to an overall increase in mafic mineral content. The lowest seismic velocities were in the lower felsic norite layer, although this layer showed an increase in density relative to the thicker felsic norite layer (Fig. 18). Within the norite sublayer, electrical resistivity decreased significantly (conductivity increased) and magnetic susceptibility increased significantly, relative to other rocks of the SIC (Fig. 18). Drill core samples made available by the mining companies enabled laboratory measurements of densities and compressional wave velocities (Fig. 18) that further aided interpretations of seismic, gravity and magnetic profiles.

Geophysical Data across the SIC

Two-dimensional seismic reflection data from lines 40 and 41 (Fig. 15; Wu et al. 1995) were compiled into a reflection profile across the Sudbury Structure and a composite interpretation was overlain (Fig. 19). The North Range interpretation is solidly based on borehole data and rock property measurements, enabling projection of the surface geology to depth, for example the SIC-footwall contact to ~9 km. However, the seismic data show that the symmetry that might be expected from an impact is not present; asymmetry is pronounced. This is the result of post-impact shortening that is manifest along a series

https://doi.org/10.12789/geocanj.2017.44.125

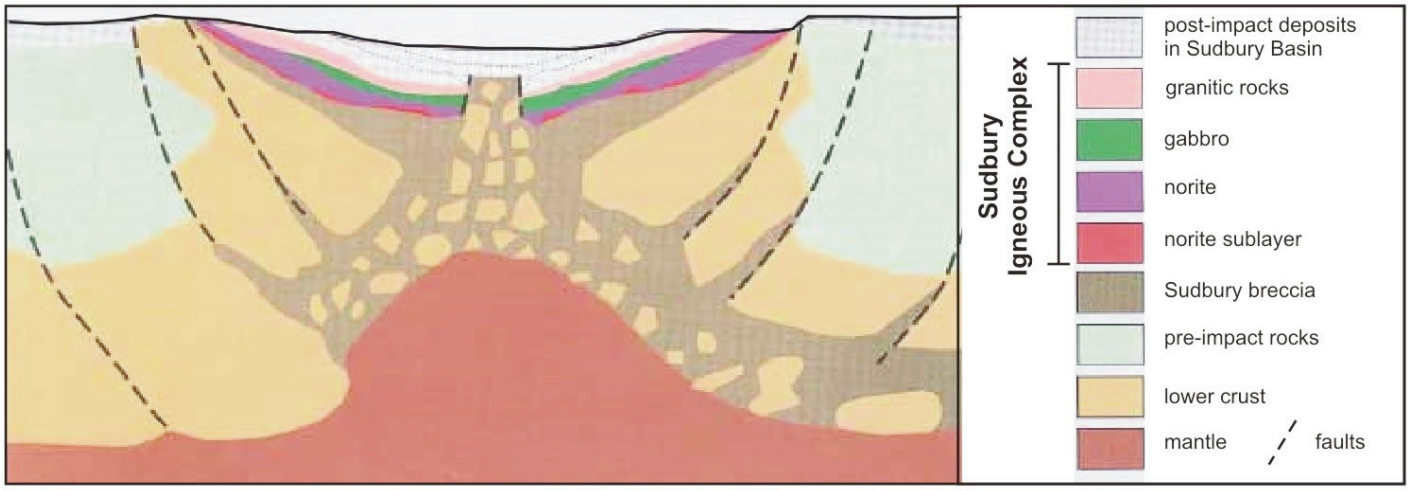

Figure 16. Generalized cross section of the Sudbury Structure following the impact event; legend on the right. Prepared, with permission, from Fensome et al. (2014).

of south-dipping reflections that represent zones of high shear strain rate, interpreted as thrust faults (Fig. 19; Boerner et al. 2000). Thus, most of the South Range of the SIC represents a north-vergent shear zone. This geometry is reinforced by electromagnetic studies that indicate a south-dipping conductive layer beneath the shear zone (Fig. 19; Boerner et al. 1994). The subsurface interpretation below the South Range shows that some of the stratigraphy is overturned, perhaps indicating positions where future deposits might be found.

Gravity data for the SIC and surrounding areas existed before the Lithoprobe studies, although some new data were acquired along the seismic lines. Using the newly interpreted seismic reflection images as a guide, McGrath and Broome (1994) showed that profile features along line 41 could be explained by defining lithological units based on the reflection interpretation and assigning these bodies the rock densities measured in the laboratory on exposed samples (Fig. 20a). Aeromagnetic and proprietary high-resolution magnetic data were also made available for Lithoprobe studies. These were supplemented by new measurements of magnetic susceptibility and natural remanent magnetization (NRM) from rock outcrops (Morris et al. 1992). Based on this information and the seismic structural interpretation, Hearst et al. (1994) were able to demonstrate that the observed magnetic field could be modelled with an appropriate assignment of susceptibilities and NRM (Fig. 20b). In the North Range, an enriched phase of the Levack gneiss complex, dykes and a depleted phase of the gneiss were interpreted. In the South Range, zones of hydrothermal mineralization (e.g. altered norite) and dykes could explain the magnetic signature. In both cases the seismic interpretation was fundamental to the potential field modelling.

TRILL 3-D Seismic Experiment

Based on the success of 2-D reflection profiling, numerous physical rock property studies in mining areas (e.g. Salisbury et al. 2003), borehole geophysical logging and forward modelling studies of seismic wave propagation, a decision was made in 1995 to conduct the first 3-D seismic survey for deep mineral exploration in Canada (Milkereit et al. 2000). The Trill area of the SIC (Fig. 15) was selected because a deep (1800 m) massive sulphide deposit had been discovered but not yet mined, thereby providing a target with relatively low background noise, since active mining infrastructure was not yet in place. A 3-D survey requires an areal distribution of sources and receivers; Figure 21a illustrates that used for the Trill experiment, is approximately 30 km^2. Extensive data processing is necessary to obtain the best quality seismic image. Borehole logs indicated that the lower contact of the SIC and associated footwall topography could be imaged. As shown by the vertical cross-section in Figure 21b, this prediction was justified. The norite sublayer and associated topography of the footwall complex are well imaged.

Typically, a massive sulphide deposit is not sufficiently large to generate a seismic reflection, even with its high impedance contrast with host rocks. This is the result of limitations in resolution of the method. However, such a deposit can generate scattered waves that have some coherency [think of a pebble dropped into a pond and the ensuing circular waves]. Modelling studies had validated that a local high impedance contrast (a dipping lens) at depth could generate observable scattered waves. Figure 21c summarizes the main results from the Trill 3-D study. The steeply dipping footwall contact, the location of the known mineralization and the associated seismic scattering response caused by the ore deposit are shown. The experiment was highly successful.

URANIUM DEPOSITS, ATHABASCA BASIN, NW SASKATCHEWAN

The Mesoproterozoic Athabasca Basin, located in northwestern Saskatchewan and northeastern Alberta (no. 5, Fig. 1), comprises an undeformed sedimentary sequence that unconformably overlies basement rocks of the Archean Hearne and Rae provinces. It is one of the world's most prolific producers of uranium from its characteristically high-grade unconformity-type deposits and is the only current uranium producer in

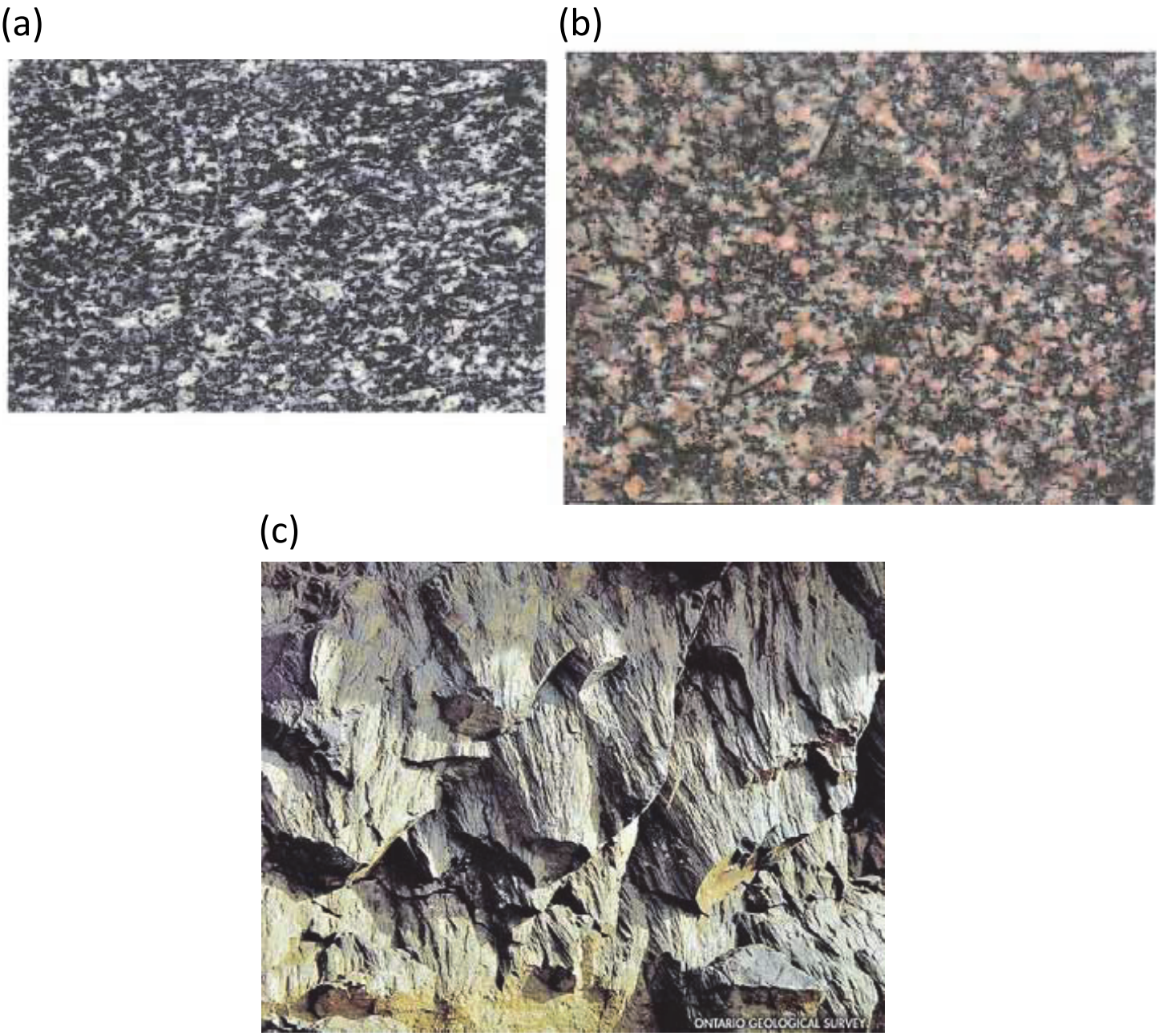

Figure 17. Photographs of rocks derived from the Sudbury Structure: a) lower noritic melt; b) upper granitic melt; c) shatter cones developed in Paleoproterozoic (Huronian) metasandstone. Prepared, with permission, from Fensome et al. (2014); a) and b) courtesy Tom Muir, Ontario Geological Survey; c) courtesy Ontario Geological Survey.

Canada. The eastern part of the basin, which includes most of the uranium mines, is underlain by the Mudjatik and Wollaston domains of the Hearne Province and the transition zone between them (Fig. 22). Archean granitic to granodioritic to tonalite orthogneiss units mainly comprise these domains. They are stratigraphically overlain by and structurally intercalated with the Paleoproterozoic Wollaston Group supracrustal package (Annesley et al. 2005). The basement rocks were intensely deformed and metamorphosed as a result of the collision of the Hearne and Superior provinces during the Trans-Hudson orogeny (ca. 1.8 Ga), which led to the development of the Wollaston fold and thrust belt. The western part of the basin, which includes one mine and an active prospect, is underlain by the Lloyd, Clearwater and Tantato domains of the Rae Province (Card et al. 2007; Fig. 22). However, the basement geology of these domains below the basin is not well established. The Paleoproterozoic Clearwater domain, comprising biotite granite that intruded older granitic gneiss, is younger than the Lloyd domain and is juxtaposed between the latter's eastern and western segments.

Lithoprobe became involved with seismic reflection studies in the Athabasca Basin as part of the project's Trans-Hudson Orogen transect (e.g. Hajnal et al. 2005a). Line S2B, acquired in 1994 for crustal studies, extended northward from the west-

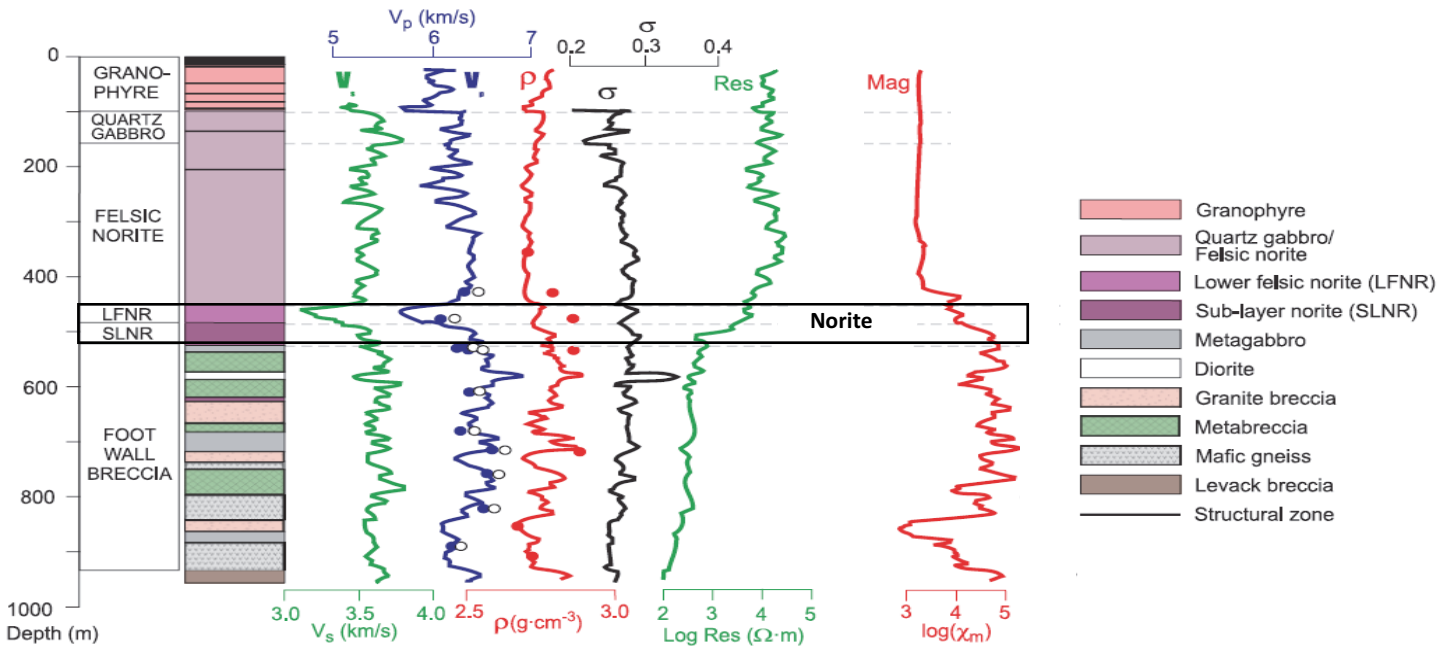

Figure 18. *In situ* geology and logging results from a 980 m borehole in the North Range of the Sudbury Structure. V_p and V_s, compressional- and shear-wave velocity, respectively; ϱ, density; σ, Poisson's ratio; Res, resistivity; Mag, magnetic; χ_m, magnetic susceptibility. Circles on the V_p log represent laboratory measurements on water-saturated cores at lithostatic pressure (solid circles) and 600 MPa (open circles). Solid circles in the relative density log are from core sample measurements. Norite layers are highlighted. Modified from Boerner et al. (2000); after White et al. (1994).

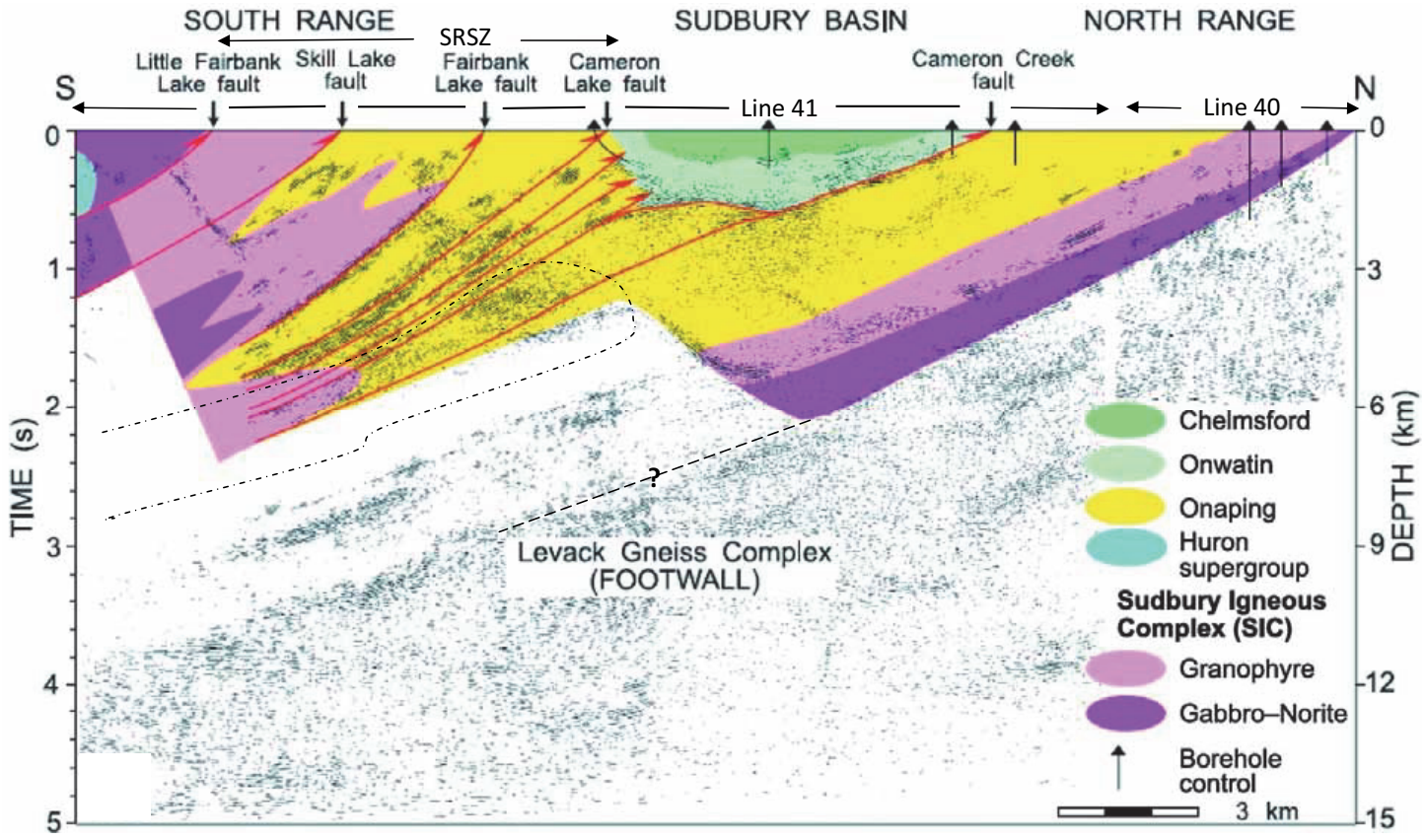

Figure 19. Geological interpretation of the composite migrated seismic section, lines 41 and 40; line locations in Figure 15. The dash-dot line below the South Range outlines the area of high conductivity interpreted by Boerner et al. (1994). SRSZ, South Range shear zone. Modified from Eaton et al. (2010); after Wu et al. (1995).

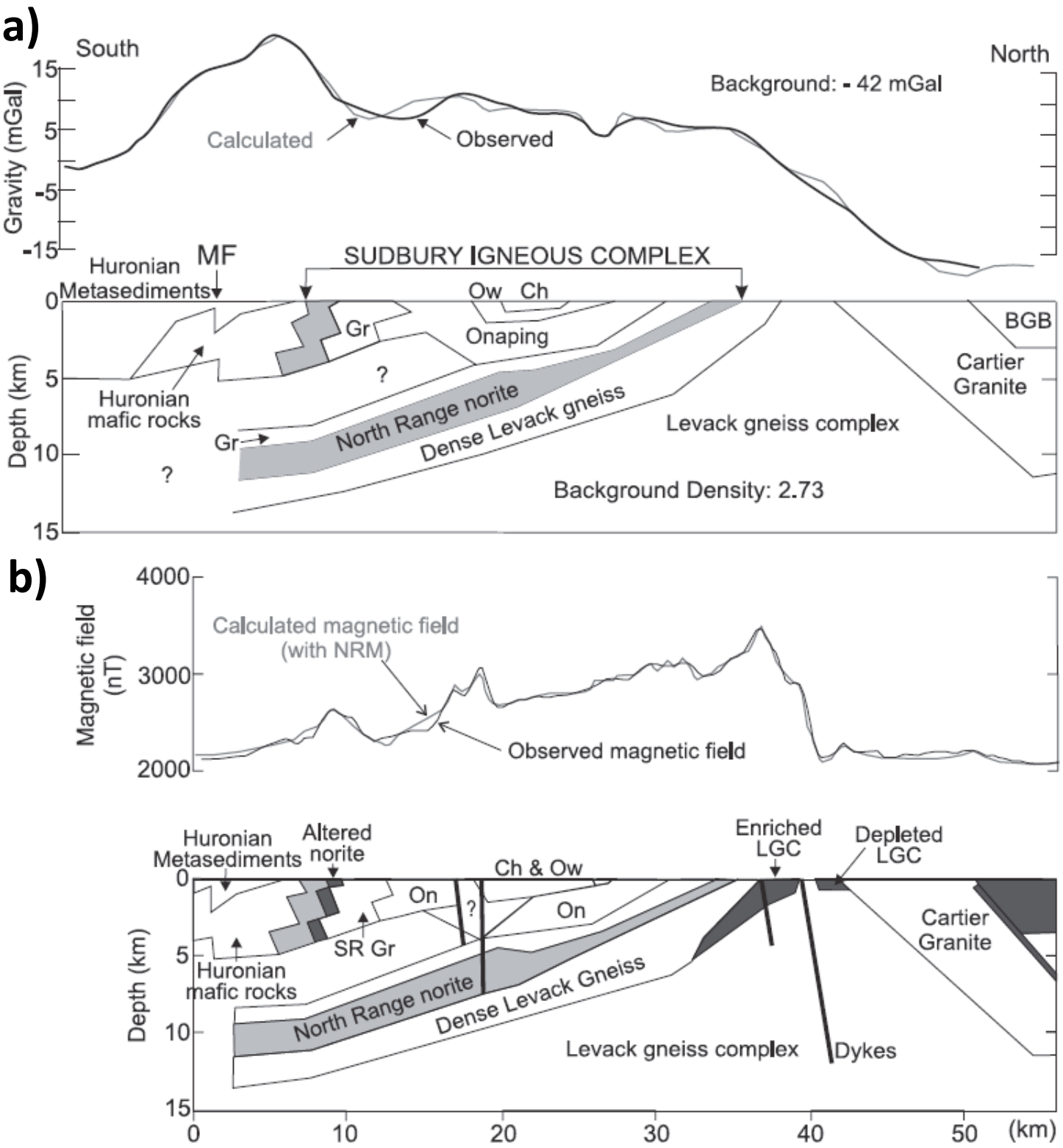

Figure 20. a) Gravity profile data and interpreted density model; location in Figure 15. Norite is shaded grey. From Boerner et al. (2000), after McGrath and Broome (1994). b) Magnetic profile and interpreted susceptibility model; location in Figure 15. From Boerner et al. (2000), after Hearst et al. (1994). BGB, Benny greenstone belt; Ch, Chelmsford; Gr, granophyre; LGC, Levack gneiss complex; MF, Murray fault zone; NRM, natural remanent magnetization; On, Onaping; Ow, Onwatin; SR, South Range.

https://doi.org/10.12789/geocanj.2017.44.125

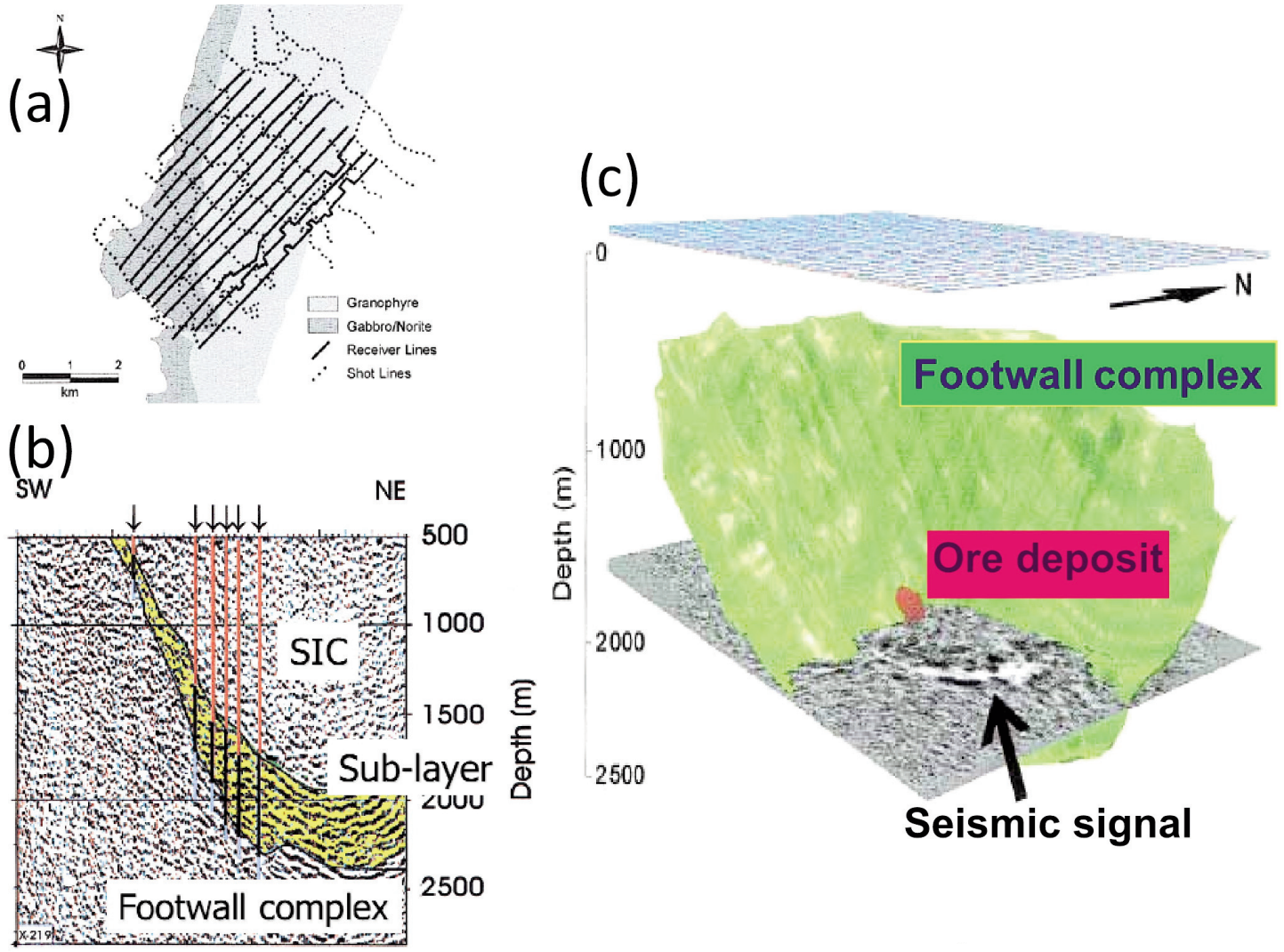

Figure 21. a) Plan view of the survey grid for the Trill 3-D seismic experiment and Trill area geology. b) Depth-migrated vertical section from the processed Trill 3-D survey with interpretation overlay showing the Sudbury Igneous Complex (SIC), the sublayer and the footwall complex. Arrows identify boreholes: red line segments, SIC; black line segments, sublayer; blue line segments, footwall complex. c) Composite perspective view of interpreted footwall contact (green) derived from migrated reflection data, known mineralization at 1800 m depth (red), and seismic scattering event (indicated by the arrow), evident on the time slice at 612 ms (~1600 m), caused by the mineralization. The pixelated grid is shown at the surface. Figures modified from Milkereit et al. (2000).

ern part of the internides of the orogen, across the Wathaman Batholith, Peter Lake domain, Wollaston domain and into the easternmost Athabasca Basin (Fig. 22; Hajnal et al. 2005b). With funds and supporting logistics from uranium companies operating in the eastern Athabasca Basin, a 32 km-long high resolution line, S2D, was run from the Wollaston domain into the basin (Fig. 22). The objective was to image the unconformity and the underlying basement structures, two fundamental requirements of any exploration program in the basin. The results (see below) were highly successful. As a result of this success, various uranium companies continued to support the acquisition of high-resolution seismic reflection data in areas of prime interest. In addition to Line S2D, this section highlights results from the western basin, the Shea Creek study, and the eastern basin, the McArthur River project that included a low-fold, irregularly sampled 3-dimensional study tied to borehole information.

Geological Background – Athabasca Basin

The Athabasca Basin consists of up to 1800 m of Mesoproterozoic sedimentary rocks comprising mainly fluvial sandstone units of the Athabasca Group unconformably underlain by peneplaned tectonometamorphic complexes (e.g. Ramaekers et al. 2007; Hajnal et al. 2010). The Athabasca Group is overlain by Quaternary till deposits varying in thickness from 0 to 90 m (Schreiner 1983). Figure 23 illustrates the lithostratigraphy of the basin, which comprises four sequences bounded by unconformities (e.g. Ramaekers et al. 2007). These indicate repeated deposition and erosion over a period of about 200 m.y. (Jefferson et al. 2007). The Fairpoint Formation comprises sequence 1 but is confined to the western part of the basin. Sequence 2, including the Smart, Read and Manitou Falls formations, represents the bulk of the Athabasca Group. It overlies basement except in the west, where it unconformably overlies the Fairpoint Formation. Within sequence 2,

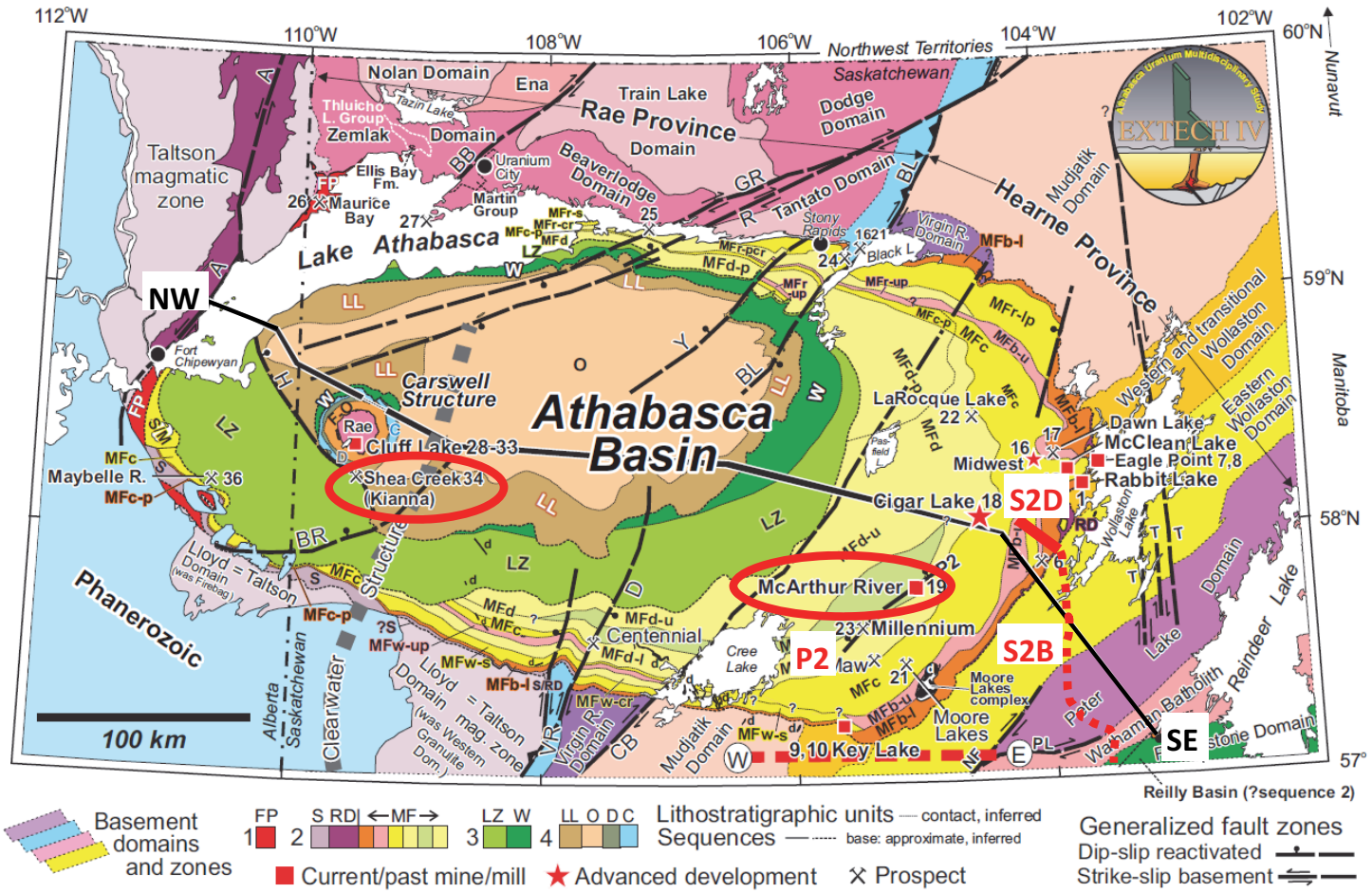

Figure 22. Geological setting and unconformity-associated uranium occurrences (numbered) of the Athabasca Basin region of northern Saskatchewan and Alberta. Symbols and fonts are slightly larger for more significant occurrences. Abbreviations for geological sequences, formations and members shown in the legend: Sequence 1: FP, Fair Point; Sequence 2: S, Smart; RD, Read; MF, Manitou Falls (members identified with different colours and letters on map); Sequence 3: LZ, Lazenby Lake; W, Wolverine Point; Sequence 4: LL, Locker Lake; O, Otherside (also called William River); D, Douglas; C, Carswell. P2 identifies the P2 reactivated thrust fault. The black line NW–SE is the location of the cross-section in Figure 23. Seismic lines S2D and S2B are located. Red ellipses highlight the two deposit areas discussed in this section. For further information, see Jefferson et al. (2007) from which the map was extracted.

the dominant Manitou Falls Formation comprises five members, as illustrated. The Lazenby Lake and Wolverine Point formations form sequence 3. They are overlain by sequence 4, comprising the Locker Lake, Otherside, Douglas and Carswell formations. Most of the Athabasca Group consists of sandstone units, mainly quartz arenite. The Fairpoint and Manitou Falls formations include subordinate and discontinuous mudstone. Moderate but distinctive amounts of mudstone and siltstone are found in the Wolverine Point Formation. These same units are abundant in the Douglas Formation, whereas the uppermost Carswell Formation is primarily dolostone.

To constrain the timing of deposition and to provide quantitative constraints on a regional provenance model for the Athabasca Group, detrital zircon ages from five samples representing a variety of stratigraphic levels (Fig. 23) were determined using U–Pb SHRIMP procedures (Rayner et al. 2003; Rainbird et al. 2007). Figures 24a and b illustrate such studies for samples from the Dunlop member of the Manitou Falls Formation; Figure 24c shows cumulative results for all five samples. In terms of timing of deposition, the youngest detrital zircon in each sample provides a maximum age of sediment deposition. For the 5 samples, the youngest zircon grains represent ages from 1662 Ma (the youngest age) for the Wolverine Point Formation to 1819 Ma for the Bird member of the Manitou Falls Formation. The Fair Point Formation is the oldest unit and has a youngest zircon age of 1810 Ma, indicating that the Athabasca Basin formed after that time. Considering these detrital zircon ages and geological information, interpretation of basin development suggests that the major basal section was deposited from about 1740 Ma to 1730 Ma whereas deposition of the upper section took place around 1640 Ma to 1630 Ma (Rainbird et al. 2007). Paleocurrent studies for the region show a predominantly westerly directed flow (Ramaekers et al. 2001). In a much earlier study but consistent with this result, Fraser et al. (1970) suggested that the Athabasca Group, among other Mesoproterozoic sedimentary basins in northwest North America, is the remnant of a once broad sand sheet deposited by a westerly directed fluvial system onto the Canadian Shield. In an alternative view based on geometry, sequence architecture, east-west elongation and dish-shaped outline of the basin, Rainbird et al. (2007) suggest that the Athabasca Basin was formed by a broad thermal subsidence

https://doi.org/10.12789/geocanj.2017.44.125

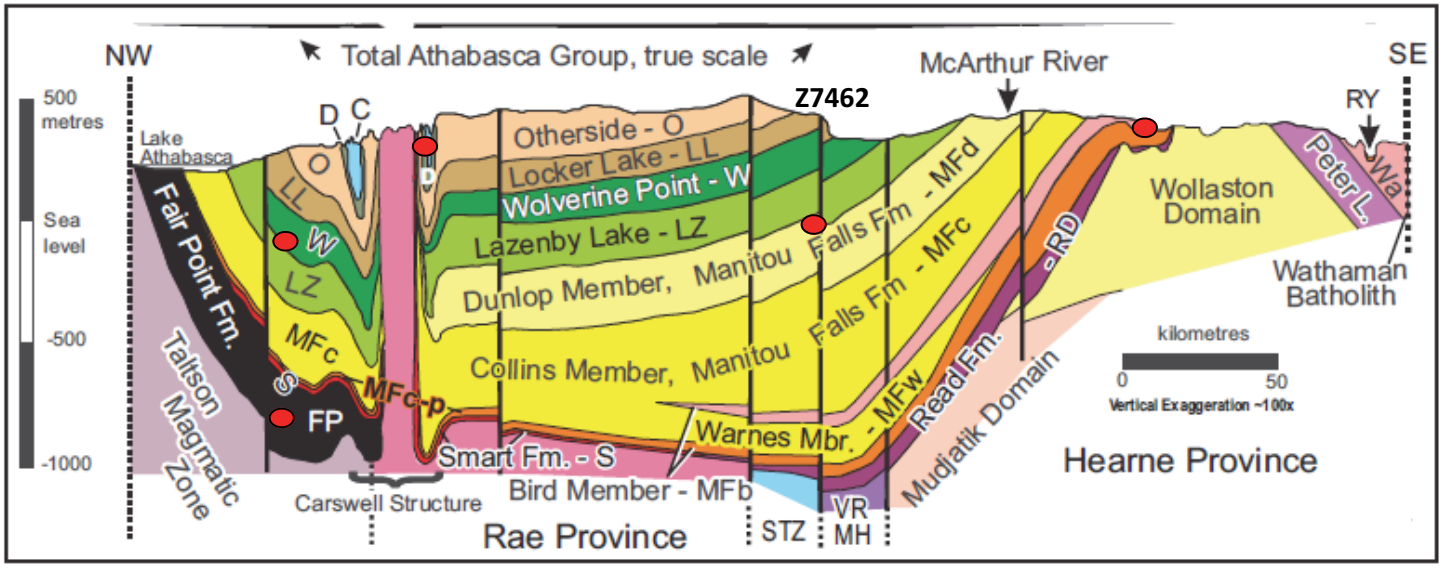

Figure 23. Lithostratigraphic cross-section of the Athabasca Basin; line of section is shown as NW–SE in Figure 22. True 1:1 scale is shown at top. Stratigraphic units in the vertically exaggerated section are formations except those starting with MF, which are members of the Manitou Falls Formation. Basement domains are diagrammatic. Black vertical lines are projected drill holes; Z7462 is the location of detrital zircon samples from the Manitou Falls Formation (see Fig. 24). Red dots show the locations of the detrital zircon samples with respect to the stratigraphy (from Rainbird et al. 2007). Figure modified from Jefferson et al. (2007).

mechanism that was probably unrelated to the Trans-Hudson Orogen to the east.

As shown in Figure 24c, ages of detrital zircon grains from the five samples display a clear bimodal distribution into Neoarchean and Paleoproterozoic components (Rainbird et al. 2007). More specifically, sequences 1 and 2 (representing the early part of development of the Athabasca Basin and the bulk of the Athabasca Group) have ages that indicate older provenance from the Rae Province and Sask craton (sequence 1) and from the Hearne Province (sequence 2). The younger provenance was influenced by an extensive mountain belt in the east, the now-exhumed Trans-Hudson Orogen. The Wolverine Point Formation of sequence 3 shows similar provenance but also includes some enigmatic younger detrital zircon grains (ca. 1770–1650 Ma) from which Rainbird et al. (2007) suggested a source more than 1000 km to the south, the Yavapai and Mazatzal orogens south of the Archean Wyoming Province. Results for the Douglas Formation of sequence 4 are similar to those for the Wolverine Point Formation without the younger zircon grains; Rainbird et al. (2007) suggested this indicates reworking of lower units from the Athabasca Group.

The unconformity with basement, which is the locus of the uranium deposits, is a red, hematitic regolith, 0 to 70 m thick, that grades downward through green, chlorite-altered rock into fresh basement rocks. Jefferson et al. (2007) have interpreted the regolith as being due to regional paleoweathering overprinted by hydrothermal alteration of basement gneiss beneath the unconformity. In addition to these processes, two other types of regional-scale alteration have been recognized: basin-wide pre-ore diagenetic sandstone alteration and sub-basin-scale alteration halos that outline trends and clusters of uranium deposits. The alterations are significant because Kyser et al. (2000) have suggested from a three-basin comparison that more intense alteration is associated with higher overall potential for uranium deposits. The sandstone and underlying basement rocks have been subjected to several episodes of brittle deformation, including repeated brittle reactivation of older ductile structures with offsets on the order of tens to hundreds of metres (Jefferson et al. 2007).

The Uranium Deposits

The unconformity-type uranium deposits are pods, veins and semi-massive bodies located close to the basement unconformity and are generally near re-activated crustal shear zones associated with the Trans-Hudson Orogen (Annesley et al. 2005; Jefferson et al. 2007). They consist principally of uraninite that is dated mainly between 1600 and 1350 Ma. While the morphology and other details of individual deposits vary considerably, they range between end-member styles that reflect both stratigraphic and structural control (Fig. 25; Thomas et al. 2000; Jefferson et al. 2007).

At one end of the generalized range are monometallic deposits, containing only uranium (Fig. 25). These are usually spatially associated with basement fracture zones with steep to moderate dips that extend along strike for hundreds of metres and down dip for tens to hundreds of metres below the basement unconformity. The high-grade ores are found in individual lenses ranging from massive pods that can be 100 m or more in vertical extent, 90 m in length and 50 m in width to small pods that are only 1 to 2 m thick and 3 to 5 m in vertical dimension (Jefferson et al. 2007). Mining grades typically run at 0.5 to 2% U but the world-class McArthur River deposit (see below) grades about 20 to 25%.

At the other end of the general range are polymetallic deposits that contain variable amounts of U, Ni, Co, As and traces of Au, PGEs, Cu, REEs and Fe (Fig. 25). They are generally developed along and just above the unconformity in the overlying sandstone and conglomerate of the Athabasca

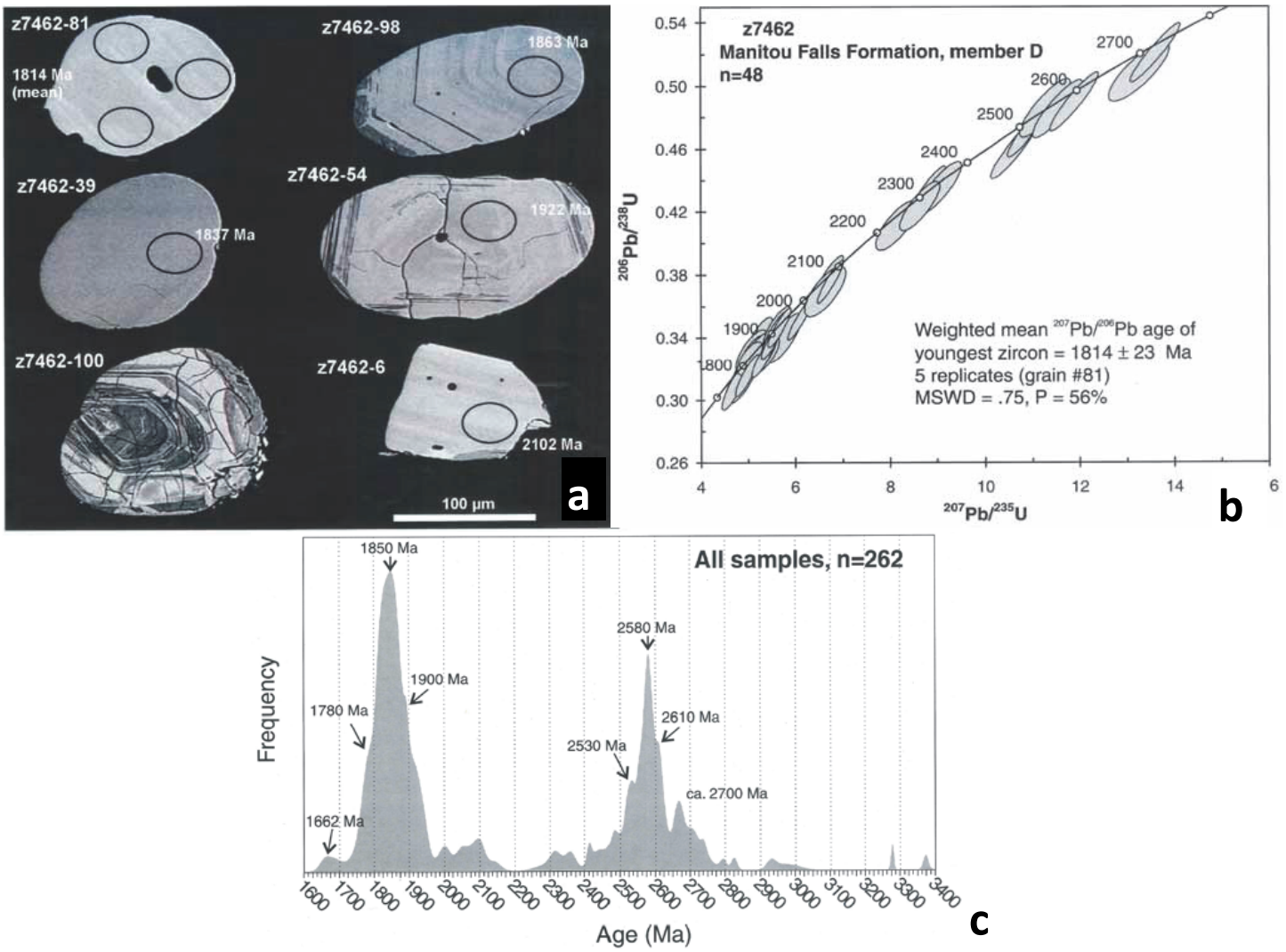

Figure 24. a) Backscattered-electron images of a representative selection of zircon grains from sample Z7462 from the Dunlop member (MFd), Manitou Falls Formation. Ellipses represent approximate locations of SHRIMP analysis. Spot $^{207}Pb/^{206}Pb$ ages are shown. b) Concordia diagram of U–Pb results for sample Z7462 showing an age of 1814 Ma. Error ellipses are 2σ. c) Cumulative probability curve of compiled SHRIMP U–Pb detrital zircon age results for five samples from the Athabasca Basin sandstone. All figures from Rayner et al. (2003).

Group. The ore is typically formed as flattened elongate pods to flattened linear ore bodies and may have root-like extensions into the basement, giving a T-shaped cross-section (Jefferson et al. 2007). Sizes of the unconformity-hosted ore deposits range about the same as fault-hosted ones but their major dimensions are horizontal. They are typically characterized by a low-grade halo with less than 1% U surrounding a high-grade core of 1 to 15% U. However, the major Cigar Lake deposit (Fig. 22) has an average grade of about 21%. It is huge with a strike length of 1900 m, a width of 50 to 100 m and an upward convex lens-shaped cross-section up to 20 m thick.

High-Resolution Seismic Studies

In order for high-resolution seismic reflection methods to be applicable for uranium exploration, the acoustic properties of the rocks within the basin and the basement must have sufficient contrast to generate reflected energy. Prior to the 1994 Lithoprobe seismic survey, Hajnal et al. (1983) presented some petrophysical studies of rocks in the Athabasca Basin and showed that, at least in some cases, appropriate contrasts did exist. With the successful test reflection profile of Line S2D in 1994 (see below), further efforts to determine acoustic properties of such rocks were undertaken. These included geophysical logging surveys, laboratory measurements on core samples, measured mineral properties and results from vertical seismic profiling (e.g. Mwenifumbo et al. 2004; White et al. 2007).

The stratigraphic units of the Athabasca Basin (Fig. 23) show no distinct acoustic properties and thus the basin-fill sedimentary rocks generally have weak reflectivity. The unconformity is characterized by complex, laterally variable chemical alteration and thus shows variable acoustic properties. Normally, the unaltered sandstone–basement contact is a strong reflector but if the overlying sandstone is silicified, reflections will not be as strong but still readily visible (Hajnal et al. 2010). The presence of a pronounced regolith can further reduce the strength of the reflected energy. When unconformity-related

https://doi.org/10.12789/geocanj.2017.44.125

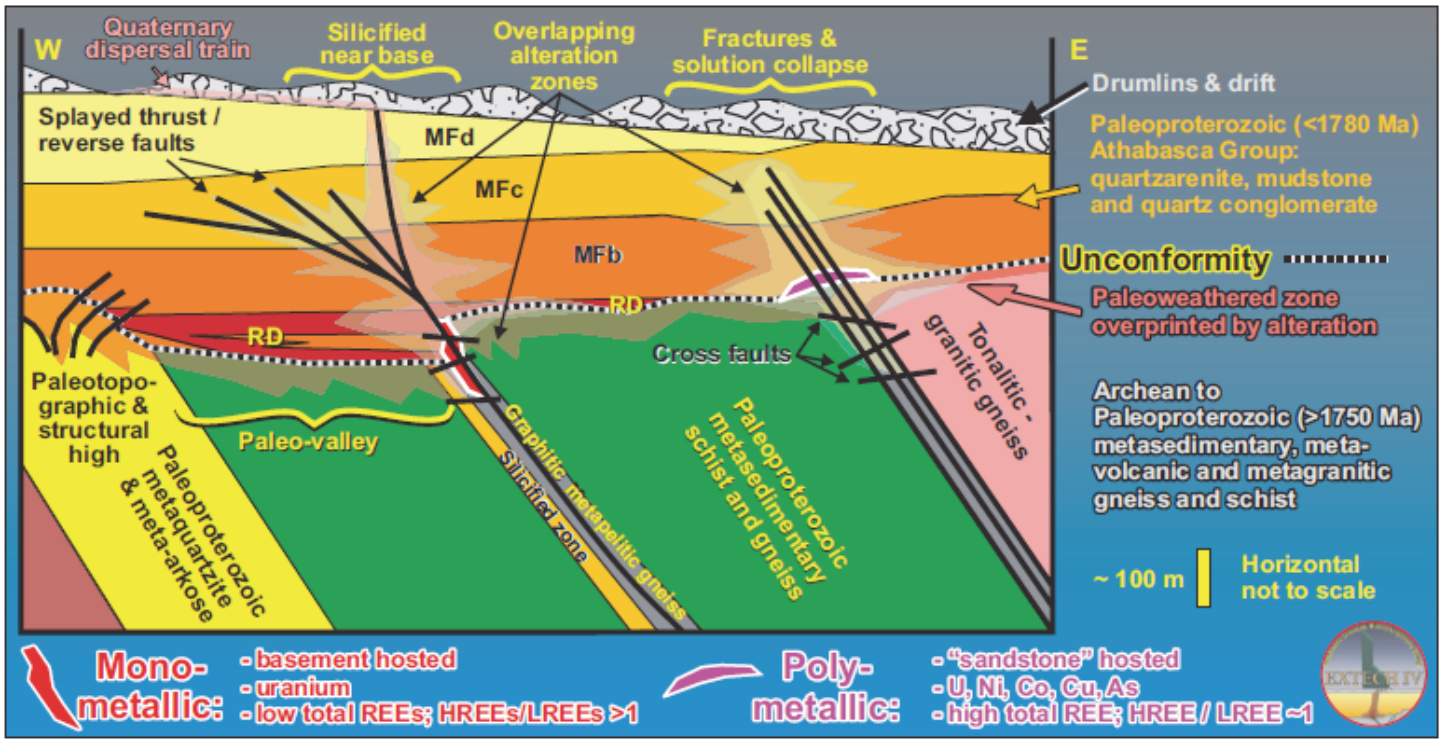

Figure 25. Generalized geological elements of mono- and polymetallic unconformity-associated uranium deposits in the eastern part of the Athabasca Basin. The empirical geological model illustrates two end-member styles of ore exemplified by McArthur River (monometallic) and Cigar Lake (polymetallic) ore deposits (locations in Fig. 22). A complete spectrum of styles between the end members is known, even within single deposits and deposit groups. MFb, MFc and MFd, members of the Manitou Falls Formation; RD, Read Formation. Figure from Jefferson et al. (2007).

reflections are observed on the seismic section, faults within the basement are often revealed by small offsets in the reflections.

The Lithoprobe Test – Line S2D, Eastern Athabasca Basin

To determine the efficacy of high-resolution seismic for the purpose of uranium exploration in the Athabasca Basin, a 32 km-long reflection line, S2D, was recorded in the eastern basin along the northernmost extent of Lithoprobe's regional reflection line S2B (locations in Fig. 22). The unconformity was well imaged along the line and its depth, determined from traveltimes and velocity information, was well constrained, having an accuracy of ± 5% or better when compared with borehole information (Fig. 26; Hajnal et al. 2010). On the basis of reflection offsets along the unconformity, numerous steeply dipping faults that penetrate from the basement into the overlying sandstone were recognized (Fig. 26). Where the basin ended toward the southeastern end of the 32 km-long line, the reflection from the unconformity was lost (Hajnal et al. 2010). However, a slightly deeper reflection from the exposed basement showed that the latter can be reflective when pelitic gneiss and Archean volcanic rocks are in contact (Hajnal et al. 1997). The success of Line S2D led to continued application of high-resolution seismic surveys in areas with substantial geological information that were funded entirely by the uranium industry. Essentially, Lithoprobe demonstrated a new approach for exploration in the Athabasca Basin.

Shea Creek, Western Athabasca Basin

Following the success of the Lithoprobe test line in the eastern basin, a reflection survey was carried out in the western basin in 1997. The Shea Creek study was conducted ~15 km south of an existing uranium mine, Cluff Lake (Fig. 22). An unusual feature of the mine is that it is located at the southern margin of the basement core of the Carswell Structure (Figs. 22, 23), which is interpreted as a meteorite impact structure (e.g. Grieve and Masaitis 1994). Uplift of the central core of the structure is considered to be responsible for transport of the uranium deposits to the near-surface (Baudemont and Fedorowich 1996). However, no genetic relationship between the ore and the impact structure exists; the main mineralization is the result of a hydrothermal event at ~1100 ± 50 Ma (Hajnal et al. 2015).

Within the Shea Creek study area (Fig. 27a), borehole logging has shown that the lithostratigraphic succession from depth to surface comprises Manitou Falls Formation's MFc and MFd of sequence 2, Lazenby Lake and Wolverine formations of sequence 3 and Locker Lake Formation of sequence 4. Subsequent well-log data investigations (SHE-105 and -22, Fig. 27a) demonstrated that *P*-wave velocity, measured density and fracture density can be used to identify contrasting lithological features and anomalous zones, due mainly to porosity variations, within the Athabasca Group and at the basement unconformity (Fig. 27b; Mwenifumbo et al. 2004). The crossplot of Figure 27b shows a well-separated diversity of the alteration clusters. Variations and differences in seismic imped-

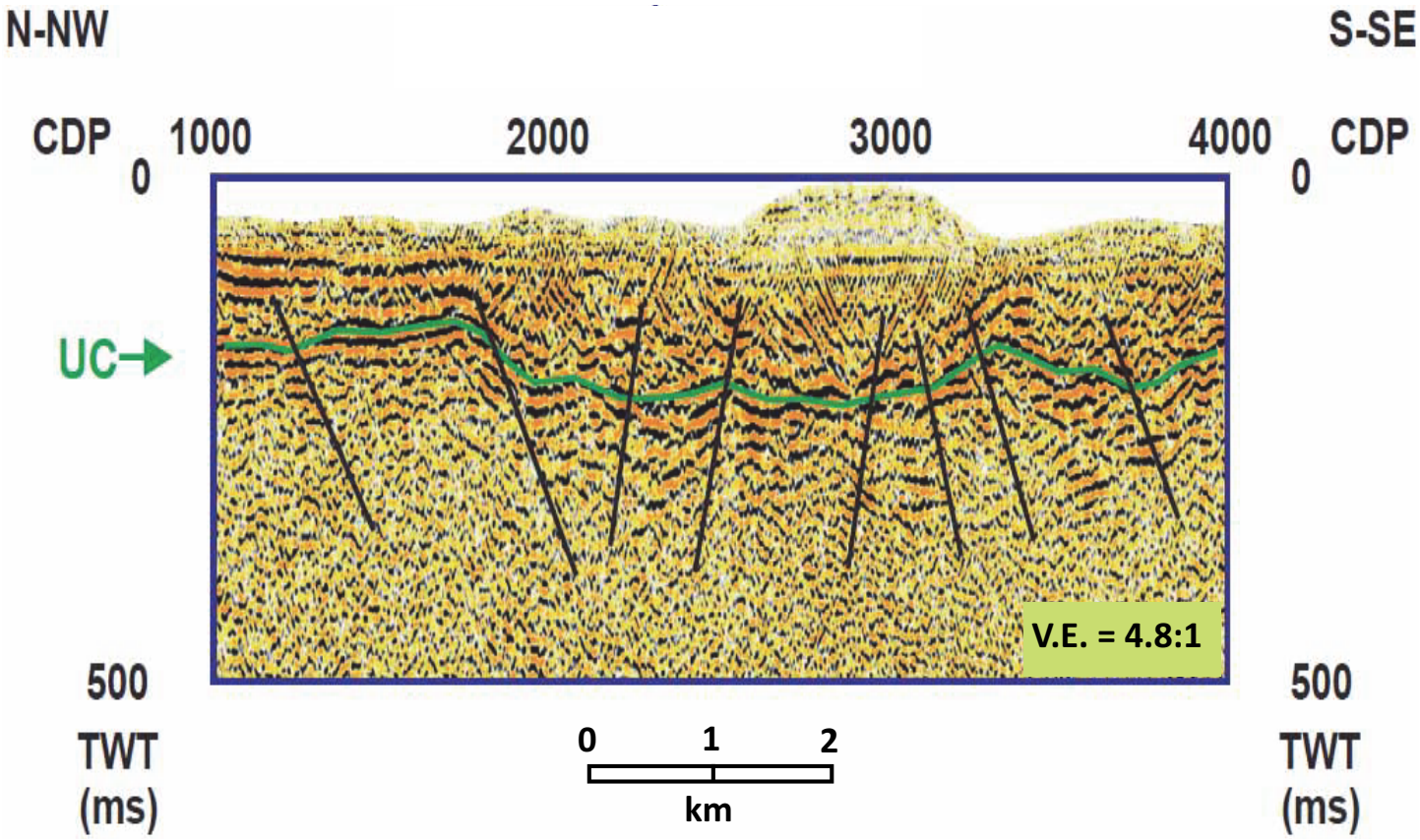

Figure 26. Enlarged example of the seismic image of the unconformity (UC) and associated fault system that extends from the basement into the overlying sandstone as observed on Lithoprobe's high resolution seismic profile S2D (location in Fig. 22). Figure from Hajnal et al. (2010).

ance, the product of velocity and density, control the seismic response in a survey. Thus, such surveys may identify target regions of mineralization that are associated with highly altered basement structural zones.

The reflection survey in the Shea Creek area (Fig. 27a) was the first fully industry-sponsored seismic survey in the Athabasca Basin. Its objectives included establishing the conditions by which such surveys can be effectively used for exploration in this geological setting, mapping the unconformity and its depth variations, and imaging the structural variations within the underlying basement complex. Figure 28 shows the migrated depth section and its interpretation for the 32 km, N–S trending line WAS-1. The northern 5 km (common-depth-point (CDP) locations 12000 to 10000) are within the Cluff Lake mine area and investigate the most southerly part of the basement uplift. The locally consistent incoherent images outline the uplift; interruption of short horizontal segments of reflectivity mark high-angle fracture zones. South of this region, the unconformity is identified by strong reflections in the basement forming an arcuate shape, part of the ring graben associated with the impact structure, within which up to 1.5 km of Athabasca Group sedimentary rocks reside. Within the sedimentary rocks, normal faults are identified, steeply dipping between CDPs 10000 and 8000, and more listric between CDPs 8000 and 6000. This interpretation is consistent with borehole geological data (e.g. DGS-4). The unconformity (UC) also is clearly identified in the remaining half of the section (south of CDP 6000, Fig. 28). Within the basement, strong and consistent reflectivity is observed (Fig. 28). The steeply north-dipping faults (A), just below the unconformity, are features generated by the impact process. The gently southwest dipping shear zones (B), just on the right side of the figure, reveal the brittle reactivation of the original tectonic structures. The gently curving, subparallel dotted lines (C) are recognized as the remnant of the first phase ductile deformation of the area (Hajnal et al. 2015). Elsewhere in the basin, the interconnection of the fracture zones with the unconformity has been recognized as pathways for the fluid migrations responsible for the ore mineralization deposition (e.g. Hajnal et al. 2007).

One of the characteristics noted on all four seismic lines (Fig. 27a) is local anomalous variations in seismic reflectivity in the vicinity of distinct basement structures (e.g. Fig. 28c). Reduction in the reflectivity of the unconformity accompanied by a depression of 25–30 m indicated variable alterations within the overlying sandstone. The spatial projection of the four anomalous zones outlines a northwest-trending line that correlates with a basement fault. Subsequent drilling along the trend delineated new ore deposits (Hajnal et al. 2015).

https://doi.org/10.12789/geocanj.2017.44.125

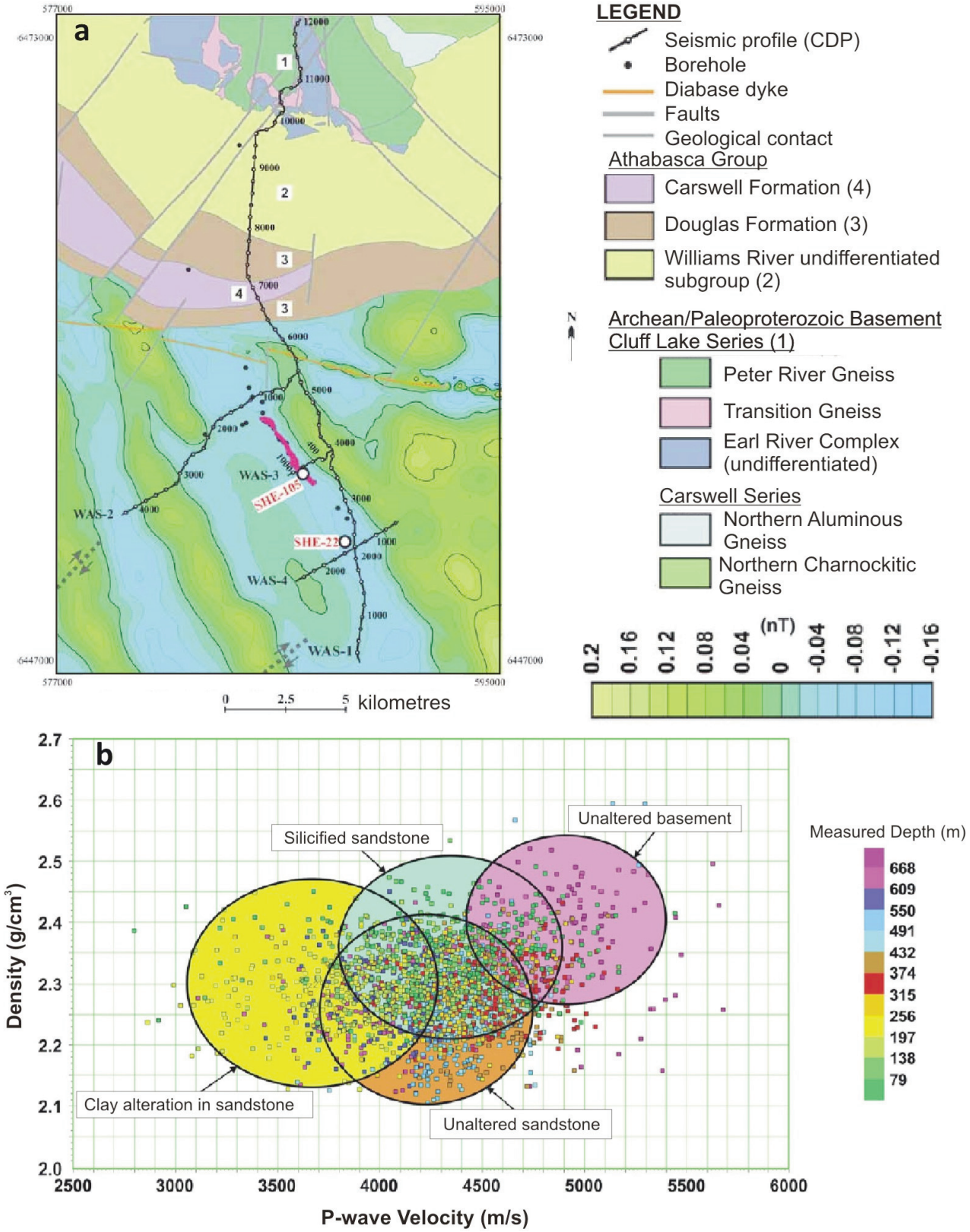

Figure 27. a) Shea Creek study area. Surface geology and structural map of the Carswell impact structure (upper half); residual magnetic map of the area of study (lower half; colour scale in lower right). Seismic profiles WAS-1, 2, 3 and 4 are shown with common-depth-point (CDP) numbers. SHE-105 and SHE-22 identify boreholes used to tie seismic results to subsurface geology. The thick, purplish, NW-trending feature crossed by WAS-3 shows the area of the Shea Creek ore deposit. From Hajnal et al. (2015). b) Density versus V_p cross-plot showing the clusters of different lithologies in the SHE-105 borehole; measured sample depths are colour-coded. From Hajnal et al. (2015).

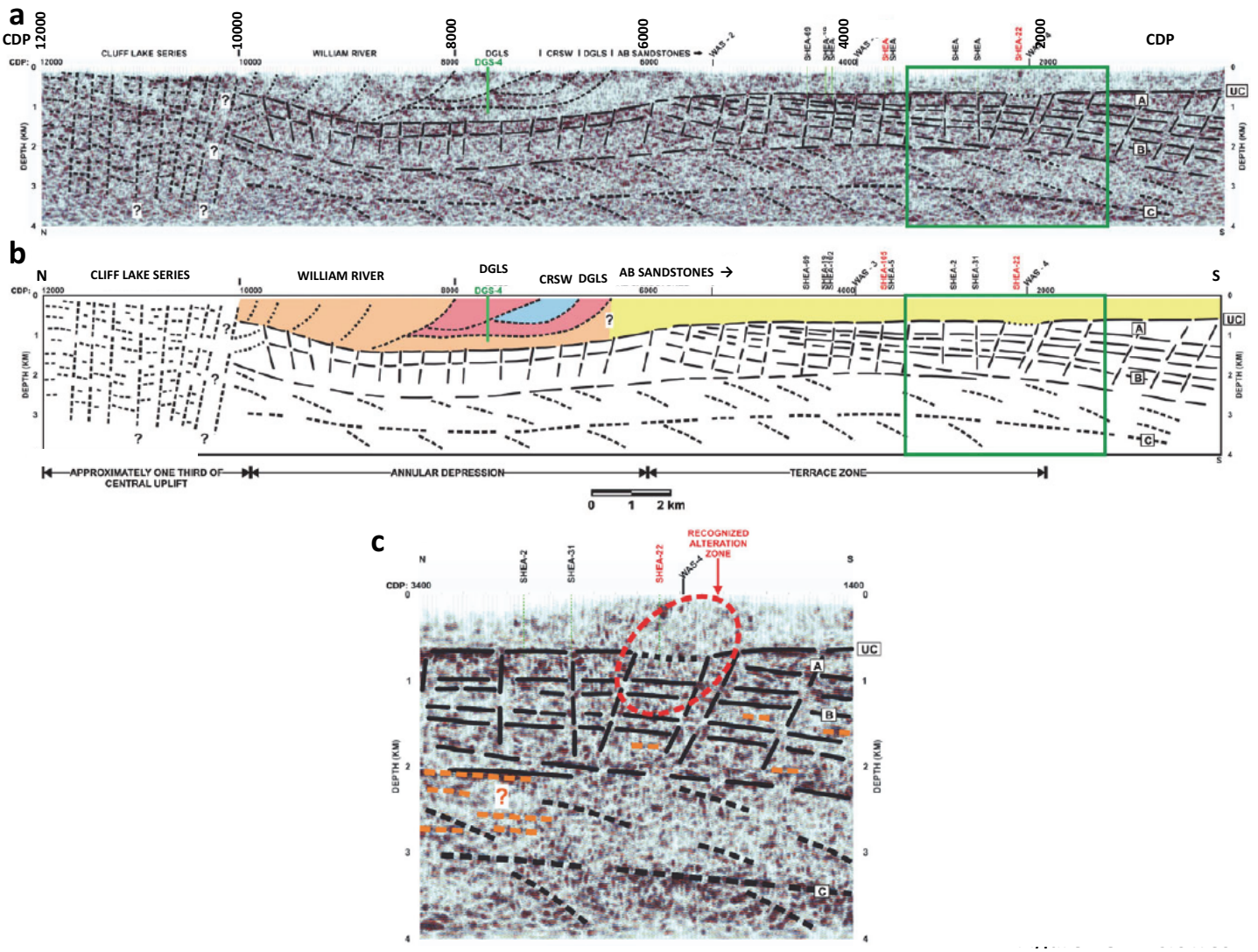

Figure 28. a) Migrated depth section for WAS-1 (location in Fig. 27a; common-depth-point (CDP) positions are marked) with interpreted correlations. Known surface geology and boreholes to which the seismic section was tied are marked at the top of the figure (William River Formation is also called the Otherside Formation). Abbreviations: DGLS, Douglas Formation; CRSW, Carswell Formation; AB, Athabasca Basin; UC, unconformity. Locations of crossing seismic lines, WAS-2, 3 and 4 are marked. Rectangle identifies the part of the section enlarged in c). b) Interpreted depth section. Colours show Athabasca Group; legend in Figure 27. Abbreviations as in a). The major elements of the impact structure are outlined below the coloured part; see text for description of labels [A], [B], and [C]. c) Enlarged anomalous portion of WAS-1. Red ellipse outlines the unique alteration and structural anomaly, a characteristic seismic feature identifiable on all four lines. Orange sub-horizontal reflector segments are inferred as remnants of earlier ductile deformation. A, B and C as in text. All illustrations from Hajnal et al. (2015).

McArthur River 2-D and Low-fold 3-D Investigations, Eastern Athabasca Basin

The McArthur River mining camp, located in the southeastern part of the Athabasca Basin (Fig. 22), was the site of further high resolution seismic studies in 2001 with the general objective of developing new or improved exploration tools for deeply buried unconformity-associated uranium deposits. As indicated in Figure 23 for the McArthur River region, the Athabasca Group sedimentary rocks comprise the Read (MFa) Formation overlying the Hearne Province basement, in turn overlain by the Bird (MFb), Collins (MFc) and Dunlop (MFd) members of the Manitou Falls Formation. Within the region of the seismic program, a substantial number of boreholes provided subsurface geological information that could be related to the seismic results. The most important structure is the P2 reactivated dip-slip fault (Fig. 22) that is associated with ore deposits.

The seismic program ranged from two regional profiles, A–A' and B–B', and two high-resolution lines, 12 and 14, to a low-fold 3-D survey (Fig. 29a) and a vertical seismic profile study (not discussed here). A segment of regional line B–B' that crosses the P2 structure and the ore zone is shown in Figure 29b. The unconformity zone is identified by the flat-lying, curvy reflection segments with strong amplitudes relative to the overlying sandstone units, whereas the P2 fault zone is identified by southeasterly dipping, high amplitude reflections that indicate it is almost 2 km thick. The fault zone intersects the unconformity below the MAC-214 borehole in which the fault is recognized as a reverse fault with 80 m of offset. The most prominent feature on the seismic section is the multi-

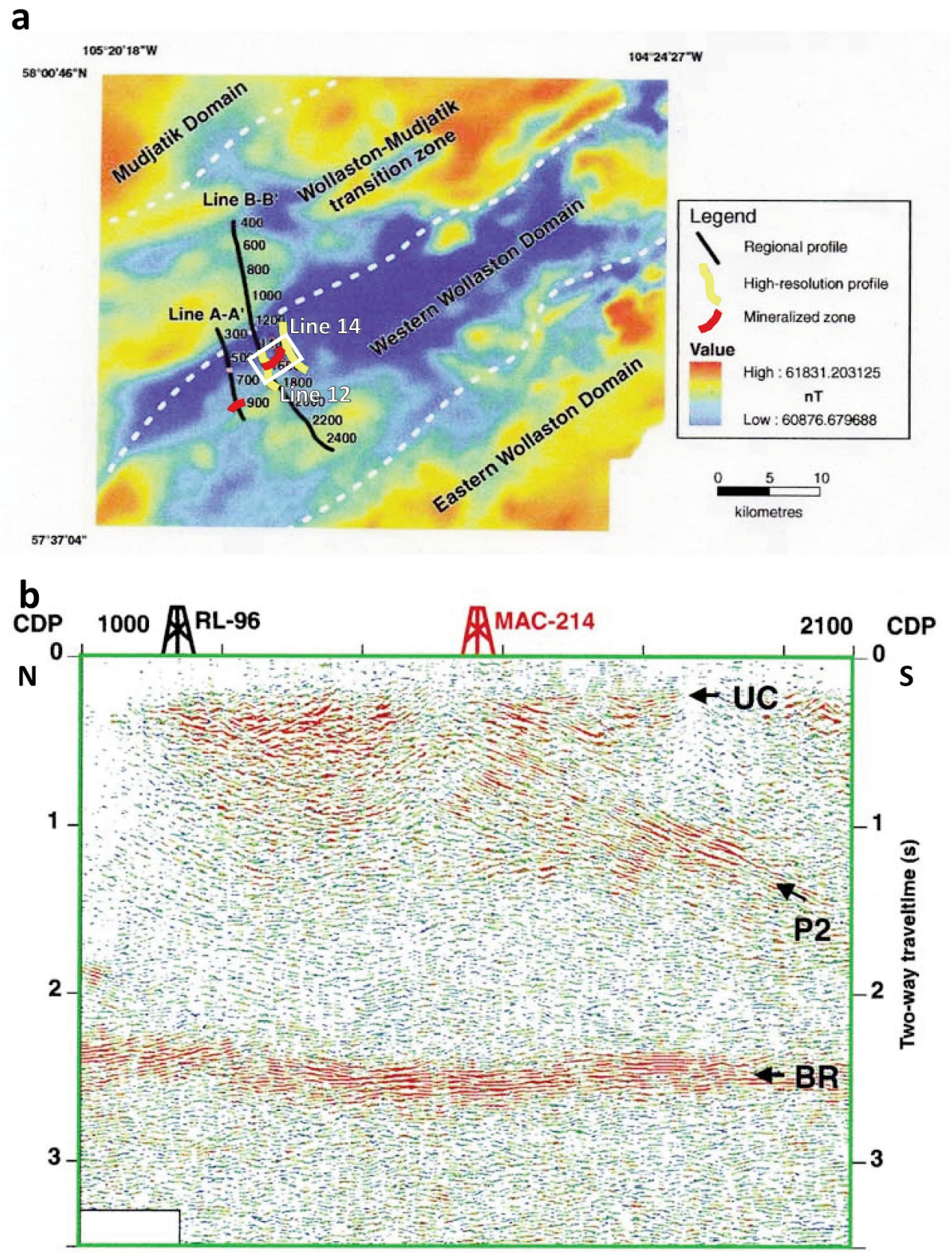

Figure 29. a) Total field magnetic map of the McArthur River study area with lithotectonic domains shown. Seismic lines are identified. Numbers are common-depth-point (CDP) locations. The white rectangle outlines the location of the low-fold 3-D acquisition program. b) Enlarged portion of line B-B', CDPs 1000 to 2100 (~12 km). Drillhole locations are marked. UC, unconformity; P2, the P2 reverse fault zone; BR, bright reflector. From Hajnal et al. (2007).

cyclic bright reflector, BR, located about 7 km below the unconformity, which was also clearly observed on earlier Lithoprobe seismic sections (Mandler and Clowes 1997) but is not relevant to the Athabasca Basin.

On line 12 (and on line 14, not shown), the unconformity shows as an undulating, sub-horizontal zone of reflectivity below which the underlying reflectivity within the basement dips to the southeast (Fig. 30a). Geological information from drill holes provides the framework that confirms the interpreted position of the unconformity and enables correlation of markers throughout the Athabasca Group as displayed in the figure. Brittle reverse faults extend from the shallowest part of the basement into the overlying sandstone units, generally offsetting the unconformity. For example, geological results from drill hole RL-068 (Fig. 30a) indicate a vertical offset of the basement of 45 m (~20 ms; Hajnal et al. 2010). McGill et al. (1993) demonstrated the relationship between reactivated faults and uranium deposits for the McArthur River area. The many drill hole results combined with the multiple and contrasting dip domains below the unconformity on lines 12 (Fig. 30a) and 14 (not shown) suggest that the basement has undergone significant structural changes (Hajnal et al. 2010).

A low-fold, irregularly sampled 3-D survey, including lines 12 and 14, was undertaken in the McArthur River mining camp to image the central area where known ore bodies are located (Fig. 29a). Its main objective was to provide areal constraints on the structural framework in the vicinity of the main P2 fault and associated ore zones. The 3-D survey was complemented by detailed geological information from 71 boreholes that extended to the depth of the unconformity (Hajnal et al. 2010). One result from analysis of the 3-D data was a structure map of the 'depth' (in time) of the unconformity that indicated its depth is controlled by a subtle and complicated network of brittle faults. These have variable dips ranging from moderate to sub-vertical and are characterized by reverse kinematics (Hajnal et al. 2010). The main structural elements and the unconformity surface are portrayed in Figure 30b. The major P2 inverse fault zone is clearly identified and above it, antithetic inverse faults form a flower structure system. The uranium ore pods are located at the intersections of the different fracture zones.

High-resolution seismic reflection studies with appropriate survey design parameters and processing procedures, combined with geological results from boreholes, continue to be an important component of exploration for uranium ore deposits in the Athabasca Basin. Lithoprobe can be credited with introducing this new exploration tool for the uranium industry.

DIAMONDIFEROUS KIMBERLITE DYKE, SLAVE CRATON, NORTHWEST TERRITORIES

In the 1990s, the Slave craton in the Northwest Territories was the locale of the largest staking rush in Canadian history, surpassing the Klondike gold rush of the 1890s. Diamonds found in kimberlite intrusions were the objective. By the end of the decade, more than 150 kimberlite occurrences had been identified (Fig. 31). Pell (1997) provided an excellent review of the history and the science associated with the kimberlite discoveries.

The Slave geological province is one of the principal Archean components of the North American craton (Fig. 31; Bleeker and Davis 1999). It includes interspersed granitoid intrusions, supracrustal sequences and basement core complexes but is dominated by voluminous granitoid intrusions (Padgham and Fyson 1992). The latter were emplaced before, during and after deformational episodes but formation of the Slave was completed by ~2.6 Ga. During the Paleoproterozoic, the Slave Province was incorporated into the North American craton and is bounded by fault systems that have been inactive since 1.27 Ga. A series of Proterozoic dykes, ranging in age from 2.21 to 0.72 Ga, have sliced through the Slave (LeCheminant et al. 1996).

With its old, stable and cool mantle root, the Slave Province is a classic setting for diamondiferous kimberlite pipes because such characteristics are necessary for the development of diamonds within the cratonic root zone (e.g. Haggerty 1986). Mantle-derived kimberlite intrusions, which are volatile-enriched, potassic, ultrabasic magmas that rise to the surface from depths greater than 150 km, host the diamonds. At or near the surface, they are emplaced as small volcanic pipes (the most common form), dykes and sills, but only a fraction are diamondiferous and of these only some are economically viable. Typical pipes have diameters ranging from 10s of metres to more than 1000 m and can be envisaged as downward tapering cones with steep sides (80–85°) and vertical extents of a few kilometres (e.g. Mitchell 1995). Dykes and sills are smaller features that cut across existing structures or layers (dykes) or are emplaced between pre-existing layers or along zones of weakness (sills). Within the Slave Province, many of the kimberlite features were emplaced during the Cretaceous and Tertiary (ages ranging from 97 to 52 Ma) but others erupted as early as the Cambrian to Late Ordovician (520–450 Ma) (Pell 1997).

The first two diamond mines in Canada, Ekati and Diavik in the Lac de Gras area (Fig. 31), were developed within kimberlite pipes. Another discovery was the Snap Lake kimberlite dyke (no. 6, Fig. 1; Fig. 31), which from limited sampling was shown to be rich in high quality diamonds. A substantive drilling program delineated the structure of the dyke: a 1–5 m-thick sheet gently dipping from subcrop to more than 1300 m depth and extending over an area of ~25 km^2 (McBean et al. 2003). But as the dyke plunged deeper, drilling became increasingly expensive. The principals of the two companies operating in the Snap Lake region (De Beers Canada Mining and Diamondex Resources) were aware of the successes that Lithoprobe scientists had achieved using seismic reflection techniques in other mining environments, as highlighted in previous sections of this article. Following discussions with them in the early 2000s, a project to test reflection techniques as a means of delineating the location and features of the dyke at depth was initiated with scientists at the University of British Columbia (one being the current author). The following material is extracted from two publications arising from this project (Hammer et al. 2004a, b).

While Lithoprobe had demonstrated success in other mining environments, this project posed two significant challenges:

https://doi.org/10.12789/geocanj.2017.44.125

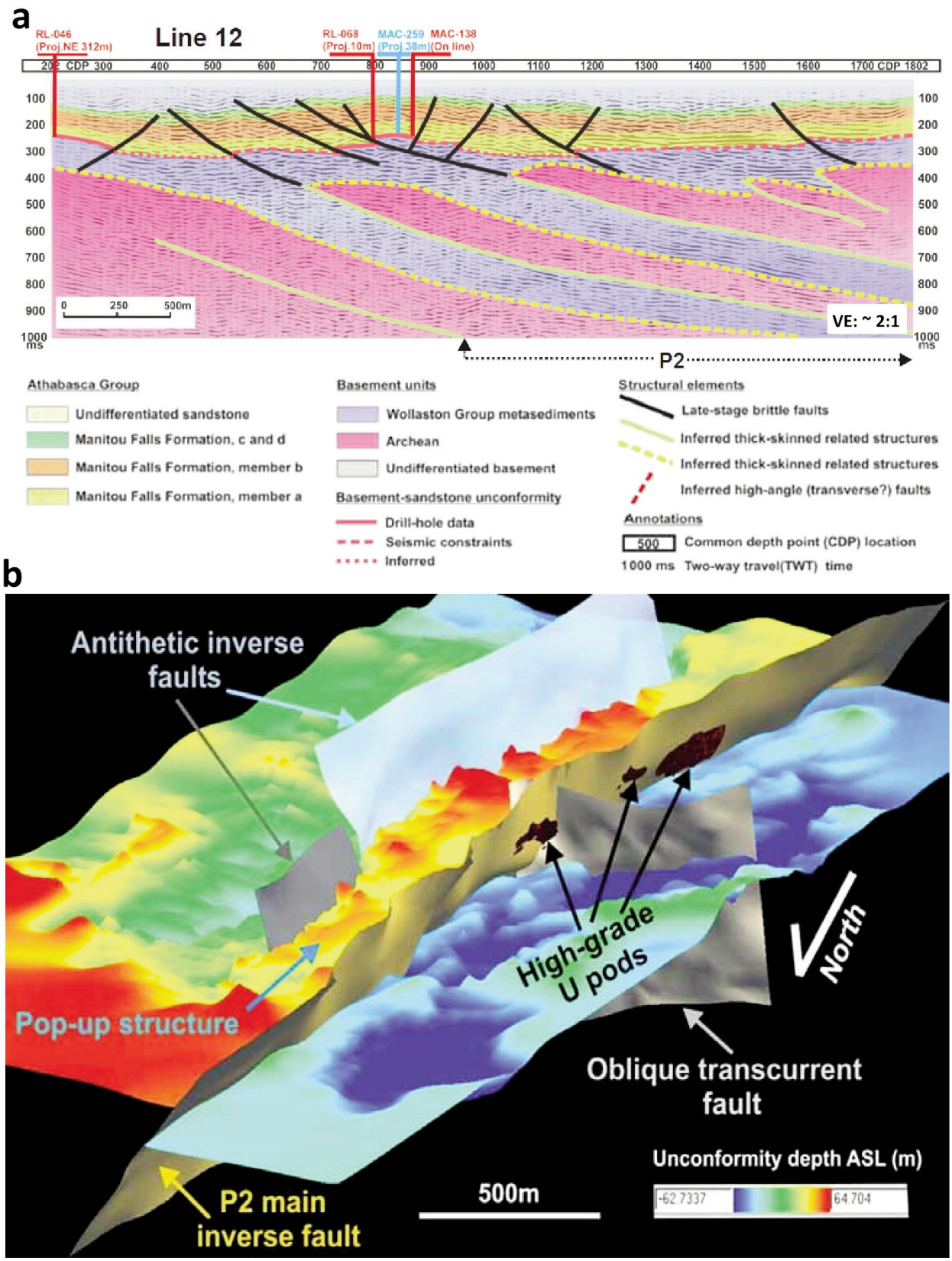

Figure 30. a) Interpreted migrated section for high-resolution line 12 (location in Fig. 29a). The interpretive section illustrates the spatial structural variation in the vicinity of the ore body and the P2 shear zone. Drill holes to which the seismic data could be tied to subsurface geology are identified along the top of the figure. UC, unconformity. b) Three-dimensional display of the structural framework of the McArthur River mining camp derived from the seismic data and tied to all boreholes within the 3-D study area (location in Fig. 29a). The horizontal slice shows the depth to the unconformity; see colour legend. From Hajnal et al. (2010).

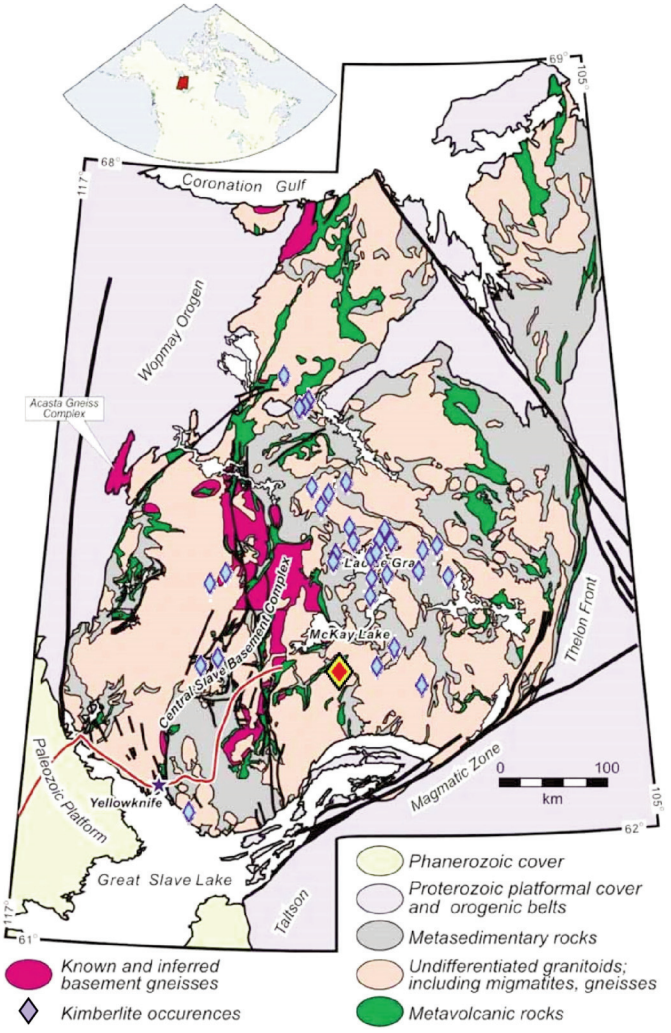

Figure 31. Geologic map of the Slave Province; inset shows location in North America. The Archean cratonic core is bounded by fault zones (bold lines), orogenic belts, and platformal cover. Red and yellow diamond, Snap Lake study location; blue diamonds, known kimberlite pipes, dykes, and sills. Modified from Bleeker and Davis (1999).

(1) The Snap Lake dyke presents an extremely thin target that extends to considerable depth. Frequencies higher than usual (> 200–250 Hz) for an exploration-scale survey were required for detection. However, higher frequencies are preferentially attenuated with depth so it was unclear if sufficient amplitudes could be returned from the dyke, particularly as the target depth increased.
(2) Impedance contrasts and attenuation are important variables in reflection surveys. However, no comparable exploration-scale surveys of thin kimberlite dykes in a granitic host-rock environment had been reported and no geophysical well log information was available. The unique nature of the survey further increased the uncertainties involved with detecting the dyke.

Based on the expectations of the two companies and the challenges associated with the project, two primary questions had to be addressed by the survey:

(1) Is the seismic reflection method an effective and cost-efficient exploration tool for the delineation of shallow-dipping kimberlite dykes and sills in a hard-rock environment and at depths that could help reduce drilling costs?
(2) Can seismic reflection studies provide information about a thin kimberlite deposit (e.g. extent, continuity and thickness) and related geology at scales that could prove useful for drill guidance and mine planning?

The opportunity to study geological samples of the kimberlite dyke and surrounding rocks and to ground-truth the seismic results with drillhole data made the Snap Lake dyke an ideal location for this unique project.

Snap Lake Dyke: Geologic Setting and Structure

Three primary geological units, granitoid, metavolcanic and metasedimentary rocks, comprise the country rocks surrounding the Snap Lake dyke (Fig. 32). The dominant granitoid is the Defeat Plutonic Suite (2610–2590 Ma) that includes granodiorite, tonalite, monzogranite and some pegmatite. The metavolcanic rocks are intensely flattened and comprise layered amphibolite and associated synvolcanic gabbroic intrusions. The metasedimentary rocks are primarily high-grade metaturbidite and migmatite. Proterozoic diabase dykes, ranging in width from a few metres to 100 m, intrude throughout the area (Le Cheminant et al. 1996). Kirkley et al. (2003) provided a detailed summary of the geology hosting the Snap Lake kimberlite.

The Snap Lake dyke is a hypabyssal kimberlite, distinctive for its high proportion of coarse-grained olivine macrocrysts (3–10 mm) (Kirkley et al. 2003). It is not associated with a known pipe and a number of theories have been advanced to explain its emplacement (McBean et al. 2003). The drilling program has shown that the dyke forms a sheet that dips from subcrop down to the northeast with dips averaging about 15° but varying from 5 to 30° (Fig. 32). Along the seismic profiles, dyke thickness is variable, ranging from 4 m to < 0.5 m (Fig. 32). Limited drilling at depths greater than 1000 m shows kimberlite intersections of less than two metres. In addition to variability in thickness, drill intersections indicate that the dyke is complex in structure, in places feathering into multiple strands or rapidly changing dip. Logging of core also shows that the dyke is accompanied by some related intrusions, fracturing and alteration in the adjacent host rock (but only within 10 cm of the dyke) (Kirkley et al. 2003).

Physical Properties

Seismic imaging of the Snap Lake dyke requires that the impedance contrast between the host rock and the kimberlite be sufficiently large that seismic waves reflected at depth have sufficient energy to be recorded at the surface (impedance is the product of velocity and density). Published data (e.g. Ji et al. 2002) suggest that the dyke would have a large impedance contrast with the granitic and metavolcanic host rocks. However, more specific data related to the Snap Lake area was necessary in order that meaningful modelling studies could be car-

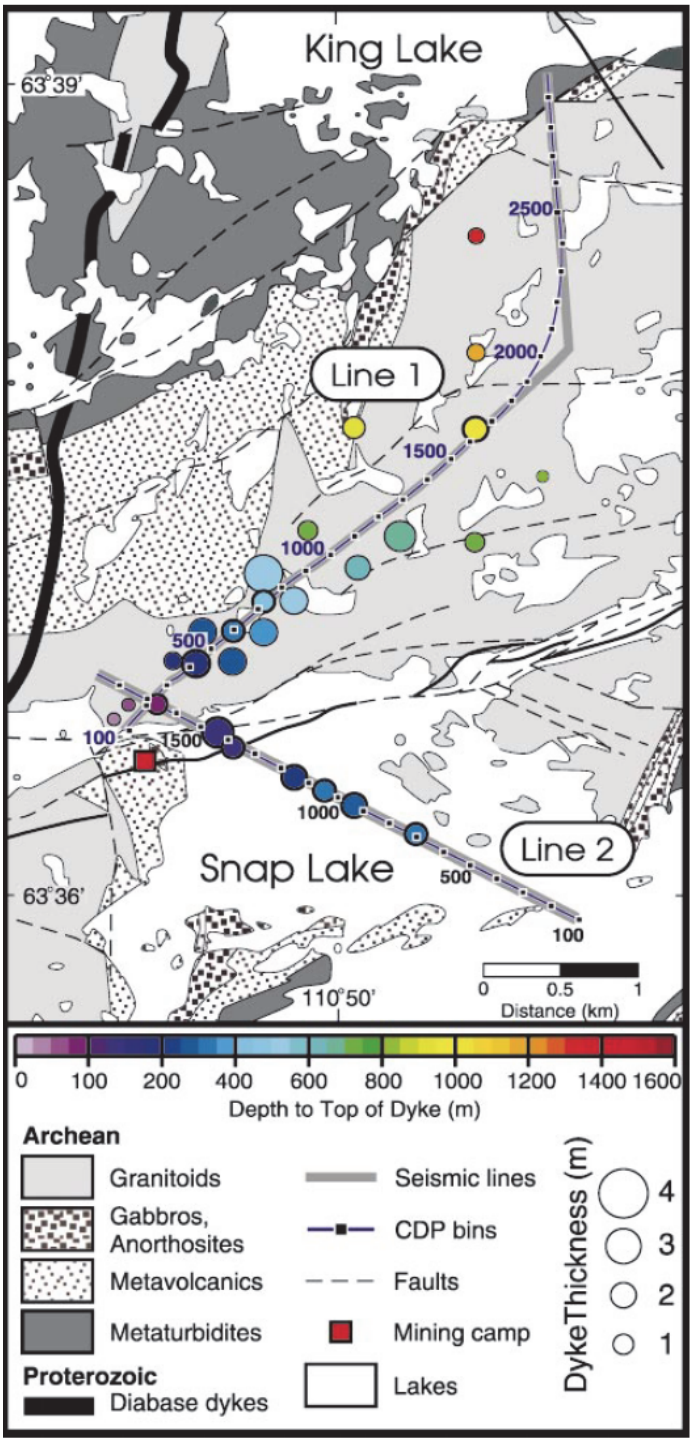

Figure 32. Locations of lines 1 and 2 on simplified geological map (M.P. Stubley, 1998, De Beers Canada Mining Inc. internal report). Drillhole locations closest to the seismic lines are noted. Depth to the intersection with the dyke is colour-coded and the dyke thickness is indicated by the circle diameter. Common-depth-point (CDP) bin centres are labeled for comparison with stacked sections. The mining camp and dyke subcrop location are noted by the red square. From Hammer et al. (2004b).

ried out to determine the best parameters for the design of the field experiment. Accordingly, core samples representing the various rock types were measured for their compressional (*P*) velocities and densities (D. Schmitt, University of Alberta, personal communication 2001). Figure 33 shows the *P*-wave velocities for all tested samples, determined for confining pressures from 0 to 300 MPa (~10 km depth). Densities were measured at laboratory temperature and pressure. As shown by average values on the right side of Figure 33, kimberlite bodies have a much lower velocity and density than the granitic host rock. As a result, the impedance contrast at vertical incidence between the kimberlite and host rocks is large, having a value of ~0.2. This indicates that significant reflected energy should be generated.

Modelling Studies

Notwithstanding the strong impedance contrast, imaging of a thin dyke still poses a significant challenge, especially as it extends to significant depths. The threshold for vertical resolution (imaging the top and bottom of the layer) is approximately 1/4 the dominant wavelength (Widess 1973). This means that resolving a 2 m-thick kimberlite dyke requires frequencies of at least 500 Hz, possible for near-surface targets but less feasible with depth due to natural attenuation of the high frequencies. If the goal is just detecting a thin layer, this can be accomplished with lower frequencies. Tuning effects involving multiple reflections can reduce the detection threshold to as little as 1/20 the wavelength (e.g. Juhlin and Young 1993; Tselentis and Paraskevopoulos 2002). This indicates that detection of a 1–2 m thick dyke may be possible if sufficient energy is returned above 200–250 Hz.

However, in terms of a field survey, many complications can arise: the laterally heterogeneous dip, thickness and structure of the dyke; signals from the deformed, metamorphosed host rocks and numerous sub-vertical dykes and faults that dissect the area could conceal reflections from the target; and accurate statics (near-surface) corrections would be required, a task made more difficult by the large lateral velocity variations in the near-surface due to alternating exposed bedrock, glacial till (permafrost) and lakes. Such issues are difficult in an environment where there were no previous studies to provide guidance. Accordingly, a synthetic modelling study, which made use of the physical properties analyses, was carried out to address these questions.

Two modelling techniques were applied: an efficient 1-D elastic reflectivity code and a computationally expensive 2-D visco-elastic finite-difference (FD) code to model complex structures. Seismic sections from many models were generated. Figure 34 shows results for a feathered dyke model using the FD code. At 400 Hz, the top and bottom of a 5 m-thick kimberlite embedded in the granitoid host rock can just be discerned but that is not the case for the 1 m-thick segment. The change in seismic signature due to the feathering is clear at 400 Hz and just distinguishable at 200 Hz in comparison with no feathering. Overall, the modelling study demonstrated the feasibility of carrying out a field survey, provided guidance for planning the acquisition geometry for the field survey and indicated some of the processing requirements that would have to be applied to the field data. Hammer et al. (2004a, 2004b) highlighted the main conclusions from the modelling study.

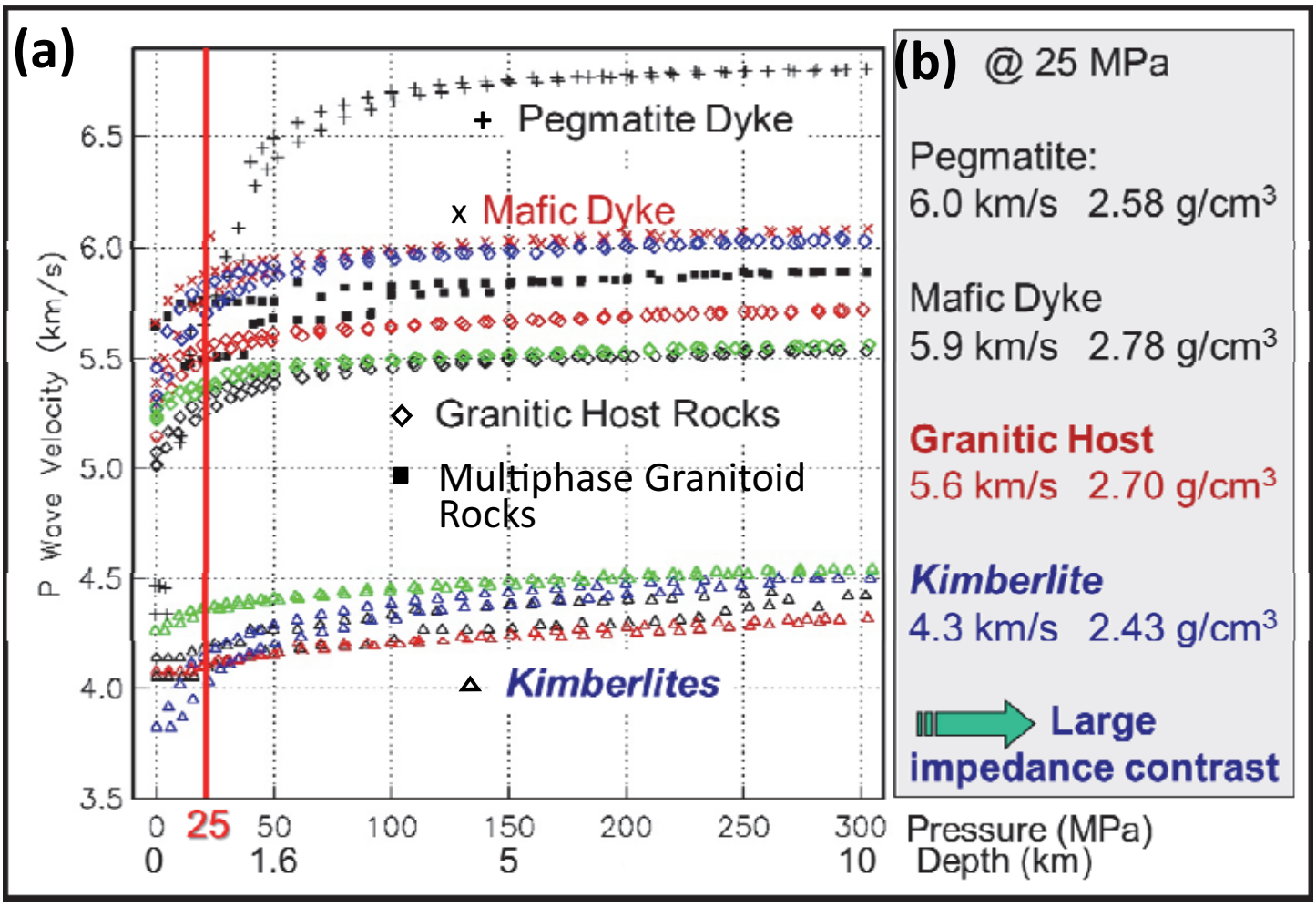

Figure 33. *P*-wave velocity response of Snap Lake core samples. Velocities were recorded as pressure was increased from 0 to 300 MPa and then reduced back to 0 MPa. Rapid changes in velocity between 0 and 5 MPa represent closure of the larger cracks. Rock types are defined by symbol shapes; individual samples denoted by symbol colours. The red line indicates the pressure at about 800 m depth. Right panel: average values of *P*-wave velocities at 25 MPa (~800 m depth) and densities (at standard temperature and pressure) of the different rock types, showing a strong impedance (product of velocity and density) contrast between the host rock and kimberlite dyke. Modified from Hammer et al. (2004b).

Seismic Surveys and Results

Using parameters indicated by the modelling studies, two seismic lines, shown in Figure 32, were run in May 2001. Line 1 was recorded on land using explosive sources (Fig. 35a) to profile down-dip dyke structure. Line 2 was recorded on land using explosive and Vibroseis (mechanical) sources and on lake ice using the Vibroseis source (Fig. 35b) to image cross-dip structure and determine the effectiveness of explosive versus Vibroseis sources and the efficacy of recording on lake ice. Acquisition parameters and processing procedures are given in Hammer et al. (2004b).

Reflections from the dyke were detected along both lines. The line 1 profile acquired using explosive shots was spectacularly successful in imaging the dyke, but the thickness of the dyke could not be resolved (Fig. 36). The line 2 profile had mixed results. Both explosive shots and the Vibroseis source generated good results on land on the western end (Fig. 32), but the on-ice experiment with the Vibroseis source recorded poor quality data with no visible reflections (see Hammer et al. 2004b). Along line 1, the dyke was superbly imaged from 30 ms (~60 m) to 425 ms (~1300 m) with faint reflections continuing to about 520 ms (~1650 m), as shown in Figure 36a. Figure 36c is an enlargement of the northern segment of the line showing the faint reflections that correlate well with detection of a 1.06 m dyke from a drillhole located ~600 m offline.

The coincident and near-coincident drillhole data correlate well with the reflection image but the seismic profile adds considerable detail to the known topography of the dyke (Fig. 36a). Reflection amplitudes vary considerably across the image. Such variations can be the result of many effects. However, we note that several zones, where amplitude drops and continuity decreases, correspond to places where drill core indicates that the dyke changes from a relatively simple planar sheet to a region with considerable variation in topography and thickness and/or the dyke becomes feathered with many thin splays being intersected (e.g. Fig. 36b, CDP ranges 500–700 and 850–1250). Such correlations could have important implications for using the seismic data for mine development.

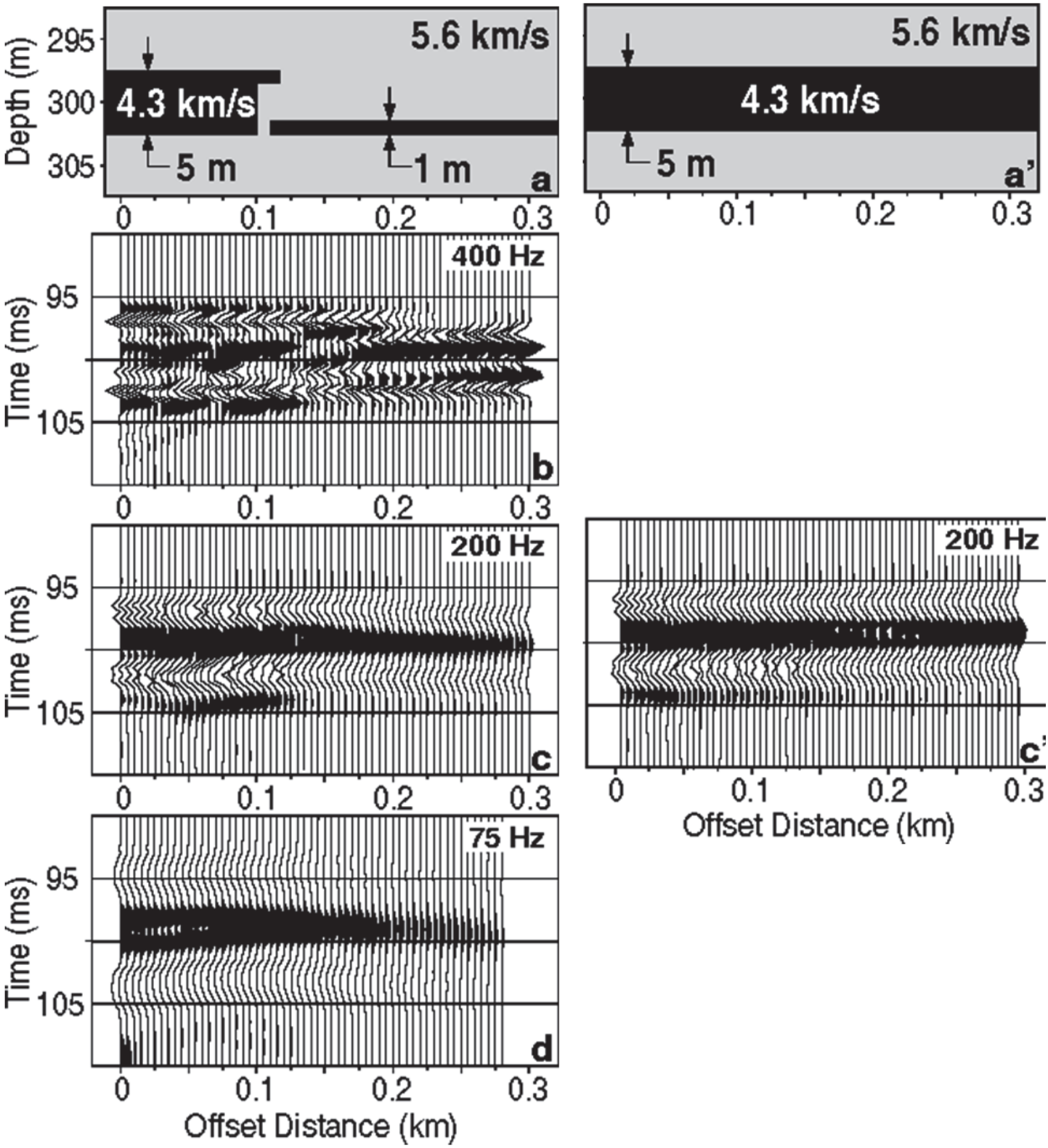

Figure 34. Finite-difference modelling of a feathered kimberlite dyke. a) Portion of model showing the kimberlite thinning from 5 m to 1 m thickness. a') Model with a constant 5 m thickness. The sequence of shot gathers [b), c), c') and d)] are normal-moveout (NMO) corrected and displayed using true relative amplitude and no correction for spherical divergence. Shot depth for all gathers is 0 m. Gathers are generated using a Ricker wavelet source centred at b) 400 Hz, c) and c') 200 Hz, and d) 75 Hz. c') is the gather for model a'). Modified from Hammer et al. (2004b).

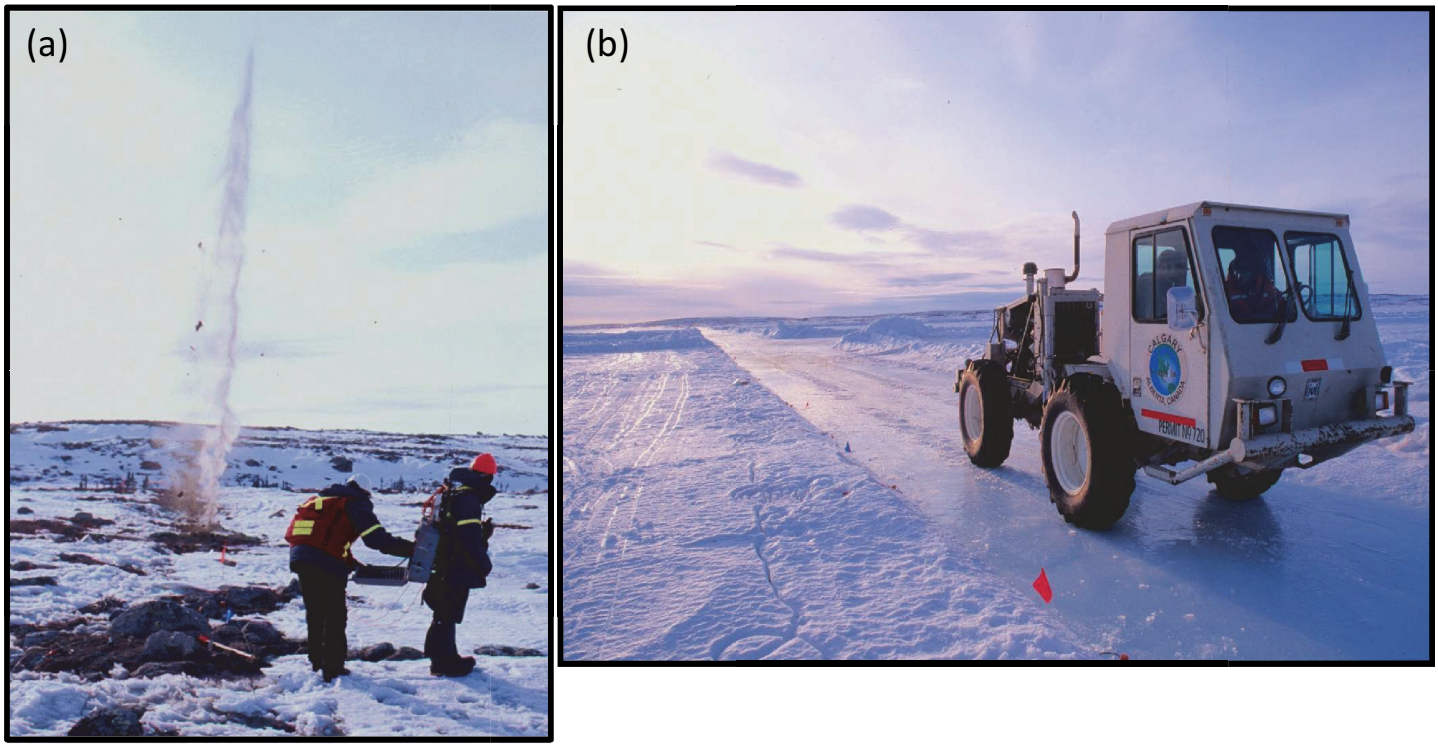

Figure 35. a) Detonation of a 0.25 kg explosive charge along line 1 during the May 2001 survey. The backpack contains the shooting box. Note that spring was early that year causing some logistical difficulties due to environmental considerations. b) The Vibroseis source along line 2 on the lake ice. The mini-vibrator generated high frequencies from 100 to 500 Hz.

As a unique experiment, the Snap Lake study demonstrated that seismic reflection methods could be a useful tool for exploration and deposit mapping of thin kimberlite dykes or sills. With an appropriate target, drilling programs that are limited by high costs and low spatial sampling could be enhanced significantly by the addition of seismic reflection profiles.

BEYOND LITHOPROBE – GEOPHYSICS AND GEOLOGY COMBINED

Examples in the previous sections are based on Lithoprobe results. They represent studies that are 15 years or more old and show interpretations based on geophysical data and a qualitative inclusion of geological data. During the last decade, some researchers have been working toward more quantitative approaches, most of which involve mathematical inversions of geophysical data constrained by geological data, to provide more reliable interpretations (e.g. Lelièvre et al. 2009). Here, I briefly describe two research examples. The first involves a method for cooperatively inverting multiple electromagnetic data sets constrained by bounds imposed by geological data from boreholes and includes an example with observed data. The second involves an approach to unifying geophysical and geological 3-D Earth models in a computational sense with the objective, not yet achieved, of seamlessly working with geological and geophysical data such that all relevant geoscience information can be included within the inversion framework.

Cooperative Geophysical Inversion Constrained by Geological Data

Many of the principal methods for mineral exploration involve electromagnetics (EM) because analyses of EM data provide estimates of the electrical resistivity in the subsurface and variations in this physical property can help distinguish mineralized zones from background lithologies. Currently, 3-D inversions of EM data generate resistivity models that can aid interpretations (e.g. Commer and Newman 2004; Haber et al. 2007). However, all such inversions are non-unique. The degree of non-uniqueness can be decreased by joint inversion or cooperative inversion of multiple EM data sets and further decreased by incorporating geological constraints. Joint inversion refers to methods in which multiple data sets are inverted simultaneously within the same inversion code (e.g. Haber and Oldenburg 1997; Sosa et al. 2013). Technically, this can be difficult due to computational issues and problematic data that can cause considerable slowing of the inversion process and possibly lead to unwanted artefacts in the final model. Cooperative inversion involves using the results from the inversion of one data set in the inversion of another data set (e.g. Oldenburg et al. 1997; Commer and Newman 2009). An advantage of this approach is that individual software packages developed for specific data sets can be used, generally providing a faster inversion process. A potential disadvantage is the need to select a workflow strategy that can find a single model that fits both data sets.

In a case history study, McMillan and Oldenburg (2014) developed a method of cooperative inversion that incorporates spatially overlapping EM data sets and borehole constraints associated with a high-sulphidation epithermal gold deposit, Antonio, located in northwestern Peru (inset, Fig.

https://doi.org/10.12789/geocanj.2017.44.125

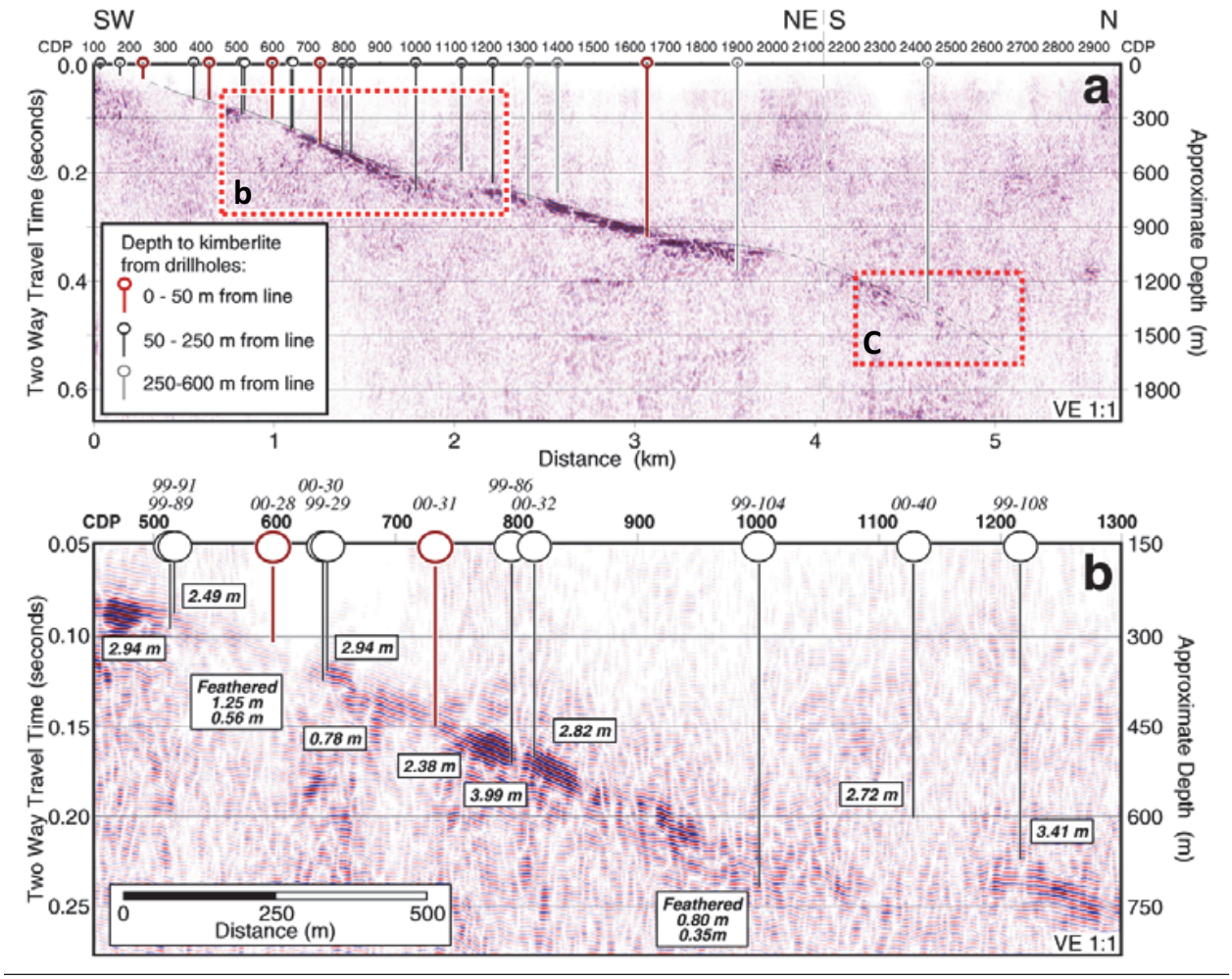

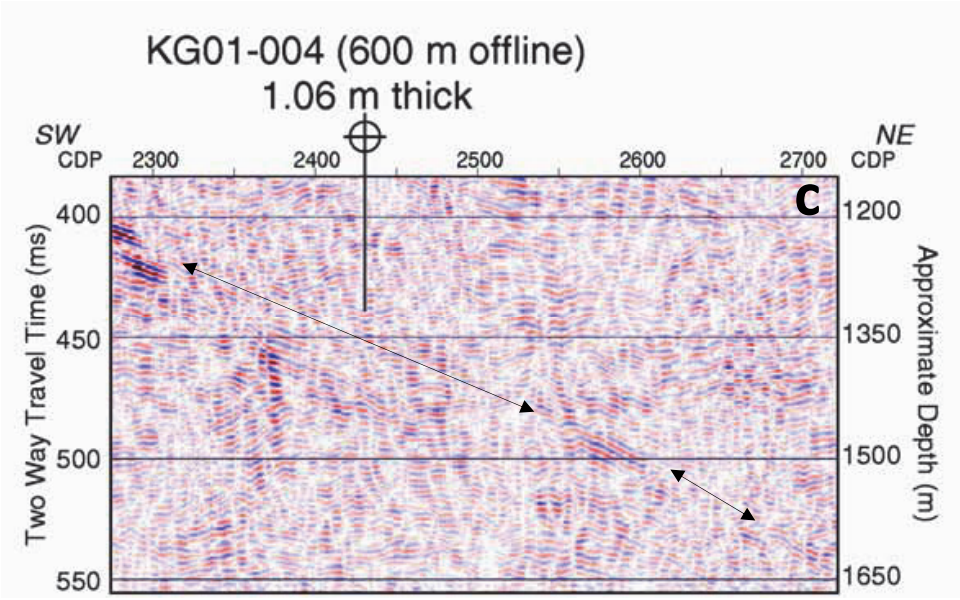

Figure 36. Migrated stacked seismic sections for line 1: a) the full profile with a thin black line tracing the top of the dyke reflection package; b) enlargement of box b in a) showing the dyke reflections through a zone with significant variations in reflector amplitude and dip; c) enlargement of box c in a) showing the low-amplitude reflector at the north end of the profile. Depths to kimberlite from nearby drill holes are indicated by the circles and vertical lines: red, 0–50 m from the line; black, 50–250 m from the line; grey, 250–600 m from the line. In b) and c) dyke thickness is labelled for each drillhole. For cores exhibiting significant feathering, the thickest kimberlite intersections are labelled. Note the correspondence between zones of low amplitude with regions that are feathered or have significant cross-dip. Approximate depths are calculated from travel times assuming 6 km/s and are corrected to a 465-m datum. Modified from Hammer et al. (2004b).

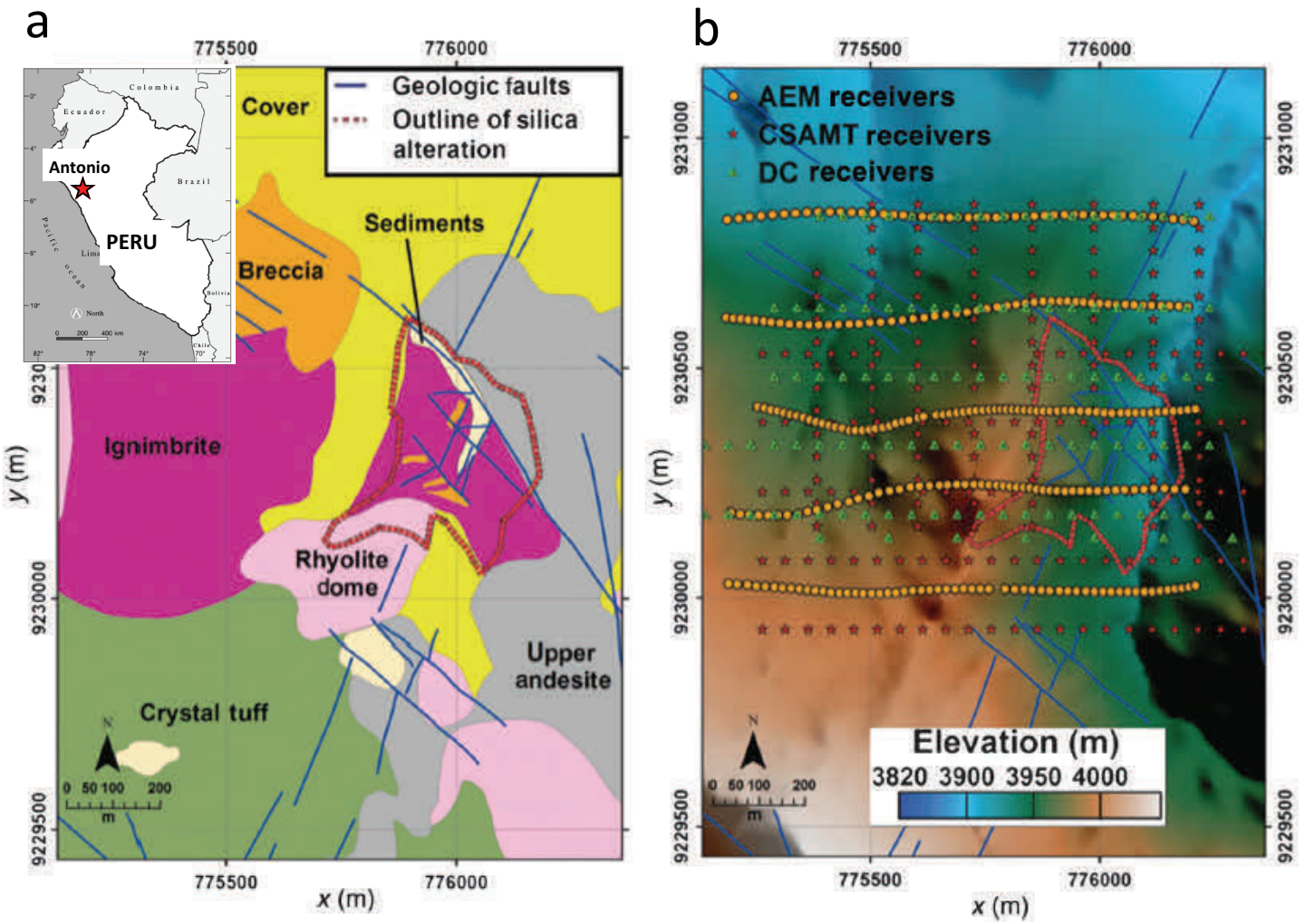

Figure 37. a) Geology in the region of the Antonio gold deposit in the Andes Mountains of northern Peru. Inset: location of Antonio within Peru. Modified from McMillan and Oldenburg (2014). b) Locations of geophysical surveys in the region of the Antonio gold deposit; background map is topography. Dotted red line outlines the mapped zone of silica alteration. Thin blue lines identify faults. AEM, airborne electromagnetics; CSAMT, controlled source audio magnetotellurics; DC, direct current resistivity. From McMillan and Oldenburg 2014).

37a). Figure 37a shows the regional geology. The area around Antonio experienced pervasive hydrothermal alteration to form a zone of massive silica alteration in the innermost region and a halo of propylitic alteration in the outer region (Fig. 37a; Teal and Benavides 2010). The quartz-rich areas of metasomatism contain the gold mineralization and these are often found near faults where confined fluid flow occurred. Structural traps associated with the intersection of faults and within favorable pyroclastic lithologies, such as ignimbrite (see Fig. 37a), are typical geological hosts to gold deposits in this region (Loayza and Reyes 2010). Silica alteration is an applicable target for EM surveys because the altered rock has a more resistive nature than the relatively conducting background rock.

The EM data-sets acquired around Antonio comprise airborne EM (AEM), controlled-source audio magnetotellurics (CSAMT) and DC resistivity (Fig. 37b). Each data set was inverted using an algorithm specifically developed for that data set. A resistor was imaged in each case, but the location of the resistor and the magnitudes of its resistivity values varied. Cooperative inversion was invoked to overcome these discrepancies and produce one resistivity model that fits all the data sets. McMillan and Oldenburg (2014) described the workflow that they selected after combining the CSAMT and DC resistivity data into one data set to be cooperatively inverted with the AEM data set. In such inversions, the calculated resistivity values are relative to a reference model, in this case a low resistivity of 23 ohm-m. Figure 38a shows a series of resistivity slices from the 3-D cooperative inversion. The authors noted that the AEM data contribute most to the cooperative result by mapping the extent of the large resistive area associated with the target region (the lighter coloured parts of each slice). The combined CSAMT/DC data better map the conductive features, the smaller blue areas within the resistive area. The cooperative model is similar to those from individual inversions of the three data sets but not identical with any of them and is interpreted to represent the resistivity signature over the Antonio deposit more accurately than any individual result.

To further improve the resistivity signature over the Antonio deposit, geological constraints were brought to bear. These

https://doi.org/10.12789/geocanj.2017.44.125

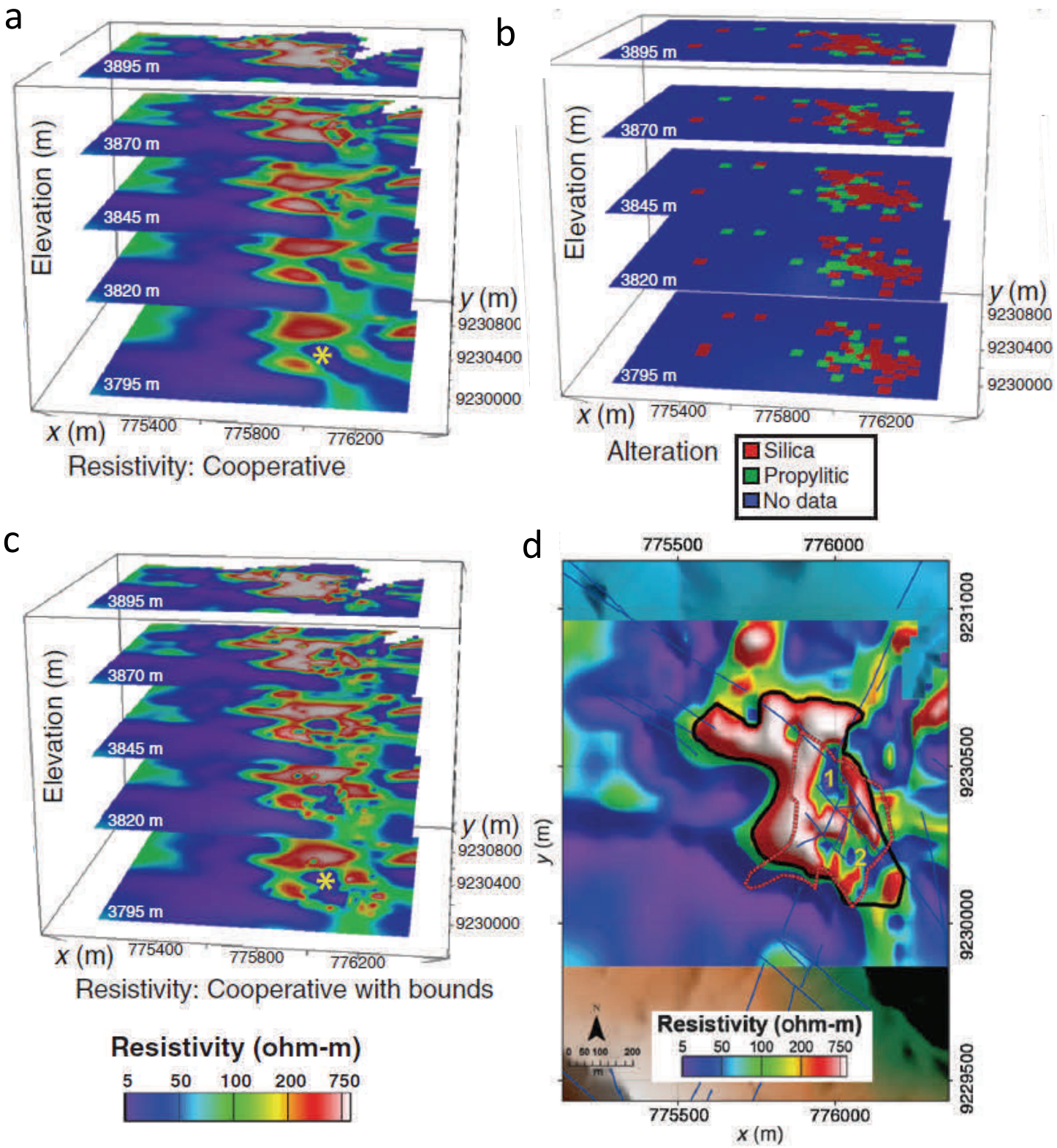

Figure 38. a) Resistivity values from 3-D cooperative inversion of AEM and combined CSAMT/DC resistivity data at five elevation slices from the 3-D model. Resistivity scale as in c). The yellow star identifies an example of a conductive anomaly potentially linked to propylitic alteration. b) Drillhole information showing silica and propylitic alteration for model cells intersected by 78 boreholes at Antonio presented as depth slices from the 3-D model. c) Resistivity values from 3-D cooperative inversion as in (a) with the addition of upper and lower bounds on resistivities as derived from a regression relationship between total alteration/sulphur content and resistivity. d) Cooperative 3-D inversions with bounds at a 3870 m elevation slice; same as 3870 m slice in c). Dotted red line, mapped zone of silica alteration; black line, outline of interpreted silica alteration at 3870 m elevation; blue lines, geologic faults. Figure adapted from figures in McMillan and Oldenburg (2014).

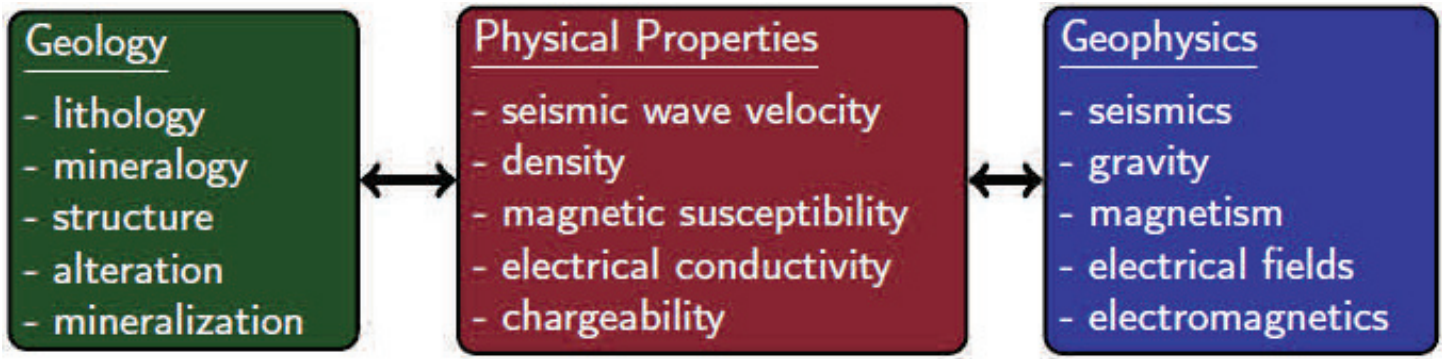

Figure 39. Schematic illustration of the interplay among components of geology, physical properties of Earth materials and types of geophysical data; all or some of which need to be included in the same model development to facilitate a unified inversion to generate the most comprehensive and realistic interpretation possible. Figure from Lelièvre and Farquharson (2016).

arise from 78 boreholes which have alteration logging and geochemical assay values but only a limited number of resistivity measurements. To augment the latter, McMillan and Oldenburg (2014) generated field constraints through a relationship between total sulphur content and resistivity that were based on laboratory rock measurements for 30 borehole samples, and then applied the regression relationship to the alteration values from the 78 boreholes. This produced a resistivity reference model (Fig. 38b) from which upper and lower bounds for resistivity values in each model cell were calculated and then incorporated into their cooperative inversion of the EM data with these constraints. Figure 38c shows the series of resistivity slices from the constrained 3-D cooperative inversion. In each slice, both the highly resistive areas (light colours) and the conductive areas within them (blue) are more clearly defined and sharper. Generally, the target silica alteration zone is mapped as a strong resistor (pink to red colours). At greater depths within the latter, many conductivity anomalies are discerned. These can be explained by the presence of propylitic alteration. A good example is shown by the star indicating high conductivity on the slice at 3795 m (Fig. 38c), which has a strong spatial correlation with a region of propylitic alteration based on borehole information (Fig. 38a).

Figure 38d shows more detail for a resistivity slice at 3870 m, an elevation corresponding to an average depth below surface of 75 m but ranging from 10 to 150 m due to the rolling topography in the region. The region north and northwest of the mapped silica alteration outline (dashed red line) shows as a resistive zone, indicating that at a depth of ~75 m the silica alteration also extends to that region. Thus, the final cooperative inversion with bounds indicates a revised zone of silica alteration at depth (black line; Fig. 38d). Within that zone, two areas of low resistivity (high conductivity) stand out (‘1’ and ‘2 in Fig. 38d). From borehole alteration logs, ‘1’ represents a small area of propylitic alteration and ‘2’ is identified with a large sulphur anomaly within the silica alteration, suggestive of extensive sulphide mineralization. Consistent with this interpretation, borehole assays show anomalous gold values. Smaller conductivity anomalies within the silica alteration zone that are not associated with propylitic alteration may indicate the presence of sulphides and thus may be prospective targets for gold mineralization.

Unified Geophysical and Geological 3-D Earth Models

In mineral exploration and mine planning, the ability to invert 3-D geophysical data sets simultaneously with 3-D geological constraints is a development that would be welcomed by the mining industry. Such ‘constrained’ geophysical inversion would provide the means to unify geological and geophysical data. As shown schematically in Figure 39, changes in geology manifest themselves as physical property contrasts that cause local variations in geophysical measurements. Constrained inversion of geophysical data with geological and physical property information incorporated into the same model would generate the most comprehensive geological interpretation. But such research is ongoing and has yet to be achieved in a way that is readily used by industry or researchers who are not inversion specialists.

One of the issues hindering such developments involves the different methods by which 3-D geological and geophysical models are digitally represented. The usual representations for 3-D geological models are wireframe surfaces, which are tessellated surfaces comprising connecting triangles. Wireframe surfaces work well because they are sufficiently general and flexible that they can be made to represent arbitrarily complicated geological structures, such as contacts between rock units, faults, ore deposits, etc., and topography. The geological structures may be known at points from borehole intersections and outcrop mapping. The contacts can be interpolated between drill holes and extrapolated outward to generate a 3-D geological model. Figure 40a shows such a geological model for the significant Voisey’s Bay nickel–copper–cobalt deposit located on the northeast coast of Labrador (Lelièvre and Farquharson 2013, 2016). The ore body that is currently being mined is the ‘ovoid,’ a massive sulphide lens, roughly ellipsoidal in shape.

In contrast, most current 3-D geophysical modelling and inversion procedures are built on rectilinear meshes because the mathematics for computations on such meshes is simpler. In rectilinear models the relevant physical properties are uniform within each brick-like cell but possibly different from cell to cell, resulting in a pixelated representation. Although discretized meshes can be made arbitrarily fine, the geophysical models will always be incompatible with geological models comprising wireframe surfaces. Also, fine meshes introduce

https://doi.org/10.12789/geocanj.2017.44.125

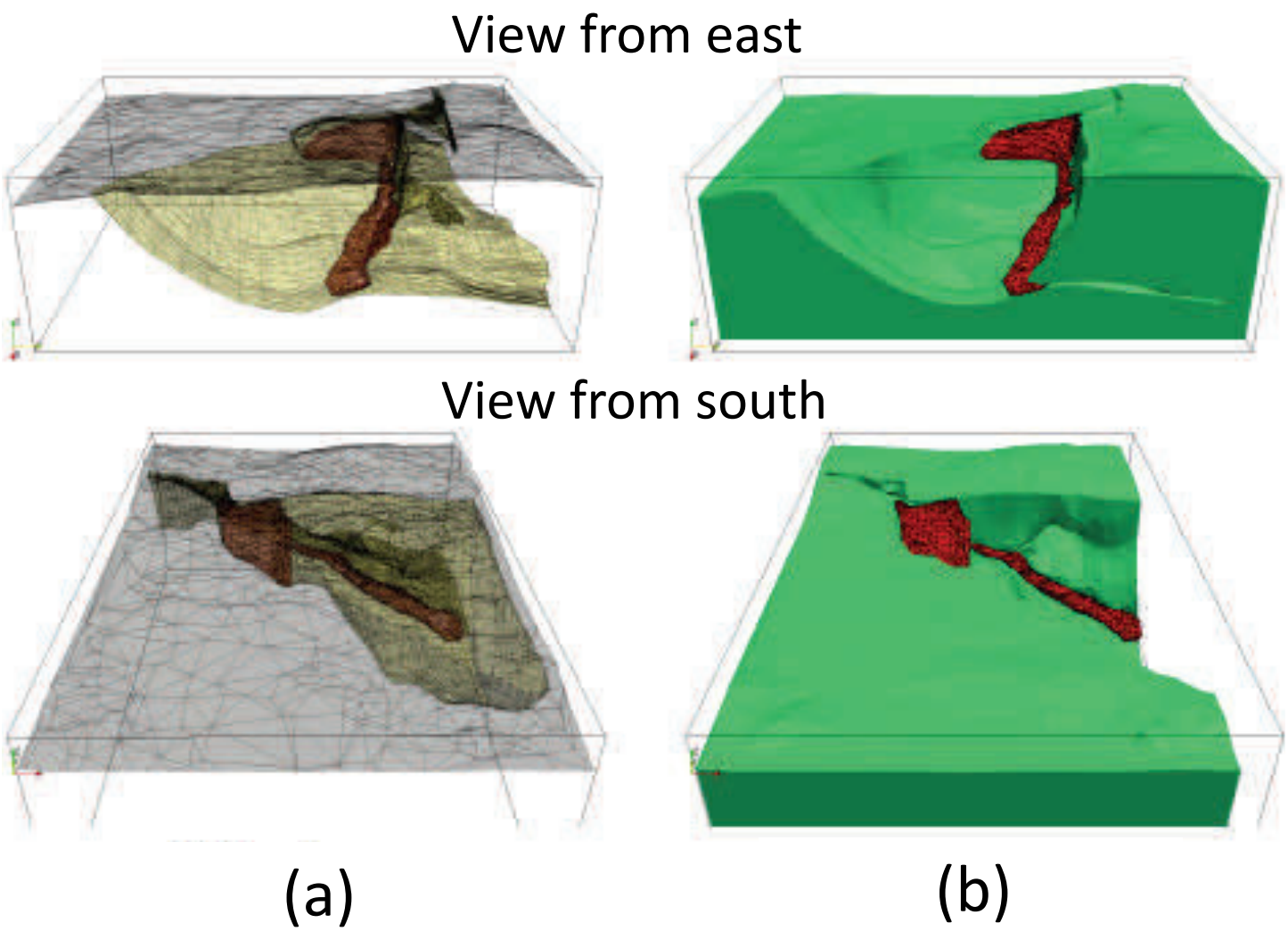

Figure 40. a) Three tessellated wireframe surfaces representing part of the geological model for the Voisey's Bay ore deposit based on over 500 drill holes and a collection of core samples. The ore deposit (red) is a massive sulphide lens roughly ellipsoidal in shape. The troctolite contact surface is shown in beige and the topographic surface in gray. b) Unstructured tetrahedral mesh developed for the same features as in a). Note that the two models are exactly the same and have enabled the geological structures in a) to be incorporated into b), which would be used for inversion of geophysical data. From Lelièvre and Farquharson (2016).

another problem: as the discretization of a model is refined, the computational resources required for 3-D numerical modelling and inversion increase dramatically.

As a result of these problems, researchers have developed and are developing procedures that make use of unstructured meshes. Within the computer science community, the generation of quality unstructured meshes is a topic of ongoing research (Si 2008; Lelièvre et al. 2012; Lelièvre and Farquharson 2013). Typical meshes of this type comprise interlocking tetrahedra although other options for the cell type are possible. They are flexible in terms of their ability to represent generally-oriented contact surfaces and this functionality is important to relate to tessellated wireframe surfaces. As described by Lelièvre et al. (2012), the unstructured meshing discretizes the volume between tessellated surfaces while exactly maintaining those surfaces. Hence, unstructured tetrahedral meshes can honour geological contacts, can incorporate prior information associated with structurally complicated subsurface geometries and can do this with an efficient discretization of the modelling domain compared to the less flexible alternative of a rectilinear mesh. This enables geophysical and geological models to share the same modelling mesh; they can be the same model, with no intermediary process required to convert from one to the other. Figure 40b shows the unstructured mesh model for the Voisey's Bay ore deposit that is depicted as a wireframe model in Figure 40a (Lelièvre and Farquharson 2016). The features of both models are the same and do not show the pixelation that would be associated with rectilinear meshes.

Nevertheless, significant challenges exist in undertaking model development and computations using unstructured meshes for the purpose of geophysical forward and inverse modelling. In terms of models, these include incorporating geological information into the modelling process and manipulating and visualizing the models. Computationally, challenges include the generation and storage of an unstructured mesh, bookkeeping requirements related to the mesh and development of appropriate numerical matrix operators. All these

challenges have not yet been met. However, Lelièvre et al. (2012) stated that "*we are developing computational methods and useful software tools to meet these challenges so that we can seamlessly work with geological and geophysical data within the framework of common Earth models built on flexible unstructured meshes.*"

CONCLUSION

The combination of geophysical studies and geological information provides the basis for greatly improved interpretations of subsurface structures associated with mineral deposits and for delineating the deposits themselves. In particular, seismic reflection studies, for which appropriate designs of field surveys and implementation of applicable processing procedures are in place, can aid exploration for mineral deposits. Such studies should be tied with physical property measurements of rock samples, drill hole geological data and results from borehole wireline logging for both survey design and interpretation of processed seismic sections. Information of this type was highly important in the successful application of reflection surveys in most of the examples presented herein. As with the current petroleum industry, which uses seismic reflection surveys and borehole information for best results, the application of 3-D procedures in mineral exploration is the direction for the future. From the seismic perspective, the Trill 3-D reflection survey of a nickel deposit in the Sudbury Structure and the McArthur River low-fold 3-D survey over uranium deposits in the Athabasca Basin, as discussed in this article, illustrate this point. Adam et al. (2003) have further discussed 3-D seismic imaging. Matthews (2002), Matthews et al. (2002) and Malehmir and Bellefleur (2009) have provided examples of direct imaging of a volcanic-hosted massive sulphide (VHMS) deposit in the Bathurst mining camp, New Brunswick, with 3-D reflection data. Other geophysical methods (e.g. magnetics, electromagnetics, gravity) for which data are available and/or appropriate for the exploration target can be the integrative tie to geological information either as the primary approach or as secondary methods that contribute to the desired exploration result. In this article, the former is illustrated by the electromagnetic studies combined with geological information that better delineated gold mineralization associated with the Antonio deposit in Peru. The secondary approach is illustrated by the contributions of magnetics and gravity to the overall interpretation of the structure of the Guichon batholith in south-central British Columbia and the contribution of electromagnetics to interpretation of structures in the Thompson nickel belt of Manitoba. Technological advances in computer hardware and software have enabled, are enabling, and will enable continuing improvement in the integration of geophysical and geological data of all kinds, particularly through mathematical inversion procedures, to further enhance success in exploration for mineral deposits.

ACKNOWLEDGEMENTS

Results presented in this article derive from publications of many Lithoprobe scientists who are cited in the reference list. I thank them for their contributions to this work and to the project as a whole. I also thank the hundreds of other Lithoprobe scientists for their contributions to the project over its 22-year history. Our work helped shape the nature of Earth Science research in Canada and beyond. Zoli Hajnal, University of Saskatchewan, kindly reviewed the section on the Athabasca Basin. Doug Oldenburg, University of British Columbia, and Colin Farquharson, Memorial University of Newfoundland, reviewed the final section on "Beyond Lithoprobe" to ensure my summary of their contributions was correctly interpreted and described. The manuscript was improved by comments from Andy Calvert, Simon Fraser University, and two other reviewers. I thank the Department of Earth, Ocean and Atmospheric Sciences at The University of British Columbia for its continuing support of my efforts.

REFERENCES

Adam, E., Milkereit, B., Arnold, G., and Pineault, R., 1996, Seismic response of the Bell Allard orebody, Matagami, Québec: Society of Exploration Geophysicists Annual Meeting Expanded Technical Abstracts with Biographies, v. 66, p. 634–637.

Adam, E., Arnold, G., Beaudry, C., Matthews, L., Milkereit, B., Perron, G., and Pineault, R., 1997, Seismic exploration for VMS deposits, Matagami, Québec, *in* Gubins, A.G., *ed.*, Proceedings of Exploration 97: 4th Decennial International Conference on Mineral Exploration, Prospectors and Developers Association of Canada (PDAC), Toronto, ON, p. 433–438.

Adam, E., Milkereit, B., and Mareschal, M., 1998, Seismic reflection and borehole geophysical investigations in the Matagami mining camp: Canadian Journal of Earth Sciences, v. 35, p. 686–695, https://doi.org/10.1139/e98-022.

Adam, E., Perron, G., Milkereit, B., Wu, J., Calvert, A.J., Salisbury, M., Verpaelst, P., and Dion, D.-J., 2000, A review of high-resolution seismic profiling across the Sudbury, Selbaie, Noranda, and Matagami mining camps: Canadian Journal of Earth Sciences, v. 37, p. 503–516, https://doi.org/10.1139/e99-064.

Adam, E., Perron, G., Arnold, G., Matthews, L., and Milkereit, B., 2003, 3D seismic imaging for VMS deposit exploration, Matagami, Québec, *in* Eaton, D.W., Milkereit, B., and Salisbury, M.H., *eds.*, Hardrock Seismic Exploration: Society of Exploration Geophysicists, Geophysical Developments Series No. 10, p. 229–246, https://doi.org/10.1190/1.9781560802396.ch15.

Ager, C.A., Ulrych, T.J., and McMillan, W.J., 1973, A gravity model for the Guichon Creek batholith, south-central British Columbia: Canadian Journal of Earth Sciences, v. 10, p. 920–935, https://doi.org/10.1139/e73-081.

Ames, D.E., Watkinson, D.H., and Parrish, R.R., 1998, Dating of a regional hydrothermal system induced by the 1850 Ma Sudbury impact event: Geology, v. 26, p. 447–450, https://doi.org/10.1130/0091-7613(1998)026<0447:DOARHS>2.3.CO;2.

Annesley, I.R., Madore, C., and Portella, P., 2005, Geology and thermotectonic evolution of the western margin of the Trans-Hudson Orogen: evidence from the eastern sub-Athabasca basement, Saskatchewan: Canadian Journal of Earth Sciences, v. 42, p. 573–597, https://doi.org/10.1139/e05-034.

Baudemont, D., and Fedorowich, J., 1996, Structural controls of uranium mineralization at the Dominique-Peter deposit, Saskatchewan, Canada: Economic Geology, v. 91, p. 855–874, https://doi.org/10.2113/gsecongeo.91.5.855.

Bleeker, W., 1990, New structural-metamorphic constraints on Early Proterozoic oblique collision along the Thompson Nickel Belt, Manitoba, Canada, *in* Lewry, J.F., and Stauffer, M.J., *eds.*, The Early Proterozoic Trans-Hudson Orogen of North America: Geological Association of Canada, Special Paper 37, p. 57–73.

Bleeker, W., and Davis, W.J., 1999, The 1991–1996 NATMAP Slave Province Project: Introduction: Canadian Journal of Earth Sciences, v. 36, p. 1033–1042, https://doi.org/10.1139/e99-053.

Boerner, D.E., Kellett, R., and Mareschal, M., 1994, Inductive source EM sounding of the Sudbury Structure: Geophysical Research Letters, v. 21, p. 943–946, https://doi.org/10.1029/93GL02316.

Boerner, D.E., Milkereit, B., and Davidson, A., 2000, Geoscience impact: a synthesis of studies of the Sudbury Structure: Canadian Journal of Earth Sciences, v. 37, p. 477–501, https://doi.org/10.1139/e99-062.

Calvert, A.J., and Li, Y., 1999, Seismic reflection imaging over a massive sulfide deposit at the Matagami mining camp, Québec: Geophysics, v. 64, p. 24–32, https://doi.org/10.1190/1.1444521.

Calvert, A.J., Perron, G., and Li, Y., 2003, A comparison of 2D seismic lines shot over the Ansil and Bell Allard mines in the Abitibi greenstone belt, *in* Eaton, D.W., Milkereit, B., and Salisbury, M.H., *eds.*, Hardrock Seismic Exploration: Society of Exploration Geophysicists, Geophysical Developments No. 10, p. 164–177, https://doi.org/10.1190/1.9781560802396.ch11.

Card, C.D, Pana, D., Stern, R.A., and Rayner, N., 2007, New insights into the geological history of the basement rocks to the southwestern Athabasca Basin, Saskatchewan and Alberta, *in* Jefferson, C.W., and Delaney, G., *eds.*, EXTECH IV: Geology and uranium EXploration TECHnology of the Proterozoic Athabasca Basin, Saskatchewan and Alberta: Geological Survey of Canada Bulletin 588, p. 119–134.

Clowes, R.M., 2001, Deep structure and seismic-reflection studies in Precambrian mining regions: Examples from the Canadian LITHOPROBE project: Mining Engineering, v. 53, p. 35–42.

Clowes, R.M., 2010, Initiation, development, and benefits of Lithoprobe – shaping the direction of Earth science research in Canada and beyond: Canadian Journal of Earth Sciences, v. 47, p. 291–314, https://doi.org/10.1139/E09-074.

Clowes, R.M., 2015, Logan Medallist 2. Geophysics and geology: An essential combination illustrated by LITHOPROBE interpretations – Part 1, lithospheric examples: Geoscience Canada, v. 42, p. 27–60, https://doi.org/10.12789/geocanj.2014.41.064.

Commer, M., and Newman, G.A., 2004, A parallel finite-difference approach for 3D transient electromagnetic modeling with galvanic sources: Geophysics, v. 69, p. 1192–1202, https://doi.org/10.1190/1.1801936.

Commer, M., and Newman, G.A., 2009, Three-dimensional controlled-source electromagnetic and magnetotelluric joint inversion: Geophysical Journal International, v. 178, p. 1305–1316, https://doi.org/10.1111/j.1365-246X.2009.04216.x.

Cook, F.A., Varsek, J.L., Clowes, R.M., Kanasewich, E.R., Spencer, C.S., Parrish, R.R., Brown, R.L., Carr, S.D., Johnson, B.J., and Price, R.A., 1992, LITHOPROBE crustal reflection cross section of the southern Canadian Cordillera, 1, Foreland thrust and fold belt to Fraser River Fault: Tectonics, v. 11, p. 12–35, https://doi.org/10.1029/91TC02332.

Cowan, E.J., and Schwerdtner, W.M., 1994, Fold origin of the Sudbury basin, *in* Lightfoot, P.C., and Naldrett, A.J., *eds.*, Proceedings of the Sudbury-Noril'sk Symposium: Ontario Geological Survey, Special Volume 5, p. 45–55.

Dietz, R.S., 1964, Sudbury structure as an astrobleme: The Journal of Geology, v. 72, p. 412–434, https://doi.org/10.1086/626999.

Dressler, B.O., 1984, Sudbury geological compilation: Ontario Geological Survey, Map 2491, scale 1:50000.

Eaton, D.W., Adam, E., Milkereit, B., Salisbury, M., Roberts, B., White, D., and Wright, J., 2010, Enhancing base-metal exploration with seismic imaging: Canadian Journal of Earth Sciences, v. 47, p. 741–760, https://doi.org/10.1139/E09-047.

Fensome, R., Williams, G., Achab, A., Clague, J., Corrigan, D., Monger, J., and Nowlan, G., *editors*, 2014, Four Billion Years and Counting: Canada's Geological Heritage: Canadian Federation of Earth Sciences and Nimbus Publishing, Halifax, Nova Scotia, 402 p.

Fraser, J.A., Donaldson, J.A., Fahrig, W.F., and Tremblay, L.P., 1970, Helikian basins and geosynclines of the Northwestern Canadian Shield, *in* Baer, A.J., *ed.*, Symposium on Basins and Geosynclines of the Canadian Shield: Geological Survey of Canada, Paper 70–40, p. 213–238.

Genna, D., Gaboury, D., and Roy, G., 2014, The Key Tuffite, Matagami Camp, Abitibi Greenstone Belt, Canada: petrogenesis and implications for VMS formation and exploration: Mineralium Deposita, v. 49, p. 489–512, https://doi.org/10.1007/s00126-013-0499-7.

Giblin, P.E., 1984, History of exploration and development of geological studies and development of geological concepts, *in* Pye, E.G., Naldrett, A.J., and Giblin, P.E., *eds.*, The Geology and Ore Deposits of the Sudbury Structure: Ontario Geological Survey, Special Volume 1, p. 3–23.

Grieve, R.A.F., and Head III, J.W., 1983, The Manicouagan Impact Structure: An analysis of its original dimensions and form: Journal of Geophysical Research, v. 88, p. A807–A818, https://doi.org/10.1029/JB088iS02p0A807.

Grieve, R.A.F., and Masaitis, V.I., 1994, The economic potential of terrestrial impact craters: International Geology Review, v. 36, p. 105–151, https://doi.org/10.1080/00206819409465452.

Grieve, R.A.F., Stöffler, D., and Deutsch, A., 1991, The Sudbury Structure: Controversial or misunderstood?: Journal of Geophysical Research, v. 96, p. 22753–22764, https://doi.org/10.1029/91JE02513.

Haber, E., and Oldenburg, D., 1997, Joint inversion: A structural approach: Inverse Problems, v. 13, p. 63–77, https://doi.org/10.1088/0266-5611/13/1/006.

Haber, E., Oldenburg, D.W., and Shekhtman, R., 2007, Inversion of time domain three-dimensional electromagnetic data: Geophysical Journal International, v. 171, p. 550–564, https://doi.org/10.1111/j.1365-246X.2007.03365.x.

Haggerty, S.E., 1986, Diamond genesis in a multiply-constrained model: Nature, v. 320, p. 34–37, https://doi.org/10.1038/320034a0.

Hajnal, Z., Stauffer, M.R., and King, M.S., 1983, Petrophysics of the Athabasca Basin near the Midwest Lake uranium deposit, *in* Cameron, E.M., *ed.*, Uranium exploration in Athabasca Basin, Saskatchewan, Canada: Geological Survey of Canada, Paper 82-11, p. 303–310.

Hajnal, Z., Annesley, I.R., White, D., Bezdan, S., Stauffer, M.R., and Thomas, M.T., 1997, Sedimentary-hosted mineral deposits: A high-resolution seismic survey in the Athabasca Basin, *in* Gubins, A.G., *ed.*, Proceedings of Exploration 97: 4th Decennial International Conference on Mineral Exploration, Prospectors and Developers Association of Canada (PDAC), Toronto, ON, p. 421–432.

Hajnal, Z., Ansdell, K.M., and Ashton, K.E., 2005a, Introduction to special issue of *Canadian Journal of Earth Sciences*: The Trans-Hudson Orogen transect of Lithoprobe: Canadian Journal of Earth Sciences, v. 42, p. 379–383, https://doi.org/10.1139/e05-053.

Hajnal, Z., Lewry, J., White, D., Ashton, K., Clowes, R., Stauffer, M., Gyorfi, I., and Takacs, E., 2005b, The Sask Craton and Hearne Province margin: seismic reflection studies in the western Trans-Hudson Orogen: Canadian Journal of Earth Sciences, v. 42, p. 403–419, https://doi.org/10.1139/e05-026.

Hajnal, Z., Takacs, E., White, D.J., Gyorfi, I., Powell, B., and Koch, R., 2007, Regional seismic signature of the basement and crust beneath the McArthur River mine district, Athabasca Basin, Saskatchewan, *in* Jefferson, C.W., and Delaney, G., *eds.*, EXTECH IV: Geology and uranium EXploration TECHnology of the Proterozoic Athabasca Basin, Saskatchewan and Alberta: Geological Survey of Canada Bulletin 588, p. 389–395.

Hajnal, Z., White, D.J., Takacs, E., Gyorfi, I., Annesley, I.R., Wood, G., O'Dowd, C., and Nimeck, G., 2010, Application of modern 2-D and 3-D seismic-reflection techniques for uranium exploration in the Athabasca Basin: Canadian Journal of Earth Sciences, v. 47, p. 761–782, https://doi.org/10.1139/E10-026.

Hajnal, Z., Takacs, E., Pandit, B., and Annesley, I.R., 2015, Uranium mineralization indicators from seismic and well log data in the Shea Creek area at the southern margin of the Carswell impact structure, Athabasca Basin, Canada: Geophysical Prospecting, v. 63, p. 861–880, https://doi.org/10.1111/1365-2478.12274.

Hammer, P.T.C., Clowes, R.M., and Ramachandran, K., 2004a, Seismic reflection imaging of thin, kimberlite dykes and sills: exploration and deposit characterization of the Snap Lake dyke, Canada: Lithos, v. 76, p. 359–367, https://doi.org/10.1016/j.lithos.2004.03.056.

Hammer, P.T.C., Clowes, R.M., and Ramachandran, K., 2004b, High-resolution seismic reflection imaging of a thin, diamondiferous kimberlite dyke: Geophysics, v. 69, p. 1143–1154, https://doi.org/10.1190/1.1801932.

Hearst, R., Morris, W., and Thomas, M., 1994, Magnetic interpretation along the Sudbury structure Lithoprobe transect: Geophysical Research Letters, v. 21, p. 951–954, https://doi.org/10.1029/93GL02610.

James, R.S., Sweeney, J.M., and Peredery, W., 1992, Thermobarometry of the Levack gneisses – footwall rocks to the Sudbury Igneous Complex: Abitibi-Grenville Lithoprobe Workshop, Lithoprobe Report 25, p. 179–182.

Jefferson, C.W., Thomas, D.J., Gandhi, S.S., Remaekers, P., Delaney, G., Brisbin, D., and 4 others, 2007, Unconformity-associated uranium deposits of the Athabasca Basin, Saskatchewan and Alberta, *in* Jefferson, C.W., and Delaney, G., *eds.*, EXTECH IV: Geology and uranium EXploration TECHnology of the Proterozoic Athabasca Basin, Saskatchewan and Alberta: Geological Survey of Canada Bulletin 588, p. 23–68.

Ji, S.C., Wang, Q., and Xia, B., 2002, Handbook of seismic properties of minerals, rocks and ores: Polytechnic International Press, 630 p.

Juhlin, C., and Young, R., 1993, Implications of thin layers for amplitude variation with offset (AVO) studies: Geophysics, v. 58, p. 1200–1204, https://doi.org/10.1190/1.1443504.

Kirkley, M.B., Mogg, B.T., and McBean, D., 2003, Snap Lake trip guide, *in* Kjarsgaard, B.A., *ed.*, 8th International Kimberlite Conference, Slave Province and Northern Alberta Field Trip Guidebook, p. 1–12.

Krogh, T.E., Davis, D.W., and Corfu, F., 1984, Precise U–Pb zircon and baddeleyite ages for the Sudbury area, *in* Pye, E.G., Naldrett, A.J., and Giblin, P.E., *eds.*, The Geology and, Ore Deposits of the Sudbury Structure: Ontario Geological Survey, Special Volume 1, p. 431–446.

Kyser, K., Hiatt, E., Renac, C., Durocher, K., Holk, G., and Deckart, K., 2000, Diagenetic fluids in Paleo- and Mesoproterozoic sedimentary basins and their implications for long protracted fluid histories, *in* Kyser, K., *ed.*, Fluids and Basin Evolution: Mineralogical Association of Canada, Short Course Series, v. 28, p. 125–262.

LeCheminant, A.N., Heaman, L.M., van Breemen, O. Ernst, R.E., Baragar, W.R.A., and Buchan, K.L., 1996, Mafic magmatism, mantle roots, and kimberlites in the Slave craton, *in* LeCheminant, A.N., Richardson, D.G., Dialbio, R.N.W., and Richardson, K.A., *eds.*, Searching for diamonds in Canada: Geological Survey of Canada Open File Report 322, p. 161–169.

Lelièvre, P.G., and Farquharson, C.G., 2013, Gradient and smoothness regularization operators for geophysical inversion on unstructured meshes: Geophysical Journal International, v. 195, p. 330–341, https://doi.org/10.1093/gji/ggt255.

Lelièvre, P.G., and Farquharson, C.G., 2016, 3D geologically constrained inversion on unstructured meshes for the Voisey's Bay Eastern Deep deposit: European Association of Geoscientists and Engineers Conference, Vienna, Austria, Workshop WS16 C06.

Lelièvre, P.G., Oldenburg, D.W., and Williams, N.C., 2009, Integrating geologic and geophysical data through advanced constrained inversions: Exploration Geo-

physics, v. 40, p. 334–341, https://doi.org/10.1071/EG09012.
Lelièvre, P., Carter-McAuslan, A., Farquharson, C., and Hurich, C., 2012, Unified geophysical and geological 3D Earth models: The Leading Edge, v. 31, p. 322–328, https://doi.org/10.1190/1.3694900.
Li, Y., and Oldenburg, D.W., 1996, 3-D inversion of magnetic data: Geophysics, v. 61, p. 394–408, https://doi.org/10.1190/1.1443968.
Lightfoot, P., 2016, Nickel Sulfide Ores and Impact Melts: Elsevier Press, Amsterdam, 680 p.
Lightfoot, P.C., and Naldrettt, A.J., *editors*, 1994, Proceedings of the Sudbury-Noril'sk Symposium: Ontario Geological Survey, Special Volume 5.
Loayza, C., and Reyes, J., 2010, Geologic survey of the Mineiro district of Yanacocha, Cajamarca, northern Peru: Presented at SIMEXMIN10 — IV Brazilian Symposium of Mineral Exploration, article 33. Available from: http://www.adimb.com.br/simexmin2010/palestras/.
Ludden, J., and Hynes, A., *editors*, 2000, The Abitibi-Grenville Lithoprobe transect part III: Introduction: Canadian Journal of Earth Sciences, v. 37, p. 115–516, https://doi.org/10.1139/e00-016.
Machado, N., Gapais, D., Potrel, A., Gauthier, G., and Hallot, E., 2011, Chronology of transpression, magmatism, and sedimentation in the Thompson Nickel Belt (Manitoba, Canada) and timing of Trans-Hudson Orogen – Superior Province collision: Canadian Journal of Earth Sciences, v. 48, p. 295–324, https://doi.org/10.1139/E10-040.
Malehmir, A., and Bellefleur, G., 2009, 3D seismic reflection imaging of volcanic-hosted massive sulfide deposits: Insights from reprocessing Halfmile Lake data, New Brunswick, Canada: Geophysics, v. 74, p. B209–B219, https://doi.org/10.1190/1.3230495.
Mandler, H.A.F., and Clowes, R.M., 1997, Evidence for extensive tabular intrusions in the Precambrian shield of western Canada: A 160-km-long sequence of bright reflections: Geology, v. 25, p. 271–274, https://doi.org/10.1130/0091-7613(1997)025<0271:EFETII>2.3.CO;2.
Matthews, L., 2002, Base-metal exploration: Looking deeper and adding value with seismic data: Canadian Society of Exploration Geophysicists Recorder, v. 27, p. 31–43.
Matthews, L., Gingerich, J.C., and Pleshko, M.J., 2002, The development of new exploration technologies at Noranda: Seeing more with hyperspectral and deeper with 3-D seismic: CIM Bulletin, v. 95, p. 56–61.
McBean, D., Kirkley, M., and Revering, C., 2003, Structural controls on the morphology of the Snap Lake kimberlite dyke: 8th International Kimberlite Conference, Expanded Abstracts, p. 69–74.
McGill, B.D., Marlatt, J.L., Matthews, R.B., Sopuck, V.J., Homeniuk, L.A., and Hubregtse, J.J., 1993, The P2 North uranium deposit, Saskatchewan, Canada: Exploration and Mining Geology, v. 2, p. 321–331.
McGrath, P.H., and Broome, H.J., 1994, A gravity model for the Sudbury Structure along the Lithoprobe seismic line: Geophysical Research Letters, v. 21, p. 955–958, https://doi.org/10.1029/93GL02247.
McMillan, M.S., and Oldenburg, D.W., 2014, Cooperative constrained inversion of multiple electromagnetic data sets: Geophysics, v. 79, p. B173–B185, https://doi.org/10.1190/geo2014-0029.1.
McMillan, W.J., Newman, K., Tsang, L., and Sanford, G., 1985, Geology and ore deposits of the Highland Valley camp, *in* Sinclair, A.J., *ed.*, Geological Association of Canada Mineral Deposits Division Field Guide and Reference Manual, Series 1.
Meldrum, A., Abel-Rahman, A.-F.M., Martin, R.F., and Wodicka, N., 1997, The nature, age and petrogenesis of the Cartier Batholith, northern flank of the Sudbury Structure, Ontario, Canada: Precambrian Research, v. 82, p. 265–285, https://doi.org/10.1016/S0301-9268(96)00055-1.
Milkereit, B., Berrer, E.K., Watts, A., and Roberts, B., 1997, Development of 3-D seismic exploration technology for Ni–Cu deposits, Sudbury basin, *in* Gubins, A.G., *ed.*, Proceedings of Exploration 97: 4th Decennial International Conference on Mineral Exploration, Prospectors and Developers Association of Canada (PDAC), Toronto, ON, p. 439–448.
Milkereit, B., Berrer, E.K., King, A.R., Watts, A.H., Roberts, B., Adam, E., Eaton, D.W., Wu, J., and Salisbury, M.H., 2000, Development of 3-D seismic exploration technology for deep nickel-copper deposits – A case history from the Sudbury basin, Canada: Geophysics, v. 65, p. 1890–1899, https://doi.org/10.1190/1.1444873.
Mitchell, R.H., 1995, Kimberlites, orangeites, and related rocks: Plenum Press, 407 p., https://doi.org/10.1007/978-1-4615-1993-5.
Morris, W.A., Hearst, R.B., and Thomas, M.D., 1992, Magnetic interpretation along the Sudbury Structure Lithoprobe transect: Abitibi-Grenville Lithoprobe Workshop, Lithoprobe Report 33, p. 129–132.
Mortensen, J.K., 1993, U–Pb geochronology of the eastern Abitibi subprovince. Part 1: Chibougamau-Matagami-Joutel region: Canadian Journal of Earth Sciences, v. 30, p. 11–28, https://doi.org/10.1139/e93-002.
Mwenifumbo, C.J., Elliot, B.E., Jefferson, C.W., Bernius, G.R., and Pflug, K.A., 2004, Physical rock properties from the Athabasca Group: designing geophysical exploration models for unconformity uranium deposits: Journal of Applied Geophysics, v. 55, p. 117–135, https://doi.org/10.1016/j.jappgeo.2003.06.008.
Naldrett, A.J., 1999, World-class Ni–Cu–PGE deposits; key factors in their genesis: Mineralium Deposita, v. 34, p. 227–240, https://doi.org/10.1007/s001260050200.
Northcote, K.E., 1969, Geology and geochronology of the Guichon Creek batholith: British Columbia Ministry of Energy, Mines and Petroleum Resources, Bulletin 56, 73 p.
Oldenburg, D.W., Li, Y., and Ellis, R.G., 1997, Inversion of geophysical data over a copper gold porphyry deposit: A case history for Mt. Milligan: Geophysics, v. 62, p. 1419–1431, https://doi.org/10.1190/1.1444246.
Osinski, G.R., Lee, P., Spray, J.G., Parnell, J., Lim, D.S.S., Bunch, T.E., Cockell, C.S., and Glass, B., 2005, Geological overview and cratering model for the Haughton impact structure, Devon Island, Canadian High Arctic: Meteoritics and Planetary Science, v. 40, p. 1759–1776, https://doi.org/10.1111/j.1945-5100.2005.tb00145.x.
Ostermann, M., and Deutsch, A., 1997, The Sudbury Igneous Complex (SIC) as impact melt layer: geochemical evidence for *in situ* differentiation (Abstract): Proceedings of the Conference on Large Meteorite Impacts and Planetary Evolution, Sudbury, 1997, LPI Contribution 922, p. 38–39.
Padgham, W.A., and Fyson, W.K., 1992, The Slave Province: a distinct Archean craton: Canadian Journal of Earth Sciences, v. 29, p. 2072–2086, https://doi.org/10.1139/e92-165.
Pell, J.A., 1997, Kimberlites in the Slave craton, Northwest Territories, Canada: Geoscience Canada, v. 24, p. 77–90.
Perron, G., and Calvert, A.J., 1998, Shallow, high resolution seismic imaging of the Ansil mining camp in the Abitibi greenstone belt: Geophysics, v. 63, p. 379–391, https://doi.org/10.1190/1.1444337.
Pye, E.G., Naldrett, A.J., and Giblin, P.E., *editors*, 1984, The geology and ore deposits of the Sudbury Structure: Ontario Geological Survey, Special Volume 1, 603 p.
Rainbird, R.H., Stern, R.A., Rayner, N., and Jefferson, C.W., 2007, Age, provenance and regional correlation of the Athabasca Group, Saskatchewan and Alberta, constrained by igneous and detrital zircon geochronology, *in* Jefferson, C.W. and Delaney, G., *eds.*, EXTECH IV: geology and uranium EXploration TECHnology of the Proterozoic Athabasca Basin, Saskatchewan and Alberta: Geological Survey of Canada Bulletin 588, p. 193–210.
Ramaekers, P., Yeo, G.M., and Jefferson, C.W., 2001, Preliminary overview of regional stratigraphy in the Late Paleoproterozoic Athabasca Basin, Saskatchewan and Alberta: Summary of Investigations 2001, v. 2, Part b: EXTECH IV Athabasca Uranium Multidisciplinary Study, Saskatchewan, Geological Survey, Saskatchewan Energy and Mines, Miscellaneous Report 2001–4.2b, CD-ROM.
Ramaekers, P., Jefferson, C.W., Yeo, G.M., Collier, D.G.F., Long, G., Drever, S., and 8 others, 2007, Revised geological map and stratigraphy of the Athabasca Group, Saskatchewan and Alberta, *in* Jefferson, C.W., and Delaney, G., *eds.*, EXTECH IV: Geology and uranium EXploration TECHnology of the Proterozoic Athabasca Basin, Saskatchewan and Alberta: Geological Survey of Canada Bulletin 588, p. 155–192.
Rayner, N.M., Stern, R.A., and Rainbird, R.H., 2003, SHRIMP U–Pb detrital zircon geochronology of Athabasca Group sandstones, northern Saskatchewan and Alberta: Geological Survey of Canada, Current Research 2003-F2, 20 p.
Rayner, N., Zwanzig, H.V., and Percival, J.A., 2006, Detrital zircon provenance of the Pipe Formation, Ospwagan Group, Thompson Nickel Belt, Manitoba, NTS 6308: Manitoba Geological Survey, Manitoba Science, Technology, Energy and Mines, Report of Activities 2006, p. 116–124.
Roberts, R.G., 1975, The geological setting of the Mattagami Lake mine, Quebec: A volcanogenic massive sulfide deposit: Economic Geology, v. 70, p. 115–129, https://doi.org/10.2113/gsecongeo.70.1.115.
Roy, B., and Clowes, R.M., 2000, Seismic and potential-field imaging of the Guichon Creek batholith, British Columbia, Canada, to delineate structures hosting porphyry copper deposits: Geophysics, v. 65, p. 1418–1434, https://doi.org/10.1190/1.1444831.
Roy, B., and Mereu, R.F., 1996, Signal enhancement using pattern recognition techniquies with application to near vertical crustal seismic reflection experiments: Geophysical Research Letters, v. 23, p. 1849–1852, https://doi.org/10.1029/96GL01587.
Salisbury, M.H., Milkereit, B., and Bleeker, W., 1996, Seismic imaging of massive sulfide deposits; Part I, Rock properties: Economic Geology, v. 91, p. 821–828, https://doi.org/10.2113/gsecongeo.91.5.821.
Salisbury, M.H., Harvey, C.W., and Matthews, L., 2003, The acoustic properties of

ores and host rocks in hardrock terranes, *in* Eaton, D.W., Milkereit, B., and Salisbury, M.H., *eds.*, Hardrock Seismic Exploration: Society of Exploration Geophysicists, Geophysical Developments No. 10, p. 9–19, https://doi.org/10.1190/1.9781560802396.ch1.

Schreiner, B.T., 1983, Quaternary geology of the NEA/IAE test area, *in* Cameron, E.M., *ed.*, Uranium exploration in Athabasca basin, Saskatchewan, Canada: Geological Survey of Canada, Paper 82-11, p. 27–32.

Si, H., 2008, Three dimensional boundary conforming Delaunay mesh generation: Unpublished Ph.D. thesis, Technische Universitat, Berlin, 144 p.

Sosa, A., Velasco, A.A., Velazquez, L., Argaez, M., and Romero, R., 2013, Constrained optimization framework for joint inversion of geophysical data sets: Geophysical Journal International, v. 195, p. 1745–1762, https://doi.org/10.1093/gji/ggt326.

Teal, L., and Benavides, A., 2010, History and geologic overview of the Yanacocha mining district, Cajamarca, Peru: Economic Geology, v. 105, p. 1173–1190, https://doi.org/10.2113/econgeo.105.7.1173.

Thomas, D.J., Matthews, R.B., and Sopuck, V., 2000, Athabasca Basin (Canada) unconformity-type uranium deposits: Exploration model, current mine developments and exploration directions, *in* Geology and Ore Deposits 2000: The Great Basin and Beyond, Geological Society of Nevada Symposium, Reno, Nevada, May 15–18, 2000, Proceedings, v. 1, p. 103–126.

Tselentis, G.-A., and Paraskevopolous, P., 2002, Application of a high-resolution seismic investigation in a Greek coal mine: Geophysics, v. 67, p. 50–59, https://doi.org/10.1190/1.1451326.

White, D., Boerner, D., Wu, J., Lucas, S., Berrer, E., Hannila, J., and Somerville, R., 2000, Mineral exploration in the Thompson nickel belt, Manitoba, Canada, using seismic and controlled-source EM methods: Geophysics, v. 65, p. 1871–1881, https://doi.org/10.1190/1.1444871.

White, D.J., Milkereit, B., Wu, J.J., Salisbury, M.H., Mwenifumbo, J., Berrer, E.K., Moon, W., and Lodha, G., 1994, Seismic reflectivity of the Sudbury Structure North Range from borehole logs: Geophysical Research Letters, v. 21, p. 935–938, https://doi.org/10.1029/93GL02609.

White, D.J., Hajnal, Z., Roberts, B., Gyorfi, I., Reilkoff, B., Bellefleur, G., and 10 others, 2007, Seismic methods for uranium: an overview of EXTECH IV seismic studies at the McArthur River mining camp, Athabasca Basin, Saskatchewan, *in* Jefferson, C.W., and Delaney, G., *eds.*, EXTECH IV: Geology and uranium EXploration TECHnology of the Proterozoic Athabasca Basin, Saskatchewan and Alberta, Geological Survey of Canada Bulletin 588, p. 363–388.

Widess, M.B., 1973, How thin is a thin bed?: Geophysics, v. 38, p. 1176–1180, https://doi.org/10.1190/1.1440403.

Wodicka, N., and Card, K.D., 1995, Late Archean history of the Levack Gneiss Complex, southern Superior Province, Sudbury, Ontario: new evidence from U–Pb geochronology (Abstract): Proceedings of the International Conference on Tectonics and Metallogeny of Early/Mid Precambrian Orogenic Belts, Precambrian '95, Program with Abstracts, p. 191.

Wu, J., Milkereit, B., and Boerner, D.E., 1995, Seismic imaging of the enigmatic Sudbury Structure: Journal of Geophysical Research, v. 100, p. 4117–4130, https://doi.org/10.1029/94JB02647.

Received August 2017
Accepted as revised November 2017